Design, synthesis and application of peptide mimetics as photoactivatable inhibitors for proteases

Inaugural-Dissertation

zur

Erlangung des Doktorgrades

Dr. rer. nat.

der Fakultät für

Biologie

an der

Universität Duisburg-Essen

vorgelegt von

Tim Van Kersavond

aus Sint-Niklaas, Belgien

Februar 2019

Die der vorliegenden Arbeit zugrunde liegenden Experimente wurden am Leibniz-Institut für Analytische Wissenschaften – ISAS – e. V., Dortmund durchgeführt.

1. Gutachter: Prof. Dr. Markus Kaiser
2. Gutachter: Prof. Dr. Steven Verhelst

Vorsitzender des Prüfungsausschusses: Prof. Dr. Michael Ehrmann

Tag der mündlichen Prüfung: 26.04.19

DOI: 10.17185/duepublico/70109
URN: urn:nbn:de:hbz:464-20190502-090211-3

Table of Contents

List of Abbreviations

A	alanine
Aβ	amyloid beta
ABP	activity-based probe
ABPP	activity-base protein profiling
Ac	acetyl
AcCl	acetyl chloride
AcOH	acetic acid
AfBP	affinity-based probe
Ahx	6-aminohexanoyl
Ala	alanine
Alloc-OSu	N-(Allyloxycarbonyloxy)succinimide
AMC	7-amino-4-methylcoumarin
AOMK	acyloxymethyl ketone
Arg	arginine
Asp	aspartic acid
Boc	*tert*-Butyloxycarbonyl
Boc_2O	di-tert-butyl dicarbonate
BP	benzophenone
Bpa	4-benzoyl-L-phenylalanine
Cat.	catalytic
CHAPS	3-((3-cholamidopropyl) dimethylammonio)-1-propanesulfonate
Click	copper(I)-catalyzed azide alkyne cycloaddition
D	aspartic acid
DCM	dichloromethane
DIEA	*N*,*N*-diisopropylethylamine
DMF	dimethylformamide
DTT	dithiothreitol
E	glutamic acid
EDTA	ethylenediaminetetraacetic acid

ESI	electrospray ionization
Et_2O	diethyl ether
EtOAc	ethyl acetate
EtOH	ethanol
Fmoc	fluorenylmethoxycarbonyl
FRET	fluorescence resonance energy transfer
FP	fluorophosphonate
FP-Rh	fluorophosphonate-rhodamine
FTMS	Fourier transform mass spectrometry
Gln	glutamine
Glu	glutamic acid
Gly	glycine
HBTU	*N*,*N*,*N*′,*N*′-Tetramethyl-*O*-(1H-benzotriazol-1-yl)uronium hexafluorophosphate
HEPES	4-(2-hydroxyethyl)-1-piperazineethanesulfonic acid
HOBt	1-Hydroxybenzotriazole
HRMS	high resolution mass spectrometry
Ile	isoleucine
iPrOH	isopropanol
LC	liquid chromatography
MALDI	matrix-assisted laser desorption/ionization
MeCN	acetonitrile
MeOH	methanol
MS	mass spectrometry
NBS	*N*-bromosuccinimide
NMR	nuclear magnetic resonance
p-azidoPhe	*para*-azidophenylalanine
Pbf	2,2,4,6,7-pentamethyldihydrobenzofuran-5-sulfonyl
PBS	phosphate-buffered saline
$Pd(PPh_3)_4$	tetrakis(triphenylphosphine)palladium(0)
Phe	phenylalanine

photoLeu	photoleucine
Pro	proline
RP-HPLC	reversed phase high performance liquid chromatography
RT	room temperature
SDS-PAGE	sodium dodecyl sulfate polyacrylamide gel electrophoresis
Ser	serin
SPPS	solid phase peptide synthesis
TAMRA	tetramethylrhodamine
tBu	*tert*-butyl
TFA	trifluoroacetic acid
THF	tetrahydrofuran
THPTA	tris(3-hydroxypropyltriazolylmethyl)amine
Thr	threonine
TIS	triisopropylsilane
TLC	thin layer chromatography
TRIS	tris(hydroxymethyl)aminomethane
Trp	tryptophan
V	valine
Val	valine

Table of Figures

Table of Tables

1 Introduction

1.1 Proteases, function and classification

Proteases are a type of enzymes that catalyze the cleavage of peptide bonds in protein and peptide substrates. This process usually goes hand in hand with the activation or deactivation of those respective substrates, which results in an ensuing biological effect. Because proteases can operate in almost any environment and are encountered in a plethora of different pathways, the biological functions and properties related to them are very diverse [1]. Many proteases are highly selective and play a role in strongly regulated processes [2], such as apoptosis [3] and blood coagulation [4], while other proteases, for example involved in digestion, can cleave a broad range of substrates. Apoptosis obviously needs to tightly controlled, and this is accomplished by an entire cascade of reactions involving caspases (Figure 1.1). They exist as inactive zymogens until they receive an apoptotic signal, either extracellular or from the mitochondria. Then, the initiator caspases are processed into a small and large subunit that dimerize to assume their active form. They in turn process the executioner caspases in the same way, and those last ones result in the actual apoptosis event.

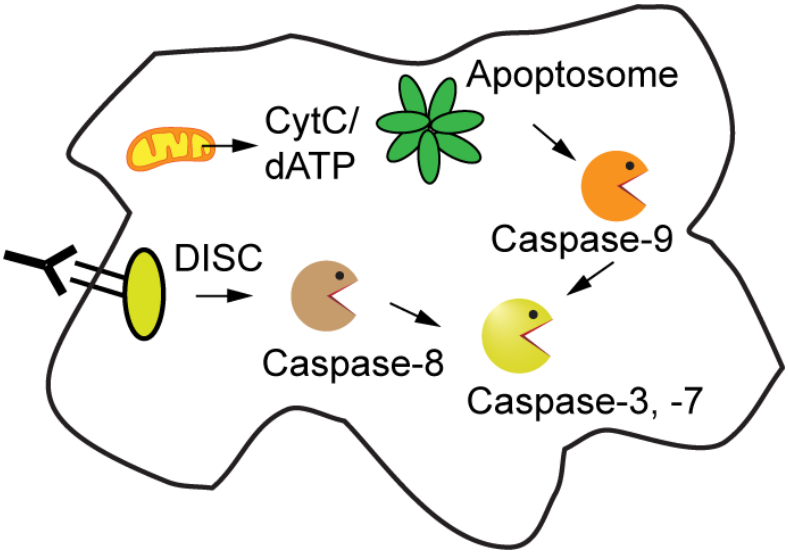

Figure 1.1 Graphic representation of the intrinsic and extrinsic apoptotic pathways involving caspases
Adapted from [5]. In the intrinsic pathway, certain stimuli are released from the mitochondria. This triggers the formation of the Apoptosome complex that cleaves the inactive procaspase-9. The two subunits that are generated this way combine to form the active caspase-9 dimer. This will in turn process the executioner caspases, caspase-3 and -7, to create their active forms that actually perform the apoptosis. In the extrinsic pathway, DISC formation leads to the autoactivation of caspase-8, which in turn cleaves caspase-3 and -7, thereby activating them.

Hypothetically, if any of these proteases are activated by a non-specific protease or due to the malfunctioning of other proteases, this could result in major complications. Hence, the importance of the regulation of proteases cannot be stressed enough. In food digestion, the involved proteases are much less selective, as their role is to process proteins to create a series of smaller peptides. An example is trypsin [6], which will cleave the peptide bond after every lysine and arginine it encounters.

In contrast to many other post-translational processes, substrate processing by proteases is an irreversible process, which also means that erroneous cleavages cannot be undone. A good example of this is the processing of the amyloid precursor protein by γ-secretase to generate amyloid beta (Aβ) peptides. These can have a variable length, with Aβ40 being the most common form. However, mutations can result in an increased production of Aβ42, which is related to Alzheimer's disease [7, 8]. Furthermore, some infectious agents depend on protease activity for their survival or host invasion. Malaria is caused by apicomplexan parasites [9, 10], and their invasion is facilitated by the *P. falciparum* signal peptide peptidase. With all of the above in mind, it is clear that proteases are involved in a variety of diseases and that they can serve as prime drug targets [11].

The substrates of proteases come in all shapes and sizes, and many of these have a specific purpose. For this reason, specialized proteases have evolved to bring about a vast array of different classes and families. Based on their catalytic residues, they can be classified in seven mechanistic classes: aspartic proteases [12], glutamic proteases [13], metalloproteases [14], cysteine proteases [15], serine proteases [16], threonine proteases [17], and asparagine peptide lyases [18]. The first six catalyze the hydrolysis of peptide bonds by using a combination of their active site residues and water molecules, but asparagine peptide lyases perform self-cleavage. Of these seven mechanistic classes, the four main ones, each with their own specific active site machinery (Figure 1.2), are: (1) Aspartic proteases, like pepsin [19], operate by coordinating a water molecule to the two active site aspartate residues. Deprotonation of the water by one of the aspartates allows it to attack the scissile peptide bond of the substrate and perform the hydrolysis. (2) In metalloproteases, such as the matrix metalloproteinases [20], a metal ion, Zn^{2+}, is suggested to coordinate to three active site residues and the carbonyl of the scissile peptide bond. This activates the carbonyl

group of that peptide bond that can in turn be attacked by a water molecule. (3) Cysteine proteases, like the caspases [3], use a catalytic dyad consisting of a cysteine and usually a histidine to cleave their substrates. In this process, the histidine deprotonates the cysteine that can then act as a nucleophile to attack the scissile peptide bond of the substrate. (4) serine proteases, like trypsin [16], perform the cleavage of substrates by a nucleophilic attack of the active site serine on the scissile peptide bond. The serine residue is usually polarized by a nearby histidine and aspartate, forming a so-called catalytic triad. This holds true for most soluble serine proteases, but the much more recently discovered intramembrane serine proteases (rhomboid proteases) utilize a catalytic dyad consisting of the active site serine and a nearby histidine residue [21, 22].

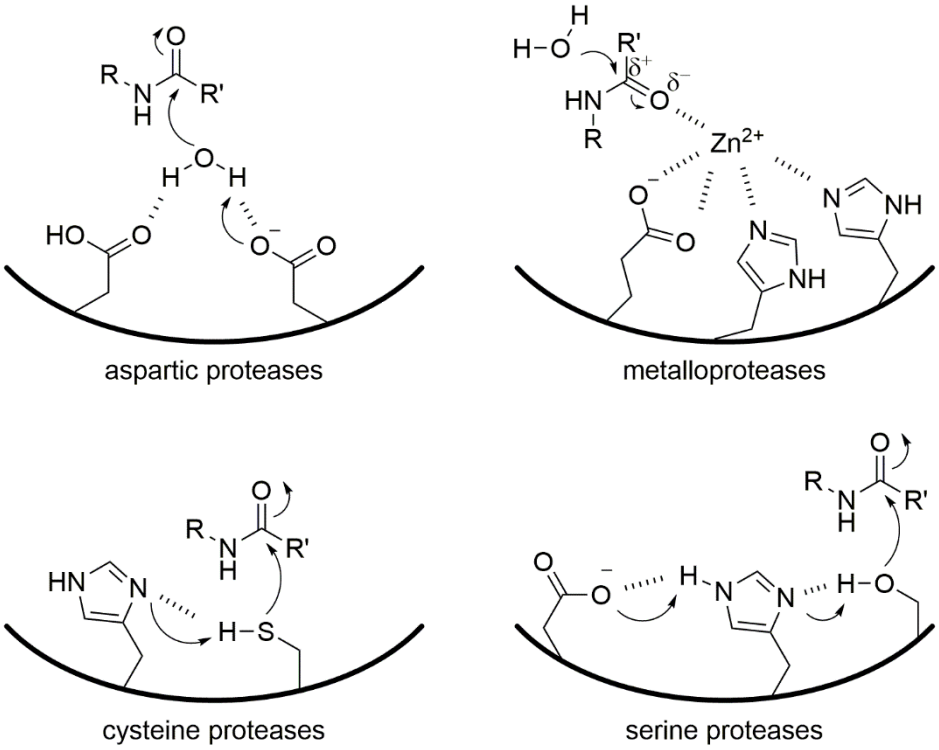

Figure 1.2 Representation of the catalytic residues of the four main protease classes and the interaction with their substrates

An example of rhomboids is *E. coli* GlpG, which is structurally the best characterized rhomboid. This protease consists of six transmembrane domains that span the lipid bilayer of membranes [23] (Figure 1.3). The active site consists of a small hydrophilic cavity in the otherwise hydrophobic protease structure that can accommodate a water molecule. Although it has recently been revealed to play an essential role in extraintestinal pathogenic gut colonization, its natural substrate is still elusive [24]. *P.*

stuartii AarA is one of the few rhomboids for which the natural substrate has been identified (TatA). Interestingly, TatA can also be cleaved by GlpG, and this protein has been the basis for most specificity related research on GlpG, including the research presented in this work.

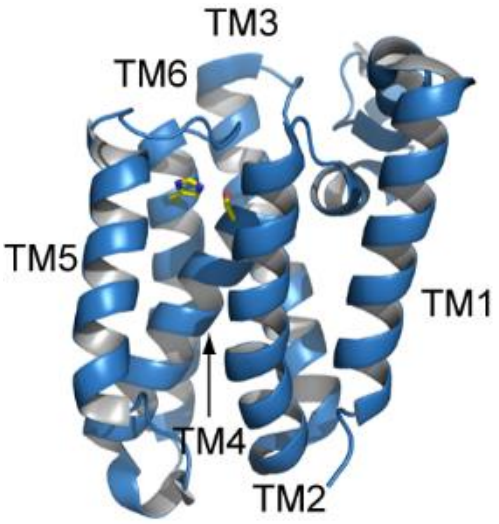

Figure 1.3 Crystal structure of *E. coli* GlpG

The six transmembrane domains that span the membrane and the catalytic residues are indicated. Adapted from [25].

1.2 The substrate specificity of proteases

Each protease has a certain degree of selectivity for its substrate(s). Depending on the specific protease, complex substrate sequences can be required for recognition. When this substrate sequence contains even minor modifications, recognition may be less efficient or not occur at all, depending on the exact location of the modification. Usually, the recognition of substrates proceeds through intermolecular interactions between the protease and its substrate. During these initial interactions, the amino acid residues close to the scissile peptide bond of the substrates are accommodated in the corresponding substrate binding pockets on the protease. These binding pockets can usually only accept certain specific amino acids, which explains why substrate mutations close to the scissile bond of substrates can have a huge impact on their recognition and subsequent processing. In this work, the terminology used to describe the amino acid residues of the substrate and the binding sites on the protease are according to the Schechter and Berger nomenclature [26]. In substrates, the non-primed site covers the amino acid residues N-terminal to the scissile bond, while the primed site covers the C-terminal amino acid residues (designated as … - P2 – P1 – P1' – P2' - …). These amino acid residues will interact with the corresponding substrate binding pockets on the protease (… - S2 – S1 – S1' – S2' - …) (Figure 1.4).

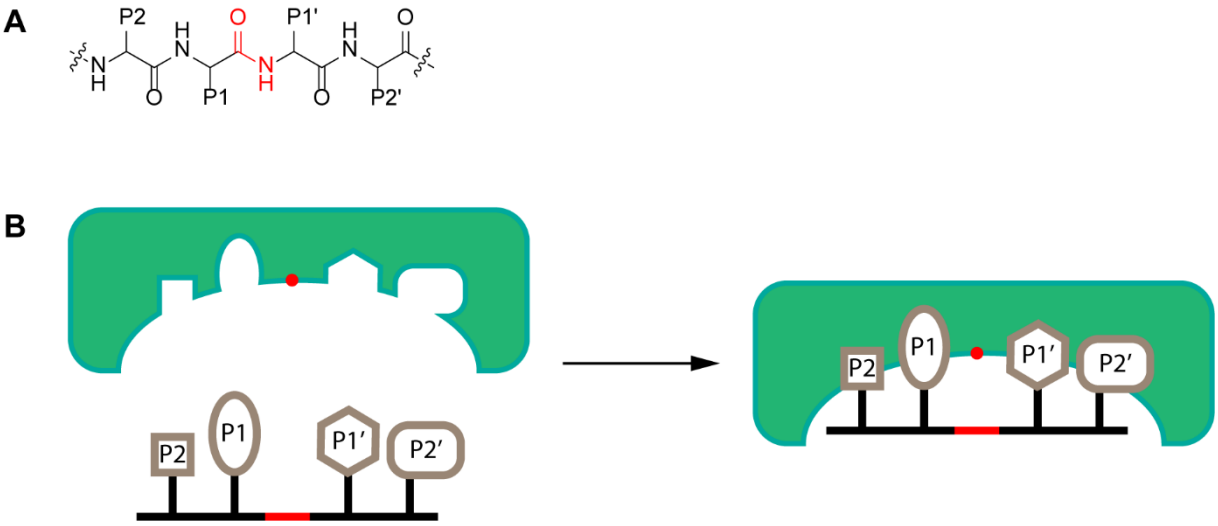

Figure 1.4 Schechter and Berger nomenclature

(A) Structural clarification, with the scissile bond highlighted in red. (B) Graphic representation of the interaction between protease and substrate, with the scissile bond and catalytic site highlighted in red.

In figure 1.5, two examples, GluC and caspase-3, are given to illustrate the importance of the substrate sequence [27]. GluC only requires a glutamic acid in the P1 position and thus has a quite low selectivity towards its substrates, where it basically cleaves after every glutamic acid it encounters. For caspase-3, the situation is a bit more complicated. While an aspartic acid in the P1 position is an absolute requirement, this alone is not sufficient. Especially a hydrophobic amino acid in the P2 position and an aspartic acid in the P4 position will increase the affinity tremendously.

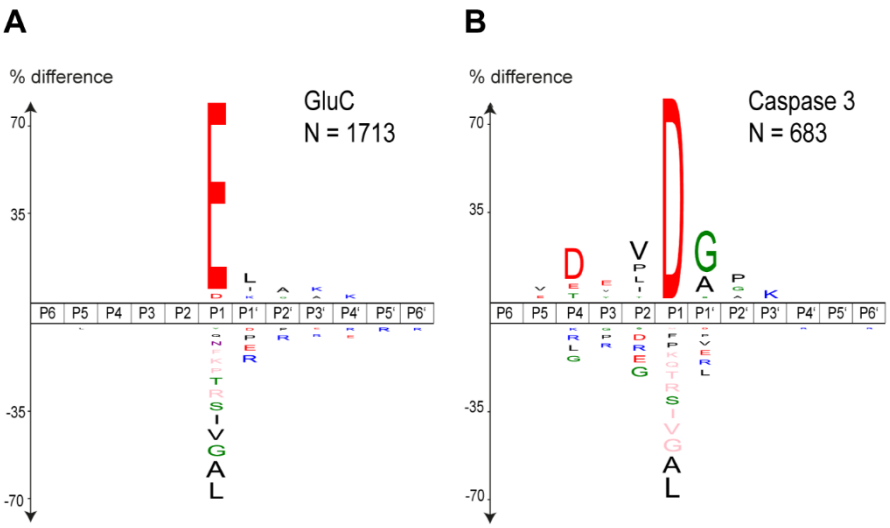

Figure 1.5 IceLogos for the proteases GluC and caspase-3

Adapted from [27]. An increasing size of the letter corresponding to a certain amino acid corresponds to a higher preference of that amino acid in that position.

1.3 Chemical tools for proteases

In order to study proteases and the interactions with their substrates, various chemical tools are available. Each of these have been designed with the substrate specificity of a certain protease in mind to a certain extent. Non-specific tools usually don't contain any specificity elements and can sometimes be used to target entire classes of proteases. Others strongly resemble the substrate structure and can even target a single specific protease.

1.3.1 Synthetic substrates

Synthetic substrates are used to measure the activity of proteases. They usually consist of a peptide covering the non-primed site of the substrate which is connected to a leaving group that replaces the primed site. Upon cleavage, this group generates a signal which is directly correlated to the protease activity. Great examples of this are the fluorogenic AMC-substrates (7-amino-4-methylcoumarin-substrates, Figure 1.6A). They consist of a non-primed site amino acid chain connected to the AMC entity via a peptide bond. Only upon processing of these substrates, the AMC fluorophore is released and generates a fluorescent signal upon irradiation. Luciferin derivatives have been designed as luminogenic substrates, and again cover the non-primed site of substrates [28]. By themselves, they don't produce a signal, but after substrate processing, aminoluciferin is produced. In a second reaction this is then recognized and processed by luciferase under consumption of ATP, and this leads to the emission of light (Figure 1.6B).

To reach higher levels of selectivity or when coverage of the non-primed site isn't sufficient for recognition, fluorescently quenched peptides (FRET peptides; fluorescence resonance energy transfer, Figure 1.6C) can be used. These peptides use a combination of a fluorophore and a quencher, located on different sides of the scissile peptide bond. That way, primed site amino acids can also be introduced in the peptide sequence, and the signal is only generated after cleavage, when the fluorophore and quencher are spatially separated.

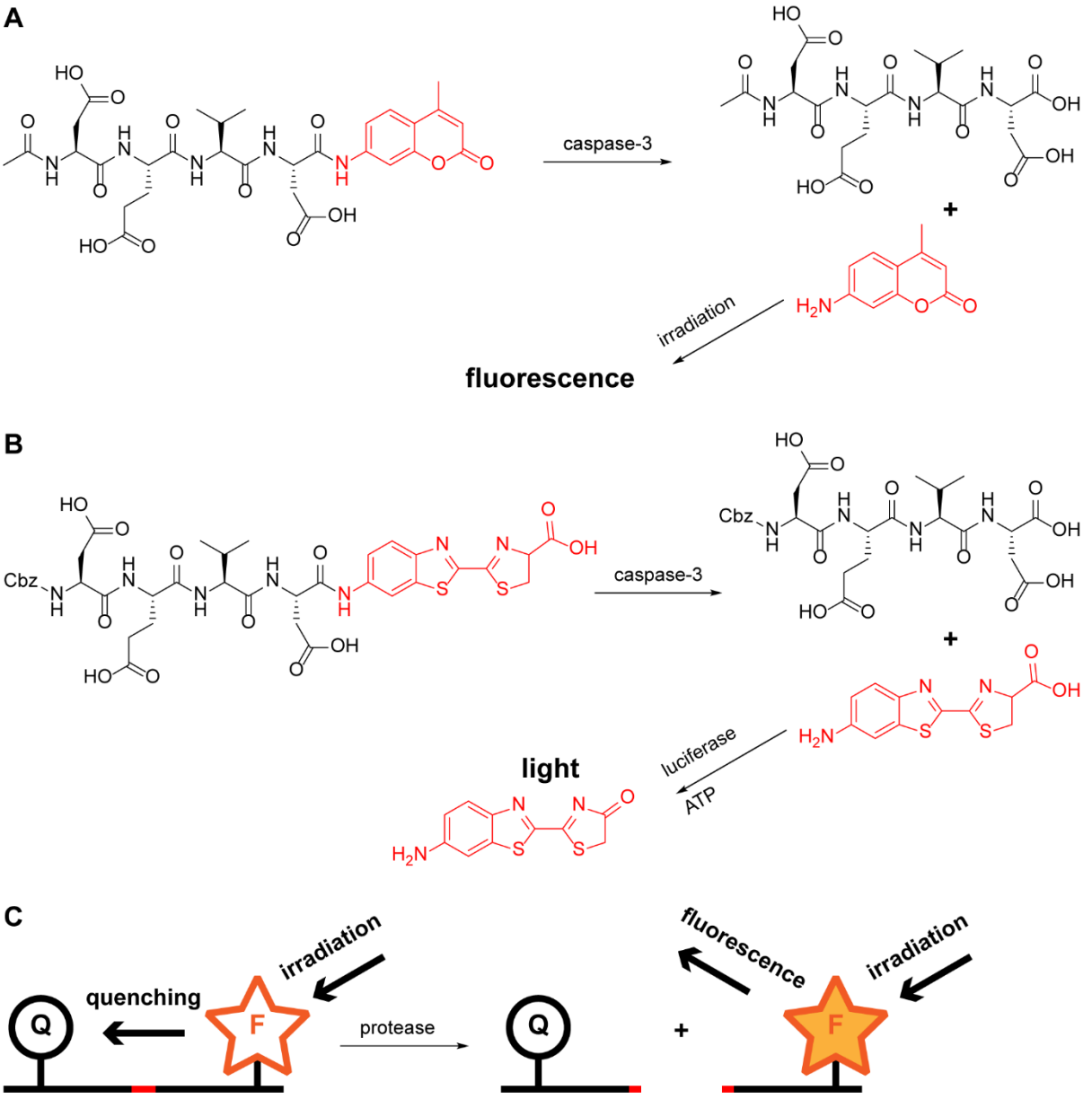

Figure 1.6 Different types of synthetic substrates

(A) the fluorogenic Ac-DEVD-AMC-substrate for caspase-3. (B) the bioluminescent Z-DEVD-luciferin derivative for caspase-3. (C) graphic representation of FRET substrates.

1.3.2 Activity-based probes (ABPs)

The primary use of ABPs is the labelling of active proteases [29, 30]. As the name suggests, they operate by directly targeting the active site residues of proteases. They usually consist of three parts (Figure 1.7): (1) the warhead is the central core of the ABP, the reactive entity that covalently binds to the active site residues, inhibiting the protease in the process. It is usually an electrophile derived from a known inhibitor against cysteine, serine or threonine proteases [31]. Different electrophiles can target

different protease classes. (2) A detection tag makes sure that the bound probe-protease complex can be detected, either directly by the incorporation of e.g. a fluorophore, or indirectly with an alkyne. This alkyne can be modified after the formation of the complex with a choice label by using click chemistry (copper(I)-catalyzed azide alkyne cycloaddition) [32, 33]. (3) The spacer separates the previous two parts, and is the origin of the selectivity of the probe. A normal alkyl chain of course doesn't introduce any selectivity, and will result in a general probe for a certain class of proteases, depending on the utilized warhead. On the other hand, a peptide chain corresponding to a certain substrate will generate a probe that is selective for a specific protease or protease family.

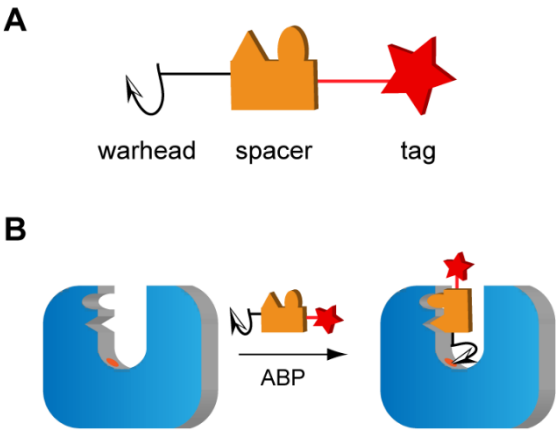

Figure 1.7 Graphic representation of activity-based probes

Adapted from [25]. (A) General design: A warhead for interaction with the active site residues, a spacer to introduce selectivity, and a tag for detection. (B) The ABP is recognized by the protease, after which the warhead can react with the active site residues, indicated with a red dot.

A drawback of most ABPs is that because of their design, they can only incorporate amino acids from one side of the scissile bond of substrates. Additionally, they cannot be used to target metallo- and aspartic proteases, as those rely on the activation of a water molecule for substrate processing and don't directly interact with their substrates. As a result, the use of an electrophile like for serine and cysteine proteases would only result in warhead hydrolysis. For this reason, AfBPs have been developed.

1.3.3 Affinity-based probes (AfBPs)

AfBPs can be used to overcome some of the drawbacks of ABPs and have some other uses as well. Just like ABPs, they contain a detection tag. As they don't depend on

protease activity, they are solely dependent on affinity between proteases and their substrates, and their use is not limited to those interactions. Therefore, AfBPs can be used to study metallo- and aspartic proteases, because they only need to be recognized in order to fulfill their role. The nature of this kind of probes suggests that they can only serve as probes when there is a strong interaction with the protease. Very selective probes can be produced when peptide chains are synthesized based on the substrate specificities of their target proteases.

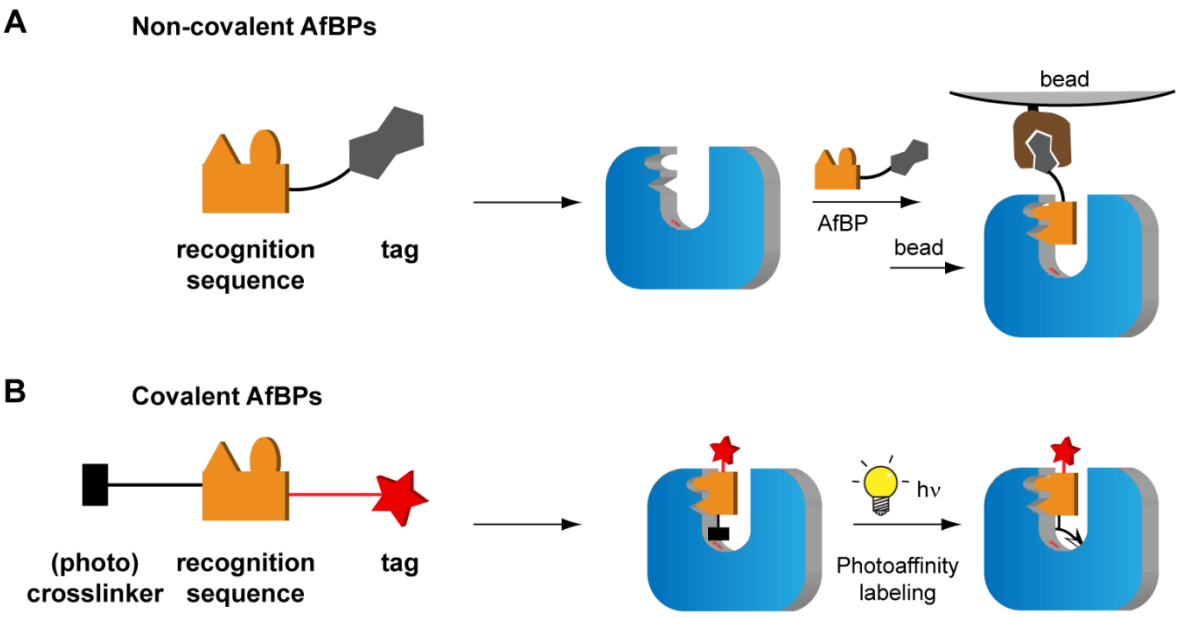

Figure 1.8 Graphic representation of affinity-based probes

(A) Non-covalent AfBPs with e.g. biotin as a tag can be a tool to purify proteases provided that the interaction between them is sufficiently strong. (B) Covalent AfBPs with e.g. a photocrosslinker can form irreversible bonds with proteases at locations other than the active site.

AfBPs come in two flavors (Figure 1.8). The non-covalent version is produced by combining the elements described until now, and can e.g. be used for isolation purposes. Covalent AfBPs additionally contain a warhead. However, they don't use an electrophile to target the catalytic residues in the active site. Instead, they employ a crosslinker, usually a photocrosslinker, for modification of the target protease upon irradiation, producing a labelled covalent complex [34]. This can be combined with other elements that increase binding, such as the non-covalent hydroxamate entity that coordinates to the metal ion in metalloproteases [35, 36]. As mentioned before, their use is not limited to activity-related interactions, and other interactions, like substrate binding sites or ligand interactions, can freely be investigated.

1.4 Activity-based protein profiling (ABPP)

The usefulness of ABPs and AfBPs becomes apparent when they are employed in ABPP [5, 37-39]. This technique has greatly advanced protease research. ABPP employs all kinds of chemical probes that can covalently label the protease active site and can be used to investigate the potency of novel potential inhibitors.

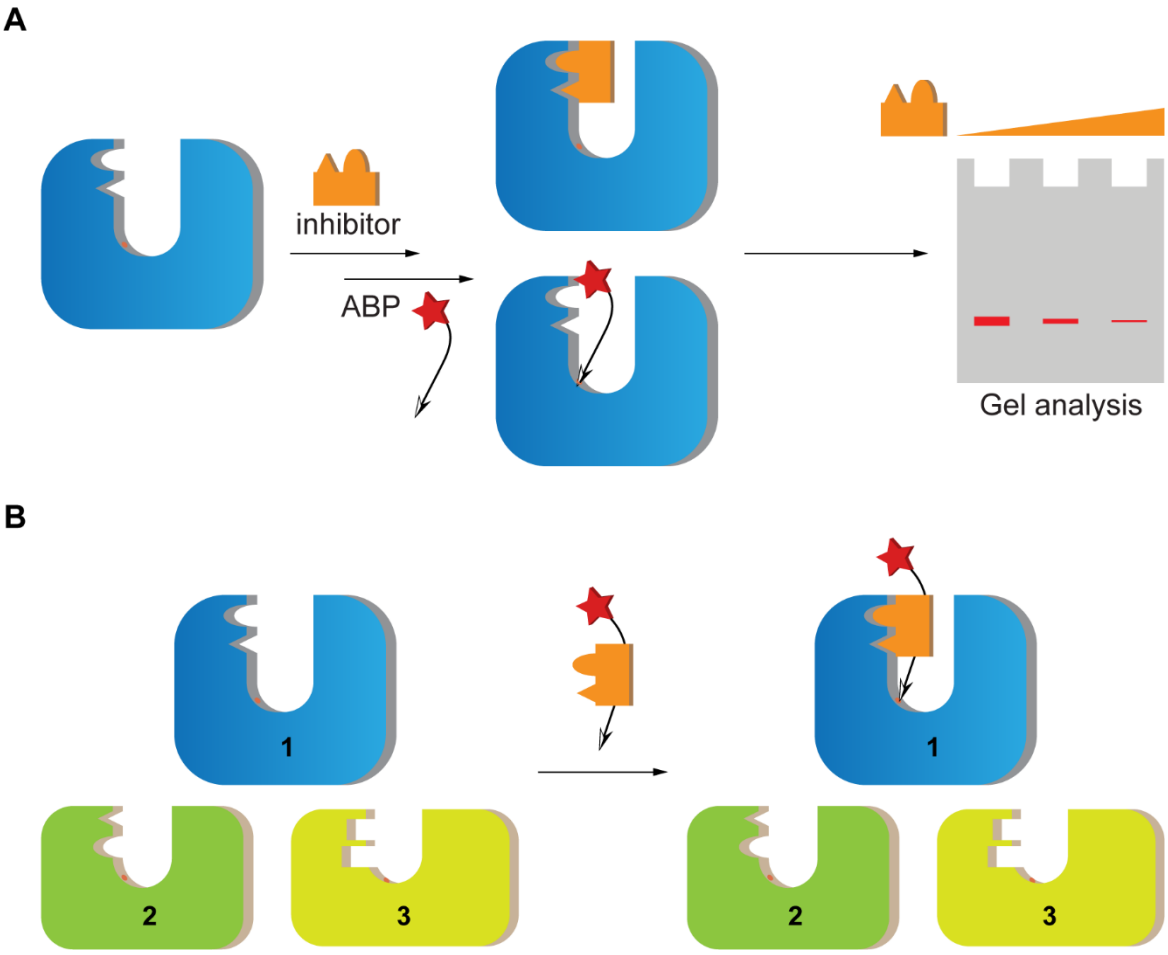

Figure 1.9 Examples of ABPP

(A) In competitive ABPP experiments, the potency of potential inhibitors can be evaluated by letting them compete with a fluorescent ABP. The fluorescence intensity of the protease band on a gel corresponds to the activity state of the protease. (B) In complex mixtures, the presence of specific proteases can be confirmed with the use of selective ABPs.

As opposed to other techniques, the read-out of these experiments conveniently directly corresponds to the protease activity and can be used to screen for selectivity or address target engagement in complex environments such as whole cell lysates, cell culture or even in vivo. In these screenings, the target protease is first incubated with the potential inhibitor. After a sufficient amount of time has passed for inhibition to occur, the sample is treated with control ABP. If fluorescence is the signal generated

by the ABP, the sample can be resolved with sodium dodecyl sulfate polyacrylamide gel electrophoresis (SDS-PAGE). When a decrease in the intensity of the protease signal appears, a loss of activity has occurred, and this can be correlated to the potency of the inhibitor (Figure 1.9A). Depending on the specificity of the ABP, multiple proteases could be investigated at the same time [40]. Alternatively, this method can be used to detect specific proteases in complex proteomes and even isolate them, or to confirm their activity state (Figure 1.9B).

All the different possible uses highlight the importance of chemical probes. However, the overview above also makes it clear that the structural nature of the probes is highly diverse. The different mechanistic protease classes require their own specific probes. This also led to the emergence of a multitude of synthetic strategies to obtain chemical probes. While AfBPs can usually be synthesized entirely on solid support, ABPs require the prior synthesis of their warheads. Some of these are easily obtainable from commercially available materials, but others can only be obtained after long and complicated syntheses. Examples of these are epoxysuccinates [41], acyloxymethyl ketones (AOMKs) [42], chloroacetamides [43], and fluorophosphonates (FPs) [44] (Figure 1.10).

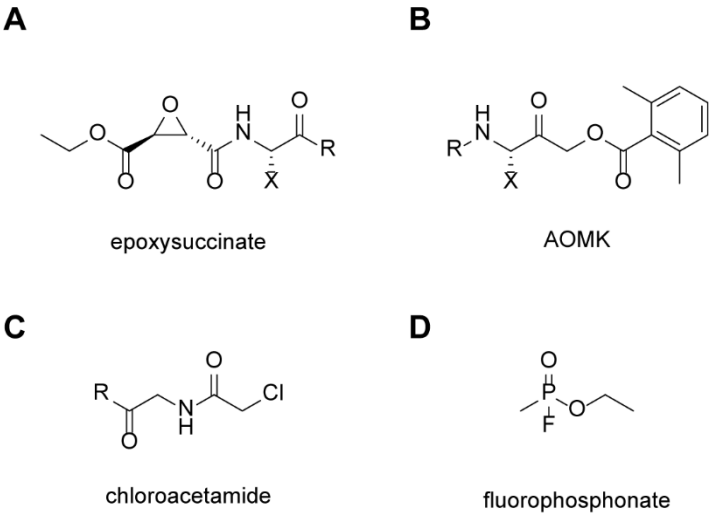

Figure 1.10 Structures of different ABP warheads

(A) epoxysuccinimates. (B) acyloxymethylketones. (C) chloroacetamide. (D) fluorophosphonates.

This raises the question of whether an alternative, more general method to obtain chemical probes, which exploits the protease substrate specificity more efficiently, would be feasible. Here, this possibility is explored with a focus on an example of a soluble protease, caspase-3, and an example of an intramembrane protease, GlpG.

2 Objectives

In this project, photoactivatable affinity-based inhibitors were synthesized for two different proteases: the main focus was on the soluble cysteine protease caspase-3, and by employing the same synthesis strategy, the first steps were also taken towards selective inhibitors for the intramembrane serine protease (rhomboid) GlpG. In order to accomplish this goal, the known substrate specificities of the target proteases were exploited. Peptides were designed based on the preferred amino acids around the scissile bond in substrates to deliver the optimal substrate sequence for the target protease. In the case of caspase-3, aspartic acid in the P1 position is by far the most crucial for recognition. Valine (P2), glutamic acid (P3), aspartic acid (P4) and alanine (P1') were added to increase the recognition efficiency and the selectivity over other proteases. This DEVDA sequence should thus only be recognized by caspase-3 and other proteases with a similar recognition motif (e.g. caspase-7), as shown in various studies [27, 45-47] (Figure 2.1).

A

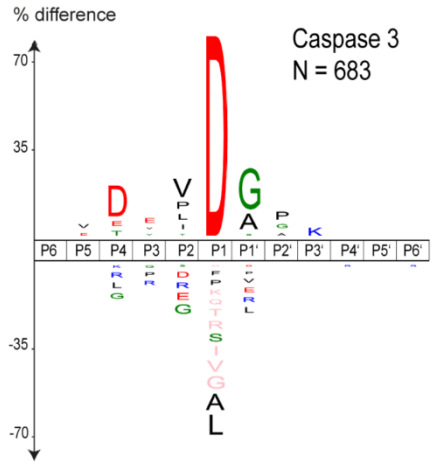

B

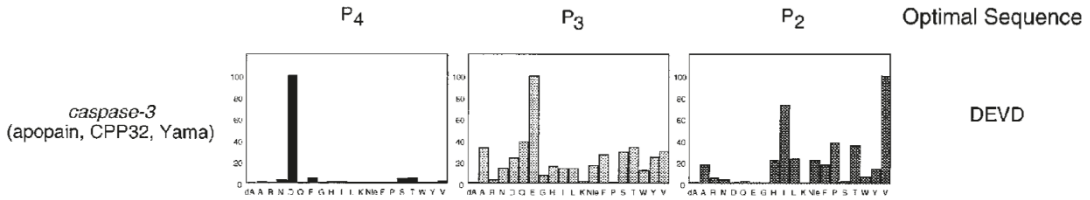

Figure 2.1 Reported substrate specificities of caspase-3

(A) adapted from [25]. (B) adapted from [45].

The proposed sequence will, by itself, not function as an inhibitor, as it would be processed by caspase-3 like any other substrate. Therefore, the strategy that is

pursued here eliminates the processing of this sequence by transforming the scissile peptide bond into an uncleavable mimic. This will allow the sequence to retain its recognition properties and reside within the protease active (Figure 2.2).

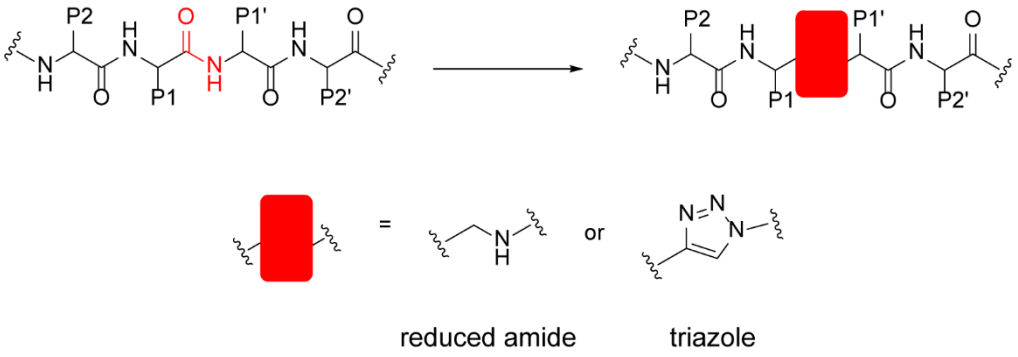

Figure 2.2 Proposed peptide bond mimics, a reduced amide and a triazole

Since there is no irreversible bond formation, this is a reversible inhibitor that can be outcompeted by any substrate recognized by caspase-3. This is avoided by introducing crosslinkers in the structure that can form a covalent bond between the inhibitor and protease to obtain an irreversible complex. These are activated through external stimuli, leading to inhibition that is possible at a specific time and place.

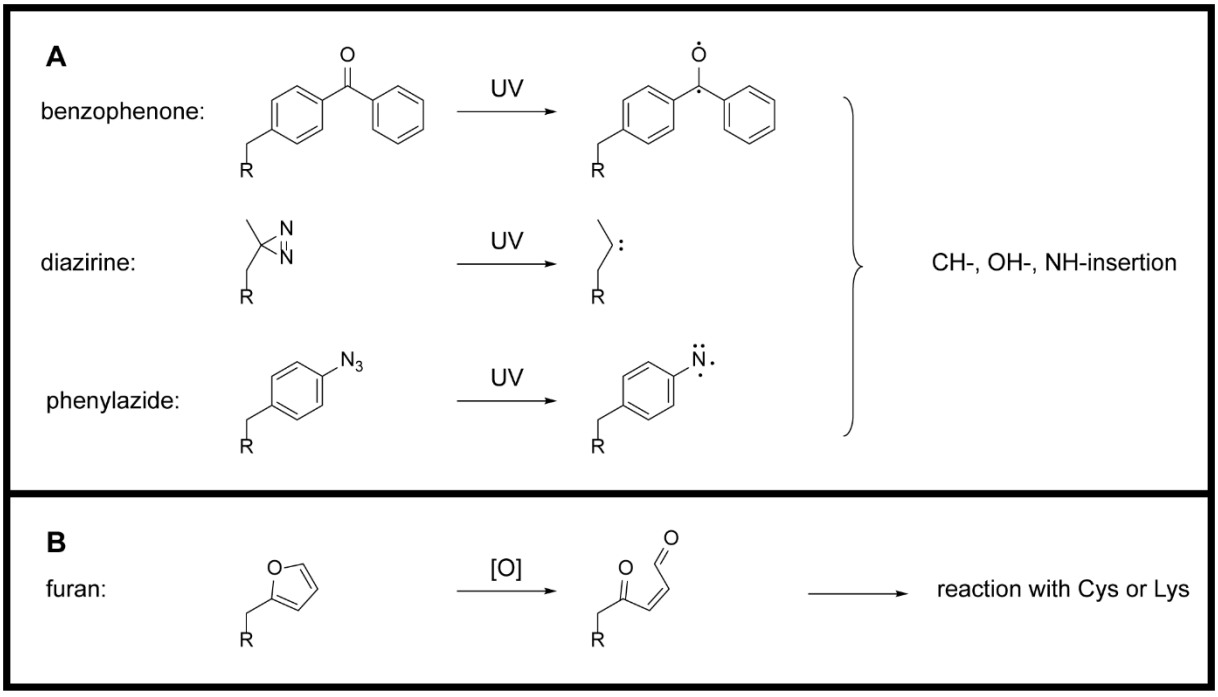

Figure 2.3 Overview of the crosslinkers

(A) The photocrosslinkers benzophenone, diazirine, and phenylazide are activated upon UV-irradiation and will insert into any nearby CH-, OH-, or NH-bond. (B) The furancrosslinker is activated by oxidation. It forms an aldehyde that can react with nearby cysteines or lysines.

The selected crosslinkers for the construction of the inhibitors are mostly photocrosslinkers that are commonly used as reagents for photoaffinity labelling: benzophenone, diazirine, and phenyl azide. Additionally, furan was used as a crosslinker that requires a different method of activation, oxidation [48] (Figure 2.3). They all have different sizes, reactivities, and result in different amounts of potential background labelling [34, 49]

Finally, the probes are also equipped with a masked detection tag, an alkyne. This can be modified post-crosslinking using click chemistry to attach any kind of tag without disrupting the probe-protease complex (Figure 2.4).

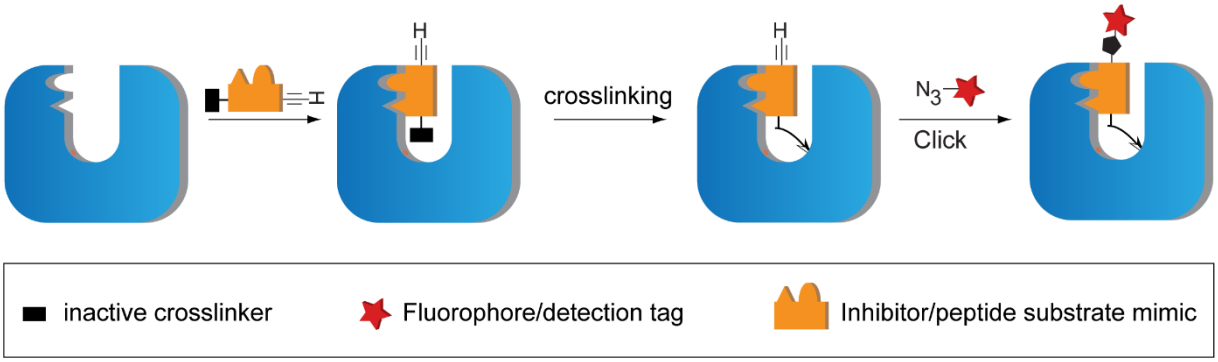

Figure 2.4 Graphic representation of a direct labelling experiment with an alkyne detection tag
After crosslinking, click chemistry is performed with a tag linked to an azide.

Two different peptide bond mimics were pursued, reduced amides and triazoles (Figure 2.2), for several reasons: (1) both were envisioned to be synthetically accessible by modified Fmoc-based solid phase peptide synthesis (SPPS). (2) The building blocks required for their synthesis can be readily obtained from commercially available amino acid analogs. (3) While reduced amides don't have the same rigidity as the normal peptide bond, they retain the conformational flexibility and the introduced modification is quite minimal, allowing the peptide to retain most of its other properties. On the other hand, triazoles are much more conformationally restricted, but their strong dipole moment make them a decent peptide bond mimic [50]. (4) The reduced amide mimic has been utilized before as protease inhibitor, e.g. for renin [51] and HIV protease [52]. All experiments concerning the triazole peptide bond mimic have been designed by Tim Van Kersavond and performed by Raphael Konopatzki under the supervision of Tim Van Kersavond.

3 Materials and methods

Parts of the Materials and method section have been adapted from [53].

3.1 Materials and equipment

All materials were purchased from Sigma Aldrich GmbH (GmbH, Darmstadt, Germany), Carl Roth GmbH + Co. KG (Karlsruhe, Germany), Thermo Fischer Scientific Inc. (Waltham, MA, USA), Rapp Polymere GmbH (Tübingen, Germany), Applichem GmbH (Darmstadt, Germany), VWR International GmbH (Darmstadt, Germany), Merck KGaA (Darmstadt, Germany), CreoSalus Inc. (Louisville, KY, USA), and Iris Biotech GmbH (Marktredwitz, Germany) and were used as received, unless otherwise noted.

TLC was performed on pre-coated ALUGRAM SIL G plates with detection by a handheld UV lamp (254 nm) and subsequent staining with potassium permanganate, p-anisaldehyde, ninhydrin or cerium ammonium molybdate.

LC-MS analysis was performed on a Thermo LCQ Fleet HPLC-MS/MS system using a gradient of 10% to 95% acetonitrile containing 0.1% formic acid.

NMR spectra were recorded on a Bruker Avance DRX 400 spectrometer with tetramethylsilane as internal standard.

High resolution ESI-FTMS was performed on a Thermo Scientific LTQ Orbitrap Velos Pro mass spectrometer.

3.2 Solution phase synthesis of building blocks

N-(9-fluorenylmethoxycarbonyl)-N'-methoxy-N'-methyl-L-isoasparagine t-butyl ester (**1**):

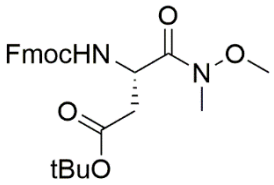

Fmoc-L-Asp(OtBu)-OH (3.0 mmol) and *N*-,*O*-dimethylhydroxylamine.HCl (4.5 mmol) were dissolved in dichloromethane (DCM, 15 mL) and cooled to 0 °C. *N*,*N*-diisopropylethylamine (DIEA) (12 mmol), HBTU (4.5 mmol) and HOBt (4.5 mmol) were added to the reaction mixture. The mixture was placed under Ar, allowed to warm up to RT and stirred overnight. The DCM was evaporated, and the residue was re-dissolved in 30 mL ethyl acetate (EtOAc) and 30 mL water. The organic phase was washed with 5% HCl (30 mL), 1 M $NaHCO_3$ (30 mL) and brine (30 mL). The organic layer was dried over $MgSO_4$ and concentrated. The crude material was purified by column chromatography (petroleum ether:EtOAc 3:1) to give **1** as a colorless oil (3.0 mmol, quantitative). ^{1}H-NMR (500 MHz, Chloroform-d) δ 7.76 (d, J = 7.5 Hz, 2H), 7.60 (t, J = 8.4 Hz, 2H), 7.40 (t, J = 7.5 Hz, 2H), 7.30 (m, 2H), 5.73 (d, J = 9.1 Hz, 1H), 5.04 (t, J = 7.0 Hz, 1H), 4.36 (d, J = 7.3 Hz, 2H), 4.23 (t, J = 7.3 Hz, 1H), 3.80 (m, 3H), 3.24 (s, 3H), 2.74 (dd, J = 15.1, 5.4 Hz, 1H), 2.58 (dd, J = 15.1, 7.0 Hz, 1H), 1.45 (s, 9H). ^{13}C-NMR (126 MHz, Chloroform-d) δ 170.9, 169.4, 155.6, 143.7, 141.2, 127.5, 126.9, 125.0, 119.8, 81.4, 67.0, 61.5, 48.3, 46.9, 38.1, 32.1, 27.8.

N-(9-fluorenylmethoxycarbonyl)-L-aspartic aldehyde t-butyl ester (**2**):

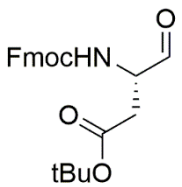

Compound **1** (3.0 mmol) was dissolved in dry THF (30 mL), placed under Ar and cooled to 0 °C. $LiAlH_4$ (3.3 mmol) was slowly added and the reaction mixture was stirred for 30 min at 0 °C. The reaction was quenched with saturated $KHSO_4$ (30 mL). The THF was evaporated and the aqueous solution was extracted with EtOAc (150 mL). The

organic phase was washed with brine (150 mL), dried over Na_2SO_4 and concentrated. The obtained crude **2** (2.30 mmol, 77%) was used without further purification. ^{1}H-NMR (500 MHz, Chloroform-d) δ 9.65 (s, 1H), 7.77 (d, J = 7.6 Hz, 2H), 7.60 (d, J = 7.6 Hz, 2H), 7.41 (t, J = 7.5 Hz, 2H), 7.32 (t, J = 7.5 Hz, 2H), 5.89 (d, J = 8.3 Hz, 1H), 4.45 (m, 3H), 4.24 (t, J = 7.0 Hz, 1H), 2.97 (dd, J = 17.3, 4.7 Hz, 1H), 2.78 (dd, J = 17.3, 4.9 Hz, 1H), 1.45 (s, 9H). ^{13}C-NMR (126 MHz, Chloroform-d) δ 198.9, 170.3, 156.1, 143.5, 141.4, 127.8, 127.1, 125.0, 120.1, 82.3, 67.3, 56.6, 47.1, 35.7, 28.0.

*N-(9-fluorenylmethoxycarbonyl)-N'-methoxy-N'-methyl-L-alaninamide (**3**):*

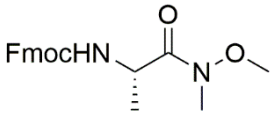

Fmoc-L-Ala-OH (15.0 mmol) and *N*-,*O*-dimethylhydroxylamine.HCl (22.5 mmol) were dissolved in DCM (90 mL) and cooled to 0 °C. DIEA (45 mmol), HBTU (22.5 mmol) and HOBt (22.5 mmol) were added to the reaction mixture. The mixture was placed under Ar, allowed to warm up to RT and stirred overnight. The DCM was evaporated, and the residue was re-dissolved in EtOAc. The organic phase was washed with water, 5 % HCl, 1 M NaHCO3, and brine. The organic layer was dried over $MgSO_4$ and concentrated. The crude material was purified by column chromatography (petroleum ether:EtOAc 3:1) to give **3** as a colorless oil (11 mmol, 73 %).

*(2S)-2-N-(9-fluorenylmethoxycarbonyl)aminopropanal (**4**):*

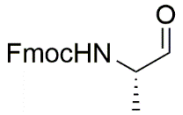

Compound **3** (5.65 mmol) was dissolved in dry THF (40 mL), placed under Ar and cooled to 0 °C. $LiAlH_4$ (6.2 mmol) was slowly added and the reaction mixture was stirred for 1 h at 0 °C. The reaction was quenched with 5 % HCl to pH 3. The THF was evaporated and the aqueous solution was extracted with EtOAc. The organic phase was washed with brine, dried over $MgSO_4$ and concentrated. The obtained crude **4** (5.2 mmol, 92 %) was used without further purification.

*L-alanine methyl ester (**5**):*

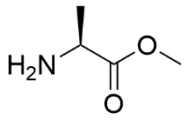

L-Alanine (11.2 mmol) was suspended in MeOH (16 mL). The suspension was cooled to 0 °C and thionyl chloride (24.6 mmol) was added. The mixture was heated to 40 °C and stirred for 3.5 h. After cooling to room temperature, the MeOH was evaporated to obtain **5**.HCl (11.2 mmol, quantitative). ^{1}H-NMR (500 MHz, Chloroform-d) δ 8.73 (s, 3H), 4.31 (s, 1H), 3.82 (s, 3H), 1.74 (s, 3H). ^{13}C-NMR (126 MHz, Chloroform-d) δ 170.6, 53.4, 49.4, 16.1.

*Fmoc-L-Asp(OtBu)-CH_2NH-L-Ala methyl ester (**6**):*

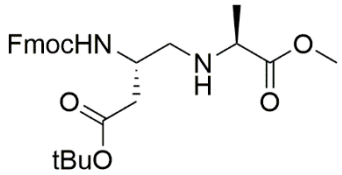

Compound **2** (6.32 mmol) was dissolved in MeOH (32 mL) and cooled to 0°C. Compound **5**.HCl (3.16 mmol), $NaBH_3CN$ (6.32 mmol), and AcOH (12.62 mmol) were added and the reaction mixture was stirred overnight. It was quenched with 1 M $NaHCO_3$ at 0 °C and extracted with EtOAc. The organic phase was washed with brine and concentrated. The obtained crude material was purified by column chromatography to give pure **6** (2.52 mmol, 80 %). ^{1}H-NMR (500 MHz, Chloroform-d) δ 7.76 (d, J = 7.5 Hz, 2H), 7.61 (d, J = 7.5 Hz, 2H), 7.40 (t, J = 7.5 Hz, 2H), 7.31 (t, J = 7.5 Hz, 2H), 5.55 (d, J = 7.6 Hz, 1H), 4.37 (d, J = 6.4 Hz, 2H), 4.23 (t, J = 6.9 Hz, 1H), 3.99 (q, J = 5.1 Hz, 1H), 3.71 (s, 3H), 3.38 (m, 1H), 2.75 (td, J = 12.2, 5.0 Hz, 1H), 2.69 (td, J = 11.5, 5.3 Hz, 1H), 2.57 (dd, J = 14.9, 4.6 Hz, 1H), 2.51 (dd, J = 14.9, 5.6 Hz, 1H), 1.45 (s, 9H), 1.29 (d, J = 6.9 Hz, 3H). ^{13}C-NMR (126 MHz, Chloroform-d) δ 175.9, 170.9, 156.0, 144.0, 141.3, 127.7, 127.1, 125.2, 120.0, 81.2, 66.7, 56.7, 51.9, 50.2, 48.5, 47.2, 38.1, 28.1, 19.0.

*Fmoc-L-Asp(OtBu)-CH_2N(Boc)-L-Ala methyl ester (**7**):*

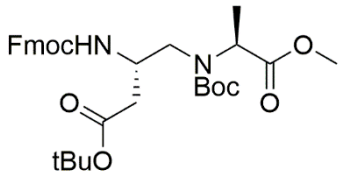

Compound **6** (2.5 mmol) was dissolved in DCM (50 mL). Di-tert-butyl dicarbonate (Boc_2O, 5 mmol) and DIEA (5 mmol) were added and the reaction mixture was stirred for 48 h. It was washed with 5 % HCl, 1 M $NaHCO_3$, and brine. The organic phase was dried over $MgSO_4$ and concentrated. The obtained crude material was purified by column chromatography to give pure **7** (2.16 mmol, 86 %). ^{1}H-NMR (500 MHz, Chloroform-d) δ 7.76 (d, J = 7.6 Hz, 2H), 7.59 (d, J = 7.4 Hz, 2H), 7.39 (t, J = 7.5 Hz, 2H), 7.30 (t, J = 7.3 Hz, 2H), 6.05 (d, J = 7.3 Hz, 1H), 4.34 (m, 2H), 4.20 (m, 1H), 4.11 (m, 1H), 4.04 (q, J = 7.1 Hz, 1H), 3.70 (dd, J = 20.6, 8.7 Hz, 1H), 3.68 (s, 3H), 3.27 (dd, J = 14.6, 4.5 Hz, 1H), 2.68 (dd, J = 16.5, 4.8 Hz, 1H), 2.42 (dd, J = 16.5, 7.6 Hz, 1H), 1.50 (d, J = 6.9 Hz, 3H), 1.45 (s, 9H), 1.42 (s, 9H). ^{13}C-NMR (126 MHz, Chloroform-d) δ 172.6, 170.6, 156.2, 143.9, 141.3, 127.7, 127.0, 125.2, 120.0, 81.2, 66.7, 56.7, 52.2, 49.4, 49.3, 47.3, 38.1, 28.2, 15.8.

*Fmoc-L-Asp(OtBu)-CH_2N(Boc)-L-Ala-OH (**8**):*

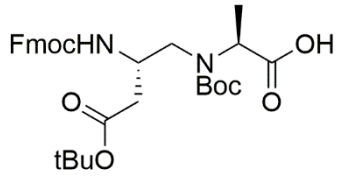

Compound **7** (1.56 mmol) and $CaCl_2$ (25 mmol) were dissolved in isopropanol (iPrOH, 21 mL). NaOH (3.12 mmol), dissolved in water (9 mL), was added dropwise and the reaction mixture was stirred for 3 h. It was quenched with saturated $KHSO_4$ to pH 3, filtered, and extracted with EtOAc. The organic phase was dried over $MgSO_4$ and concentrated. The obtained crude material was purified by column chromatography to give pure **8** (0.18 mmol, 11.5 %) and recover pure **7** (1.16 mmol, 74 %). ^{1}H-NMR (500 MHz, Chloroform-d) δ 7.75 (d, J = 7.6 Hz, 2H), 7.57 (d, J = 6.8 Hz, 2H), 7.39 (t, J = 7.3 Hz, 2H), 7.29 (t, J = 7.3 Hz, 2H), 5.98 (d, J = 7.5 Hz, 1H), 4.32 (m, 2H), 4.21 (m, 1H), 4.17 (m, 1H), 4.02 (m, 1H), 3.76 (m, 1H), 3.18 (m, 1H), 2.58 (dd, J = 16.4, 4.5 Hz, 1H), 2.45 (dd, J = 16.2, 6.9 Hz, 1H), 1.47 (d, J = 6.2 Hz, 3H), 1.44 (s, 9H), 1.40 (s, 9H). ^{13}C-

NMR (126 MHz, Chloroform-d) δ 175.2, 170.5, 157.1, 143.9, 141.3, 127.7, 127.1, 125.2, 120.0, 81.4, 68.2, 56.9, 50.0, 49.0, 47.2, 38.2, 28.1, 15.3.

Imidazole-1-sulfonyl-azide (**9**):

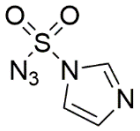

Sodium azide (9.6 mmol) was dissolved in MeCN (6.5 mL), placed under inert atmosphere (Ar), and cooled to 0 °C. Sulfuryl chloride (11.5 mmol) was added to this suspension and the mixture was allowed to warm to room temperature and stirred overnight. The reaction mixture was again cooled to 0 °C and imidazole (19.2 mmol) was added. After stirring for 4 h, it was quenched with 1 M $NaHCO_3$ to pH 9 and the aqueous solution was extracted with EtOAc. The obtained organic phase was washed with water, dried over $MgSO_4$, and filtered. A solution of HCl (14.4 mmol) in EtOH (3.5 mL), generated by the addition of AcCl to EtOH, was added dropwise to the organic phase to crystallize **9** as the HCl salt. The obtained suspension was filtered and the filter cake was washed with EtOAc to obtain **9**.HCl (2.9 mmol, 25 %).

Azido-L-alanine (**10**):

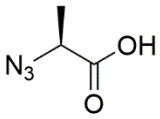

L-Ala-OH (0.8 mmol), $CuSO_4$ (0.008 mmol, cat.), and K_2CO_3 (2.2 mmol) were dissolved in methanol (40 mL) and placed under Ar. Compound **9** (1.0 mmol) was added and the mixture was stirred overnight. The mixture was concentrated, and the residue was re-dissolved in 5 % HCl (20 mL). The aqueous phase was extracted three times with EtOAc (20 mL). The organic phase was dried over $MgSO_4$ and concentrated. The crude material was purified by column chromatography (petroleum ether:EtOAc 10:1 + 1% AcOH) to give **10** (0.37 mmol, 47%) as a yellow oil. 1H-NMR (500 MHz, DMSO-d6) δ 9.78 (d, J = 7.3 Hz, 1H), 4.31 (q, J = 7.4 Hz, 1H), 1.36 (d, J = 7.4 Hz, 3H). 13C-NMR (126 MHz, DMSO-d6) δ 172.9, 48.6, 16.6.

N-(Allyloxycarbonyl)-L-aspartic acid β-t-butyl ester (**11**):

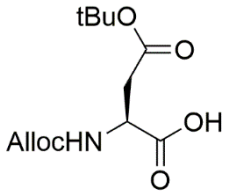

L-Asp(OtBu)-OH (5.3 mmol) and Alloc-OSu (7.9 mmol) were dissolved in THF (20 mL). K_2CO_3 (2.7 mmol, 10% in water) was added and the mixture was stirred overnight. After evaporation of THF, the mixture was diluted with 10% K_2CO_3 (10 mL) and washed four times with diethyl ether (Et_2O, 30 mL). The aqueous phase was acidified with 5% HCl to pH 3 and extracted four times with DCM (30 mL). The combined organic layers were dried over $MgSO_4$ and concentrated under reduced pressure. The obtained crude material was purified with column chromatography (DCM:MeOH 200:1) to give **11** (4.7 mmol, 89%). ^{1}H-NMR (500 MHz, Chloroform-d) δ 6.65 (s, 1H), 5.90 (m, 1H), 5.77 (d, J = 8.6 Hz, 1H), 5.23 (dq, J = 10.5, 1.3 Hz, 2H), 4.60 (m, 3H), 2.99 (dd, J = 17.2, 4.4 Hz, 1H), 2.77 (m, 1H), 1.44 (s, 9H). ^{13}C-NMR (126 MHz, Chloroform-d) δ 175.5, 170.3, 156.0, 132.4, 118.0, 82.4, 66.1, 53.5, 37.6, 28.0.

N-(Allyloxycarbonyl)-N'-methoxy-N'-methyl-L-isoasparagine t-butyl ester (**12**):

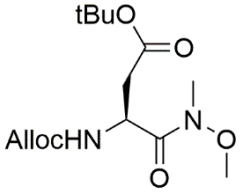

Compound **11** (4.7 mmol) and *N*-,*O*-dimethylhydroxylamine.HCl (7.1 mmol) were dissolved in DCM (20 mL) and cooled to 0 °C. DIEA (14.1 mmol), HBTU (7.1 mmol) and HOBt (7.1 mmol) were added to the reaction mixture. The mixture was placed under Ar, allowed to warm up to RT and stirred overnight. The DCM was evaporated, and the residue was re-dissolved in 30 mL EtOAc and 30 mL water. The organic phase was washed with 5% HCl (30 mL), 1 M $NaHCO_3$ (30 mL) and brine (30 mL). The organic layer was dried over $MgSO_4$ and concentrated. The crude material was purified by column chromatography (petroleum ether:EtOAc 3:2) to give compound **12** as a colorless oil (3.3 mmol, 70%).

N-(Allyloxycarbonyl)-L-aspartic aldehyde t-butyl ester (**13**):

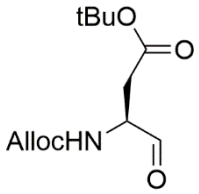

12 (1.7 mmol) was dissolved in dry THF (20 mL), placed under Ar and cooled to 0 °C. $LiAlH_4$ (2.0 mmol) was slowly added and the reaction mixture was stirred for 30 min at 0 °C. The reaction was quenched with saturated $KHSO_4$ (20 mL). The THF was evaporated and the aqueous solution was extracted with EtOAc (100 mL). The organic phase was washed with brine (100 mL), dried over Na_2SO_4 and concentrated. Crude **13** (0.9 mmol, 53%) was used without further purification.

(3S)-3-N-(Allyloxycarbonyl)amino-pent-4-ynoic acid t-butyl ester (**14**):

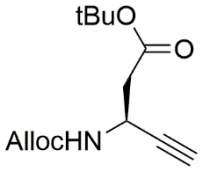

Dimethyl 2-oxopropylphosphonate (1.1 mmol) and K_2CO_3 (4.0 mmol) were dissolved in MeCN (9 mL). **9**.HCl (1.2 mmol) was added to the mixture, which was placed under Ar and stirred for 2 h. Compound **13** (0.9 mmol) was dissolved in methanol (9 mL) and added to the brown-yellow mixture, which was stirred overnight. The mixture was filtered, and the filter cake was washed three times with EtOAc. The clear filtrate was concentrated and resuspended in water (10 mL). The aqueous suspension was extracted three times with EtOAc (10 mL). The combined organic phases were washed with brine (20 mL), dried over $MgSO_4$ and concentrated under reduced pressure. The crude material was purified by column chromatography (petroleum ether:EtOAc 3:1) to give **14** (0.16 mmol, 18%). ^{1}H-NMR (500 MHz, Chloroform-d) δ 5.91 (ddq, J = 16.7, 11.4, 5.7 Hz, 1H), 5.65 (d, J = 9.5 Hz, 1H), 5.23 (ddq, J = 10.5, 2.9, 1.4 Hz, 2H), 4.82 (dd, J = 26.6, 7.3 Hz, 1H), 4.61–4.54 (m, 2H), 2.84–2.57 (m, 2H), 2.31 (dd, J = 7.1, 2.4 Hz, 1H), 1.50–1.36 (m, 9H). ^{13}C-NMR (126 MHz, Chloroform-d) δ 169.5, 155.2, 132.6, 118.0, 81.8, 81.7, 71.4, 65.9, 40.9, 39.8, 28.1.

3.3 General procedures for solid phase synthesis

3.3.1 Kaiser test

For the detection of residual primary amines on resin, a Kaiser test was performed after each peptide coupling step. Two drops of solution A, solution B and solution C were added to a glass tube. A small amount of resin was added, and the mixture was heated at 100 °C for 2 min. An almost colorless, clear solution indicated complete coupling. A dark blue solution indicated the presence of primary amines. For the detection of residual primary azides [54], an aliquot of resin was first treated with a 5% Ph_3P solution in THF (w/v) for 15 min, washed with DMF, MeOH and DCM, followed by a normal Kaiser test procedure.

Kaiser test solution A: 49 mL pyridine and 1 mL of a solution of 16.5 mg KCN in 25 mL H_2O

Kaiser test solution B: 5 g ninhydrin in 100 mL EtOH

Kaiser test solution C: phenol:EtOH 4:1

3.3.2 Chloranil test

For the detection of secondary amines on resin, a chloranil test was performed when appropriate. Two drops of solution A and solution B were added to a glass tube, to which a small amount of resin was added. After 5 min, a color change of the resin indicated the presence of primary (green) or secondary (blue) amines.

Chloranil test solution A: 2% acetaldehyde in DMF

Chloranil test solution B: 2% chloranil in DMF

3.3.3 General SPPS elongation procedure

Before loading of the first amino acid, polystyrene Rink amide resin was Fmoc-deprotected with 20% piperidine in DMF for 3 x 3 min. The resin was washed with DMF, MeOH and DCM.

The first amino acid was coupled by using 3 eq. of Fmoc-protected amino acid, 3 eq. of HBTU and 6 eq. of DIEA in DMF. The mixture was shaken for 1 h after which the mixture was flushed away and the resin was washed with DMF, MeOH and DCM. Completion of the reaction was confirmed with a Kaiser test. For elongation, the same procedure for Fmoc-deprotection and amino acid coupling were performed.

3.3.4 On resin reductive amination and Boc protection

The resin-bound amino acid was Fmoc-deprotected with 20% piperidine in DMF for 3 x 3 min. The resin was washed with DMF, MeOH and DCM.

Next, amino aldehyde **2** or **4** (15 eq.; 1 M in DMF) was added to the resin. After 10 min, $NaBH_3CN$ (15 eq.; 1 M in DCM:MeOH 3:1 + 1% AcOH) was added. The reactor was shaken for 1 h, after which the mixture was flushed away and the resin washed with DMF, MeOH and DCM. Completion of the reaction was confirmed with a Kaiser test (must be negative) and chloranil test (must be positive).

The obtained resin was treated with Boc_2O (3 eq.; 0.4 M in DMF) and DIEA (3 eq.; 0.4 M in DMF). The reactor was shaken overnight, after which the mixture was flushed away and the resin was washed with DMF, MeOH and DCM. Completion of the reaction was confirmed with a Kaiser and chloranil test, which both must be negative.

3.3.5 On resin click chemistry

The resin was treated with DIEA (90 eq.), 2,6-lutidine (90 eq.), sodium ascorbate (36 eq., 0.5 M in DMF), CuBr (13 eq., 0.6 M in MeCN), and amino alkyne **14** (3 eq.). The reactor was shaken overnight, after which the mixture was flushed away and the resin washed with water, methanol, DMF, and DCM. A modified Kaiser test (see Section 3.3.1) was performed to confirm completion of the reaction.

3.3.6 On resin Alloc deprotection

Phenylsilane (20 eq., 0.5 M) and tetrakis(triphenylphosphine)palladium(0) ($Pd(PPh_3)_4$, 8 mol %) were dissolved in DCM. This mixture was added to the resin and the reactor was placed under Ar and shielded from light. After shaking for one hour, the mixture was flushed away, and this procedure was repeated twice. The resin was washed with DMF, MeOH and DCM.

3.3.7 Resin cleavage and purification

The resin was treated 3 x 30 min with a cleavage cocktail of TFA:TIS:water 95:2.5:2.5, and subsequently washed with a small amount of cleavage cocktail. The combined fractions were added to ice cold Et_2O in order to precipitate the target compound. After centrifugation (5 min at 3000 g), most of the solvent was decanted. Any remaining volatiles were removed under a steady N_2-stream.

The crude product was purified with RP-HPLC using a linear gradient of MeCN in water with 0.1% TFA. The collected fractions containing product were combined and lyophilized.

3.4 Characterization of the synthesized inhibitors

Hexynoyl-Bpa-Asp-Glu-Val-Asp(CH_2NH)-Ala-NH_2 (**15**):

Inhibitor **15** was synthesized according to the general procedure and isolated after HPLC purification as a white solid (0.80 µmol, 4% overall yield). HRMS (ESI) calculated 878.3931 $[M + H]^+$, found 878.3918.

Hexynoyl-Ahx-Bpa-Asp-Glu-Val-Asp(CH_2NH)-Ala-NH_2 (**16**):

Inhibitor **16** was synthesized according to the general procedure and isolated after HPLC purification as a white solid (1.21 µmol, 7 % overall yield). ESI-MS calculated 991.4771 $[M + H]^+$, found 993.4.

Hexynoyl-Asp-Glu-Val-Asp(CH_2NH)-Ala-Bpa-NH_2 (**17**):

Inhibitor **17** was synthesized according to the general procedure and isolated after HPLC purification as a white solid (0.80 µmol, 7% overall yield). HRMS (ESI) calculated 878.3931 $[M + H]^+$, found 878.3916.

Hexynoyl-photoLeu-Asp-Glu-Val-Asp(CH_2NH)-Ala-NH_2 (**18**):

Inhibitor **18** was synthesized according to the general procedure and isolated after HPLC purification as a white solid (0.80 µmol, 7% overall yield). HRMS (ESI) calculated 752.3574 $[M + H]^+$, found 752.3572.

Hexynoyl-Asp-Glu-Val-Asp(CH_2NH)-Ala-photoLeu-NH_2 (**19**):

Inhibitor **19** was synthesized according to the general procedure and isolated after HPLC purification as a white solid (0.93 µmol, 8% overall yield). HRMS (ESI) calculated 752.3574 $[M + H]^+$, found 752.3560.

Hexynoyl-p-azidoPhe-Asp-Glu-Val-Asp(CH_2NH)-Ala-NH_2 (**20**):

Inhibitor **20** was synthesized according to the general procedure and isolated after HPLC purification as a white solid (0.12 µmol, 1% overall yield). HRMS (ESI) calculated 815.3683 $[M + H]^+$, found 815.3678.

Hexynoyl-Asp-Glu-Val-Asp(CH_2NH)-Ala-pazido-Phe-NH_2 (**21**):

Inhibitor **21** was synthesized according to the general procedure and isolated after HPLC purification as a white solid (1.23 µmol, 11% overall yield). HRMS (ESI) calculated 815.3683 $[M + H]^+$, found 815.3673.

Hexynoyl-2-furylalanine-Asp-Glu-Val-Asp(CH_2NH)-Ala-NH_2 (**22**):

Inhibitor **22** was synthesized according to the general procedure and isolated after HPLC purification as a white solid (1.57 µmol, 8 % overall yield). ESI-MS calculated 764.3461 $[M + H]^+$, found 765.7.

Hexynoyl-2-furylalanine-Gly-Asp-Glu-Val-Asp(CH_2NH)-Ala-NH_2 (**23**):

Inhibitor **23** was synthesized according to the general procedure and isolated after HPLC purification as a white solid (1.10 µmol, 6 % overall yield). ESI-MS calculated 821.3676 $[M + H]^+$, found 822.8.

Hexynoyl-2-furylalanine-Ahx-Asp-Glu-Val-Asp(CH_2NH)-Ala-NH_2 (**24**):

Inhibitor **24** was synthesized according to the general procedure and isolated after HPLC purification as a white solid (0.68 µmol, 4 % overall yield). ESI-MS calculated 877.4302 $[M + H]^+$, found 879.0.

Hexynoyl-2-furylalanine-O2Oc-Asp-Glu-Val-Asp(CH_2NH)-Ala-NH_2 (**25**):

Inhibitor **25** was synthesized according to the general procedure and isolated after HPLC purification as a white solid (1.32 µmol, 7 % overall yield). ESI-MS calculated 909.4200 $[M + H]^+$, found 911.1.

Ac-Asp-Glu-Val-Asp(CH_2NH)-Ala-NH_2 (**26**):

Inhibitor **26** was synthesized according to the general procedure and isolated after HPLC purification as a white solid (4.97 µmol, 27% overall yield). HRMS (ESI) calculated 575.2672 $[M + H]^+$, found 575.2664.

Hexynoyl-Asp-Glu-Val-Asp(CH_2NH)-Ala-NH_2 (**27**):

Inhibitor **27** was synthesized according to the general procedure and isolated after HPLC purification as a white solid (4.06 µmol, 22% overall yield). HRMS (ESI) calculated 627.2985 $[M + H]^+$, found 627.2975.

Hexynoyl-Bpa-Asp-Glu-Val-Asp(triazolo)-Ala-NH_2 (**28**):

Inhibitor **28** was synthesized according to the general procedure and isolated after HPLC purification as a white solid (0.33 µmol, 2% overall yield). HRMS (ESI) calculated 916.3836 $[M + H]^+$, found 916.3830.

Hexynoyl-Asp-Glu-Val-Asp(triazolo)-Ala-Bpa-Gly-NH_2 (**29**):

Inhibitor **29** was synthesized according to the general procedure and isolated after HPLC purification as a white solid (2.57 µmol, 13% overall yield). HRMS (ESI) calculated 973.4050 $[M + H]^+$, found 973.4046.

Hexynoyl-Bpa-Thr-Ile-Ala-Thr-Ala(CH_2NH)-Ala-Phe-Gly-Ser-Pro-Trp-Gln-NH_2 (**30**):

Inhibitor **30** was synthesized according to the general procedure and isolated after HPLC purification as a white solid (0.13 µmol, 0.4 % overall yield). ESI-MS calculated 790.40 $[M / 2 + H]^+$, found 803.67.

Hexynoyl-Thr-Ile-Ala-Thr-Ala(CH_2NH)-Ala-Bpa-Gly-Ser-Pro-Trp-Gln-NH_2 (**31**):

Inhibitor **31** was synthesized according to the general procedure and isolated after HPLC purification as a white solid (0.13 µmol, 0.4 % overall yield). ESI-MS calculated 717.37 $[M / 2 + H]^+$, found 729.95.

Hexynoyl-Thr-Ile-Ala-Thr-Ala(CH_2NH)-Ala-Phe-Gly-Ser-Pro-Bpa-Gln-NH_2 (**32**):

Inhibitor **32** was synthesized according to the general procedure and isolated after HPLC purification as a white solid (0.14 µmol, 0.4 % overall yield). ESI-MS calculated 697.86 $[M / 2 + H]^+$, found 710.44.

3.5 Biochemistry

3.5.1 Gel-based competitive ABPP

Caspase-3, produced in *E. coli* and purified as described before [55], was reacted in PBS with 1 mM DTT. Samples were combined with the indicated inhibitor and activated by irradiation with a handheld UV lamp at 365 nm for the indicated time at room temperature or by NBS treatment for 60 min at room temperature. For competition experiments with 'pre-activation,' the indicated inhibitors were activated prior to addition to caspase-3, and incubated for an additional 30 min. Next, ABP **SV149** was added (final concentration 1 µM) to label residual caspase-3 activity. The samples were incubated for 30 min at room temperature, after which 1/3rd volume of 4× Laemmli buffer was added. Samples were heated for 2 min at 95 °C and resolved by 15% SDS-PAGE. Gels were scanned using a Typhoon Trio+ fluorescent scanner with excitation at 532 nm and an emission filter of 580 nm. Gel images were processed with ImageJ (background subtraction with rolling ball radius of 50 pixels and automated contrast adjustment).

3.5.2 Protease kinetics experiments

Purified caspase-3 (2 nM) was pre-activated by incubation in caspase assay buffer (20 mM HEPES pH 7.4, 100 mM NaCl, 1 mM EDTA, 10% sucrose (w/v), 0.1% CHAPS (w/v), 10 mM DTT) for 15 min at 37 °C. Inhibitors **15**, **17**, and DMSO (control) were incubated with caspase-3 at 10 µM final concentration. One set was irradiated with a handheld UV lamp at 365 nm for 30 min at room temperature whereas the control set was not irradiated. After 30 min, 99 µL of the sample was added to 1 µL of Ac-DEVD-AMC fluorogenic substrate (5 mM in DMSO; 50 µM final concentration) in a black 96 well plate. The fluorescence intensity was read using an iD3 SpectraMax platereader (Molecular Devices; excitation wavelength: 340 nm; emission wavelength: 475 nm). The experiment was performed in duplicate. Activity was determined as the slope from the linear part of the progress curve by using GraphPad Prism.

3.5.3 Fluorescent labeling experiments

Inhibitors were clicked onto 5-TAMRA-azide (Carl Roth, Germany) by using the following conditions: to PBS, the inhibitor (at twice the indicated concentration) was added, together with 5-TAMRA-azide (25 µM), $CuSO_4$ (1 mM), sodium ascorbate (1 mM), and tris(3-hydroxypropyltriazolylmethyl)amine (THPTA, 50 µM),. After 60 min incubation at room temperature, the sample was added to an equal volume of purified caspase-3 in PBS with 2 mM DTT, and irradiated with a handheld UV lamp at 365 nm for 30 min at room temperature for the photocrosslinking inhibitors. For the inhibitors with a furan crosslinker, the sample was treated with NBS for 60 min at room temperature prior to the addition of caspase-3, after which it was incubated for 30 min. 1/3rd volume of 4× Laemmli buffer was added, and the samples were processed for gel analysis as described in section 3.5.1.

3.5.4 ESI-MS on caspase-3

Intact proteins were analyzed on an orbitrap Fusion Lumos mass spectrometer equipped with a nanoelectrospray ion source (Thermo Fischer, Dreieich, Germany). Sample desalting was performed using Amicon Ultra-0.5 3K NMWL centrifugal filters (Merck Millipore, Darmstadt, Germany) according to the manufacturer's protocol and samples were brought to a final concentration of approx. 1 pmol/µL (in 25% MeOH and 0.5% formic acid). Analysis was performed by directly infusing the samples using a 25 µL syringe (Hamilton, Reno, NV, USA) operated by a syringe drive maintaining a flow rate of 300 nL/min. The mass spectrometer was operated in intact protein mode with the nitrogen pressure set to 3 mtorr in the ion-routing multipole. S-Lens RF-level was set to 80% and in source fragmentation was kept at 0 V. Spectra were acquired in the orbitrap with 10 microscans at a resolving power of 240,000 (at 200 m/z) with the automatic gain control target set to 1×10^6. Spectra were deconvoluted using the Xtract algorithm of the Xcalibur suite (Thermo Scientific). Resolving power was set to 180,000 (at 400 m/z), minimum signal to noise threshold was 4 and the maximum allowed charge state 20.

3.5.5 MALDI-MS on caspase-3

A total of 10 mM DTT was added to a stock solution of caspase-3 (200 ng/µL; 100 mM TRIS, pH 8.0, 100 mM NaCl), and this was treated with 10 vol % of the indicated inhibitor (1 mM) and irradiated with a handheld UV lamp at 365 nm for 30 min. Afterwards, the samples were diluted in 0.1% TFA in water (20 ng/µL final concentration of caspase-3). Then, 1 µL of sinapic acid solution A (saturated sinapic acid in ethanol) was spotted on a BRUKER MTP 385 ground steel TF target plate, followed by 1 µL of a mixture of equal volumes of the caspase-3 sample and sinapic acid solution B (saturated sinapic acid in 3:7 acetonitrile:0.1% TFA in water). Spectra were recorded on a BRUKER ultrafleXtreme MALDI-TOF/TOF system.

3.5.6 Competitive ABPP with bisulfite aldehyde quenching

The indicated inhibitors were incubated in PBS with or without 10 mM $NaHSO_3$, with or without irradiation at 365 nm for 30 min time at room temperature before addition to caspase-3. After 30 min, ABP **SV149** was added (final concentration 1 µM) to label residual caspase-3 activity. The samples were incubated for 30 min at room temperature, after which 1/3rd volume of 4× Laemmli buffer was added. The samples were processed for gel analysis as described in section 3.4.1.

3.5.7 ESI-MS-MS on inhibitors

The data was obtained on a QTRAP 6500 (Applied Biosystems, Darmstadt, Germany) equipped with an electrospray ion source (Turbo V Ion Source). The following ESI source settings were used for positive mode: curtain gas, 20 arbitrary units; ion source gas I, 9 arbitrary units; ion source gas II, 0 arbitrary units; collision gas, medium; temperature, 0; ion spray voltage, 5500 V; declustering potential, 100V; entrance potential, 10 V; and exit potential 10 V. Fragmentation of the selected masses was performed with a collision energy of 45 V. The input was a direct infusion with a syringe (100µL) with a flow rate 10 µL/min. The scan mode was Enhanced Product Ion and the data was obtained with the software Analyst 1.6.2.

3.5.8 Docking of inhibitor **26** in the caspase-3 active site

The reduced amide inhibitor **26** was drawn as mol file and energy minimized in the program Avogadro with the MMFF94 molecular mechanics force field using the steepest descent algorithm. The resulting molecule was exported as pdb file and used as input for docking. Caspase-3 coordinates were taken from PDB file 3PD0 and used as receptor molecule. Both receptor and ligand input files were prepared using AutodockTools 1.5.6. Water molecules were removed, polar hydrogen atoms and Gasteiger charges were added to the receptor. The reduced amide ligand, with polar hydrogens and Gasteiger charges added, included 22 rotatable bonds and was docked in a box of 22x24x28 Angstrom (x, y, z) centered around the active site of the receptor using Autodock Vina. The coordinates of the pose with the lowest energy were visualized in the caspase-3 crystal structure using PyMol.

4 Results

4.1 Synthesis of the affinity-based inhibitors

4.1.1 Synthesis of reduced amide inhibitors for caspase-3

In order to access peptides with a reduced amide as the peptide bond mimic, a protocol compatible with Fmoc-based SPPS was pursued. The construction of reduced amides was possible by on-resin reductive amination, but this first required the synthesis of an aldehyde analog of the P1 amino acid. To show the feasibility of the on resin synthesis, there was a focus on caspase-3 reduced amide inhibitors, and the synthesis of inhibitor **15** is described here. Starting from the commercially available Fmoc-L-Asp(OtBu)-OH, the aldehyde was synthesized in solution in two steps via a Weinreb amide intermediate. This prevents the overreduction of the carboxylic acid to the alcohol that would otherwise occur (Figure 4.1).

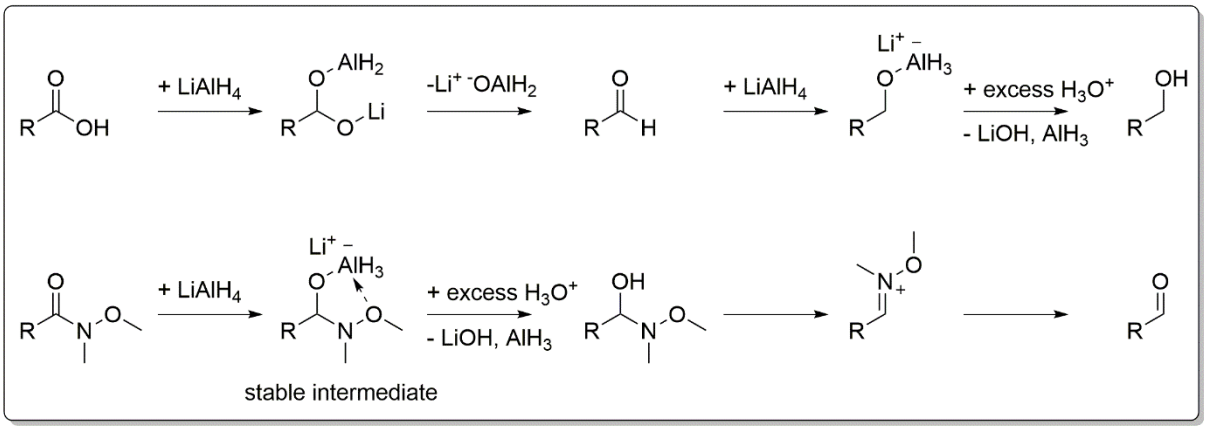

Figure 4.1 Comparison of a LiAlH4 reduction of a carboxylic acid and a Weinreb amide

Note that a stable intermediate is formed after the hydride attack only for the Weinreb amide. The cause for this is a combination of the coordination of the oxygen of the methoxylamide to the aluminum atom and the electron withdrawing effect of that same oxygen on the neighbouring nitrogen.

The Weinreb amide **1** was obtained by coupling *N*,*O*-dimethylhydroxylamine to aspartic acid using HBTU with DIEA as a base. Compound **1** was then further reduced to aldehyde **2** with lithiumaluminum hydride and subsequent acidic work-up (Figure 4.2). Initially, the acidic work-up was always performed with a 5 % HCl solution to reduce the pH to 3. However, after repeating this reaction multiple times for aspartic acid and other amino acids, inconsistent yields were obtained. The HCl (pKa -8) turned out to (partially) deprotect the side chains due to the sudden shift in pH that the strong

acid induced. To circumvent this, a saturated solution of the milder $KHSO_4$ (pKa 2) was used instead, resulting in a much more reliable synthesis (Table 4.1).

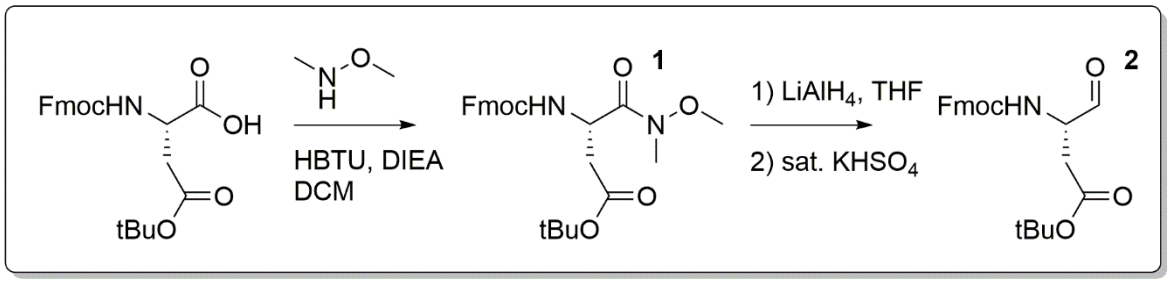

Figure 4.2 Solution phase synthesis of the Fmoc- and tBu-protected aspartic aldehyde **2**
Starting from the commercial Fmoc-L-Asp(OtBu)-OH, aldehyde **2** is synthesized in two steps.

Table 4.1 Comparison of the yields obtained after using HCl or KHSO4 as quenchers during the reduction of the Weinreb amides of the respective amino acids
Alanine had no acid sensitive protecting group and quenching with HCl resulted in high and consistent yields. The yield for arginine say a huge increase when using $KHSO_4$. The yields for aspartic acid were very inconsistent with HCl, but this was solved with $KHSO_4$.

	HCl yield (%)	*$KHSO_4$ yield (%)*
Fmoc-L-Ala-OH	98, 92	/
Fmoc-L-Arg(NPbf)-OH	39, 0	90
Fmoc-L-Asp(OtBu)-OH	72, 0, 87, 76, 0, 95, 60	76, 79, 75

With aldehyde building block **2** in hand, the probe could be entirely synthesized on solid support (Figure 4.3). The Rink amide resin was chosen as a convenient and reliable acid labile resin. It allows for an easy and straightforward coupling of the amino acids and eventually yields a C-terminal amide after cleavage of peptides from the resin. This prevents the presence of an unwanted C-terminal charge that would also be absent at that position in actual substrates. First, the coupling of the primed site alanine to the resin was performed with HBTU as coupling reagent and DIEA as a base. A negative Kaiser test after the coupling confirmed the completion of the reaction. Next, a reductive amination was performed with the previously synthesized aldehyde building block **2**. Under the influence of sodium cyanoborohydride and in the presence of acetic acid, the aldehyde was coupled to the free amine of the growing peptide chain, resulting in a secondary amine. Here, the combination of a negative Kaiser test and a positive chloranil test confirmed the complete formation of the

secondary amine. This reaction proceeds through the formation of an imine and its subsequent reduction.

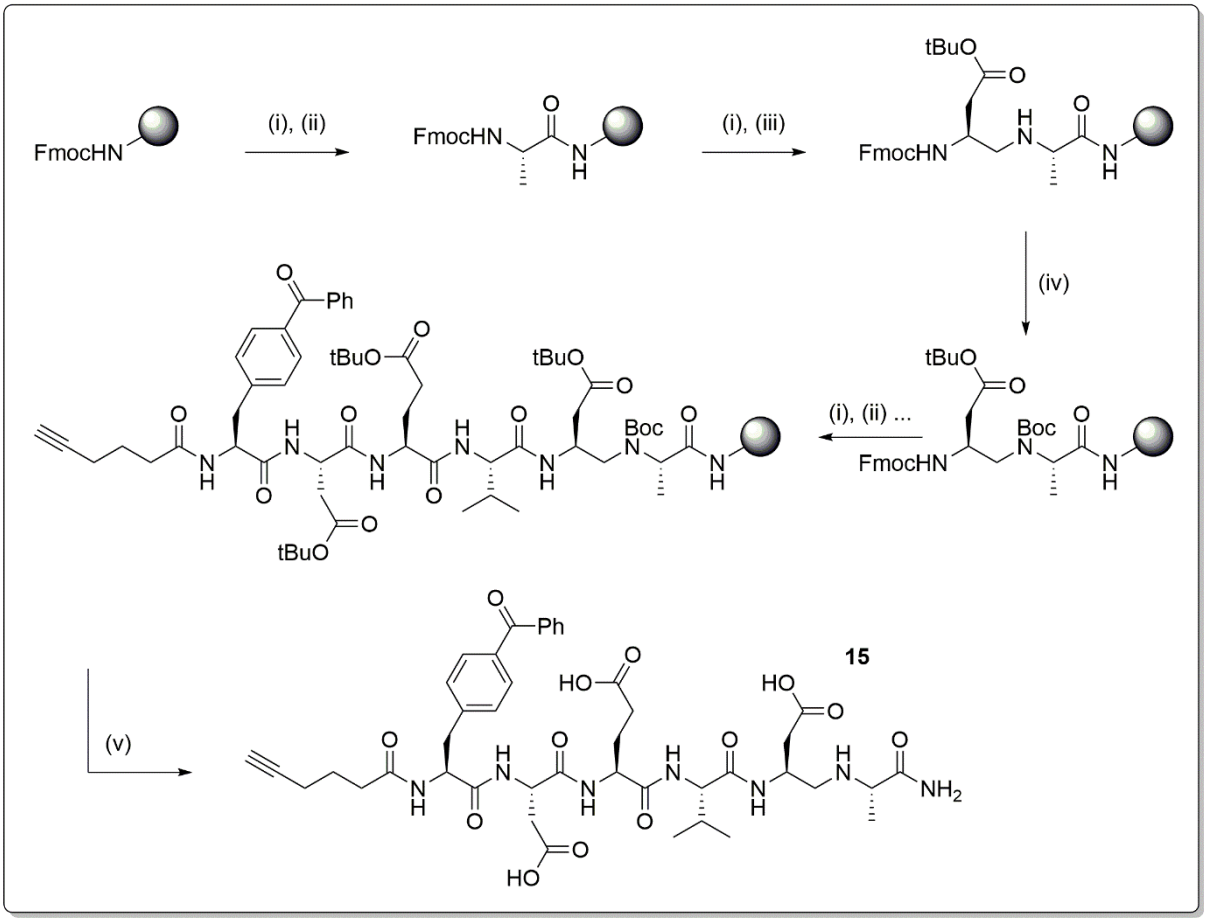

Figure 4.3 Solid phase synthesis of inhibitor **15**

(i) 20 % piperidine in DMF; (ii) Fmoc-amino acid, HBTU, DIEA, DMF; (iii) compound **2**, $NaBH_3CN$, AcOH, DMF, MeOH, DCM; (iv) Boc_2O, DIEA, DMF; (v) TFA, TIS, H_2O.

After the reductive amination, the secondary amine was protected with a Boc-group to avoid further elongation of the peptide chain at that position. The last synthesis steps were the standard amino acid couplings of valine, glutamic acid, aspartic acid, 4-benzoyl-L-phenylalanine, and the alkyne tag as described before, and the complete inhibitor **15** was obtained as a fully protected peptide mimetic on solid support. It was simultaneously deprotected and cleaved from the resin with a 95 % TFA cocktail to yield the desired crude inhibitor **15**. 2.5 % triisopropyl silane was present to scavenge any cations generated this way, e.g. the *tert*-butyl cation after aspartic and glutamic acid deprotection. Reversed phase HPLC with an optimized gradient for the inhibitor was used for its purification.

4.1.2 Synthesis of reduced amide inhibitors for GlpG

The reduced amide inhibitors for GlpG were synthesized using the same procedures described in the previous section. In this case, the amino aldehyde **4** used in the reductive amination was obtained from the Weinreb amide **3** of alanine, as opposed to aspartic acid for caspase-3.

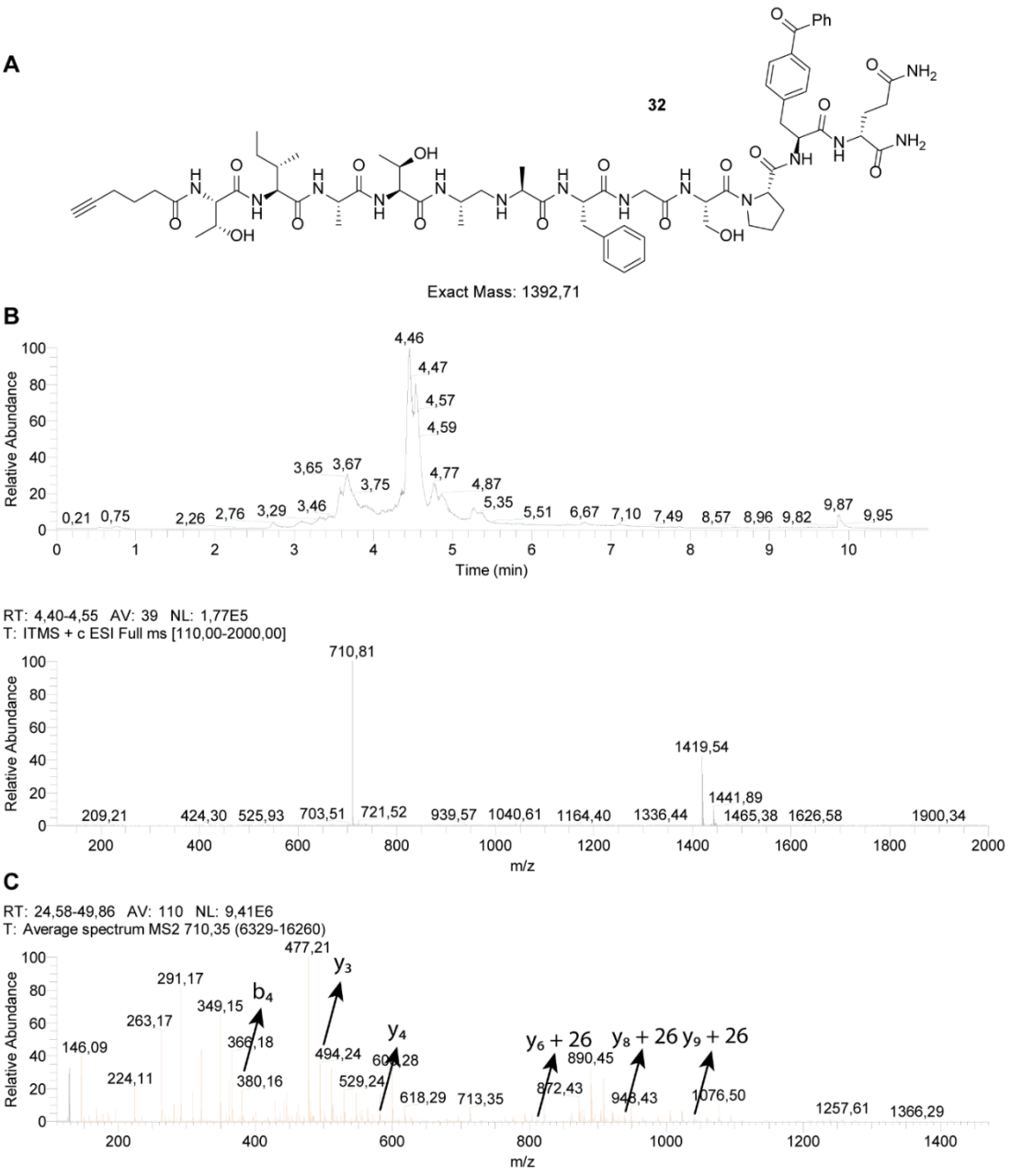

Figure 4.4 Analysis of GlpG inhibitor **32**

(A) Structure of inhibitor **32** and its exact mass. (B) LC-MS data reveals an unexpected major product (M+26+H). (C) MS-MS data reveals that the y_6-ion (consisting of the 6 most C-terminal amino acids) still has the additional mass, but the y_4-ion doesn't. Hence the unknown modification is present on either the Phe or the Gly.

Unfortunately, detailed analysis of the LC-MS data of the crude probes revealed the unexpected appearance of a major product with an extra atomic mass of 26. This did not correspond to any of the reagents that were used during the synthesis and the nature of this modification could not be elucidated. However, after inspection of MS-MS data, the point of origin could be narrowed down. It appeared that this mass always appeared on an amino acid residue C-terminal to the peptide bond mimic, meaning that it was introduced during the reductive amination (Figure 4.4).

To make the synthesis strategy generally applicable to all possible sequences, a new synthesis approach was pursued where the peptide bond mimic was completely synthesized in solution. This eliminated the possibility of the modification being introduced during the SPPS.

4.1.3 Alternative synthesis of reduced amide inhibitors for caspase-3

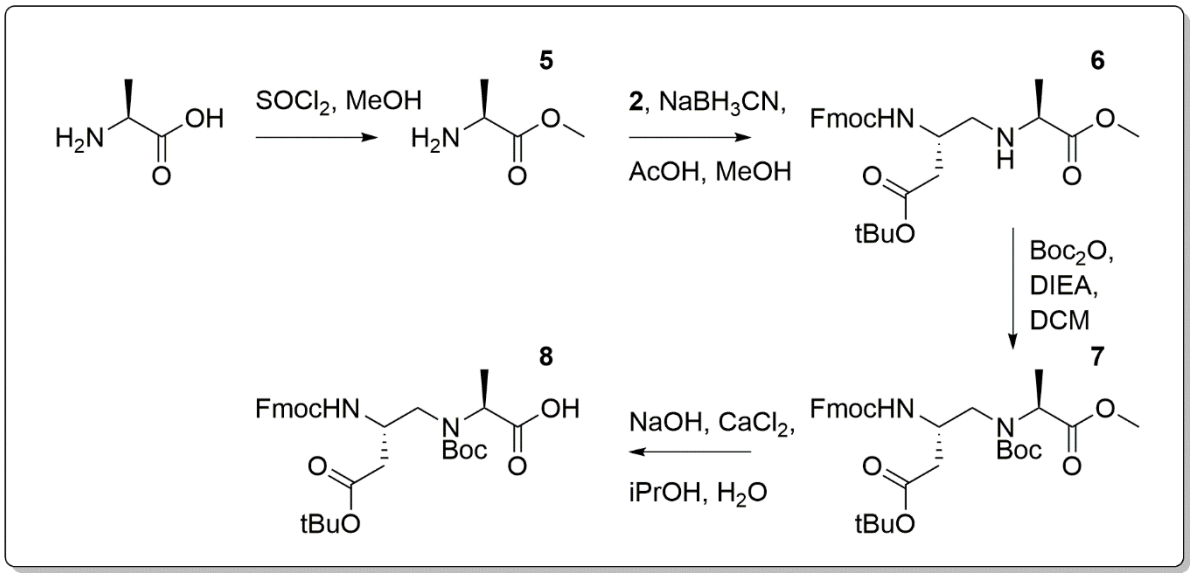

Figure 4.5 Solution phase synthesis of the reduced amide building block **8**

For the reductive amination in solution (Figure 4.5), the same aldehyde **2** as described before was required. Additionally, the other reaction partner, the amine, was introduced as the methyl ester **5** of the desired amino acid, alanine. This was obtained as the HCl salt by reacting alanine with thionylchloride in methanol. This reaction turned out to be highly dependent on the concentration and temperature, with an increase in both (0.01 to 0.7 M and 25 to 40 °C) providing a much higher yield and conversion rate. The reductive amination itself proved to be a lot more challenging. Initially, the plan was a

two-step reaction with first the synthesis of the imine and secondly its reduction with sodium borohydride to the amine **6**. This proved to be impossible, as the imine was either not formed or fell apart during work-up. Modified reaction conditions, addition of a triethylamine base or $CuSO_4$ to remove the generated water, did not improve the reaction at all. A better approach was a one-pot process with the mild sodium cyanoborohydride as reducing agent, similar to the reductive amination on solid support described previously. After optimization of the reaction conditions, yields were observed of up to 80 % with a very straightforward protocol. Next, the synthesized secondary amine **6** was again protected with a Boc group using di-tert-butyl dicarbonate and DIEA.

The final step, the hydrolysis of the methyl ester **7**, proved to be troublesome. The saponification had to be carried out in such a way that all other protecting groups remained intact. No issues were expected for the acid labile groups, but the N-terminal Fmoc-group is base labile and can be deprotected with high enough pH values. The reaction proceeded best with NaOH, addition of $CaCl_2$ and an isopropanol/water solvent system to minimize Fmoc-deprotection [56]. With these conditions, only partial conversion to the carboxylic acid **8** was observed, giving rise to yields around 10 %, but most of the remaining starting material could be recovered as there were no side reactions. This made multiple repeats of the reaction possible after isolation of the starting compound. A 30 % total yield after three reaction cycles provided enough material to synthesize all desired probes. These were again synthesized on solid support with a rink resin using standard amino acid coupling conditions. The last remaining probes for caspase-3 were synthesized this way.

Table 4.2 Overview of all synthesized reduced amide inhibitors for caspase-3 and GlpG

On the right side of the table is indicated which method was used for each inhibitor: 1 = reductive amination on solid support; 2 = reductive amination in solution.

	Inhibitor structure	***method***
15	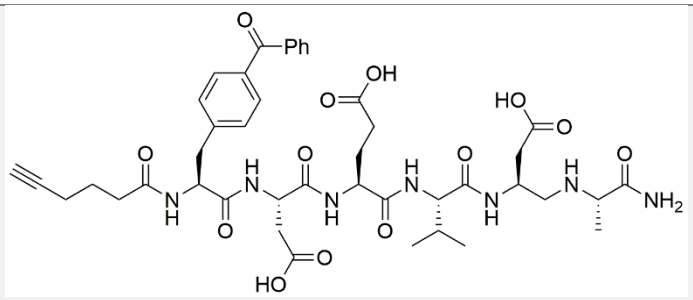	1
16	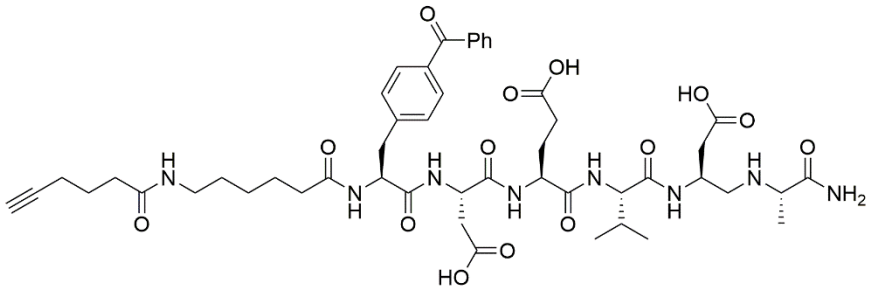	1
17	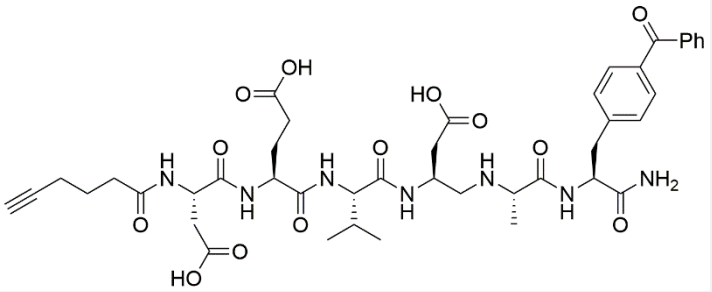	2
18	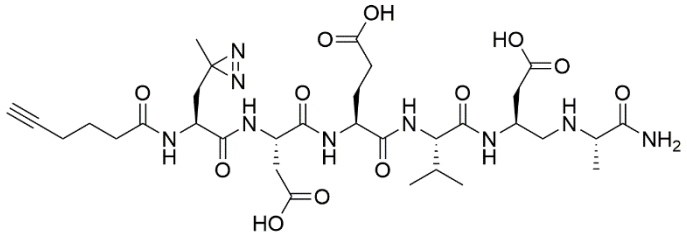	2
19	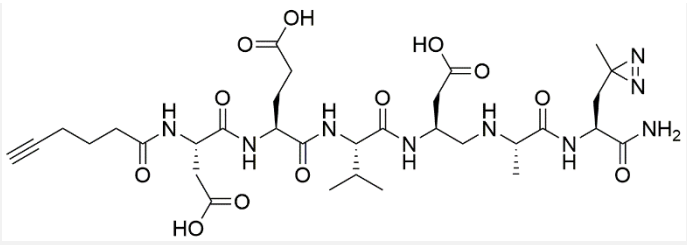	2

	Inhibitor structure	Method
20	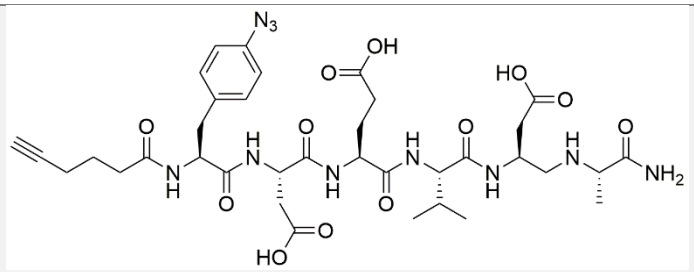	2
21	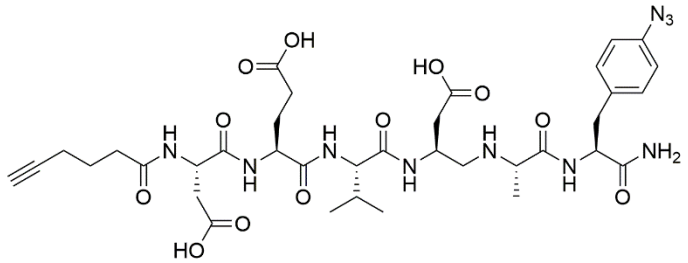	2
22	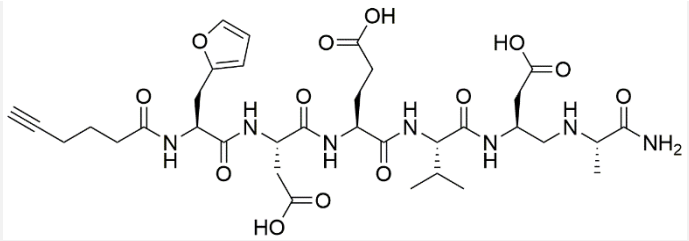	1
23	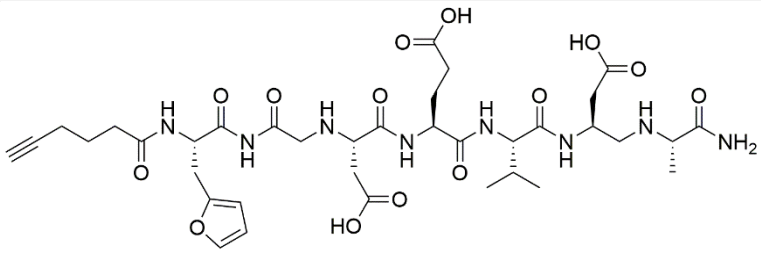	1
24	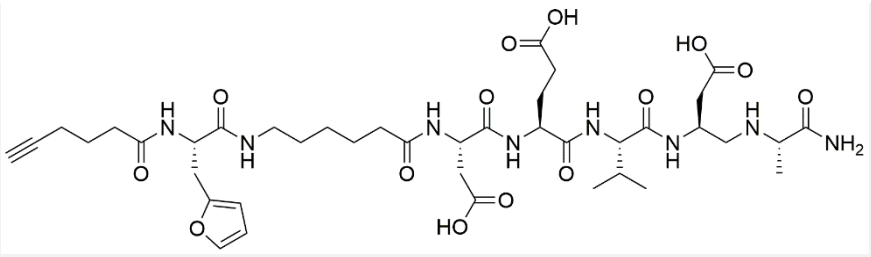	1
25	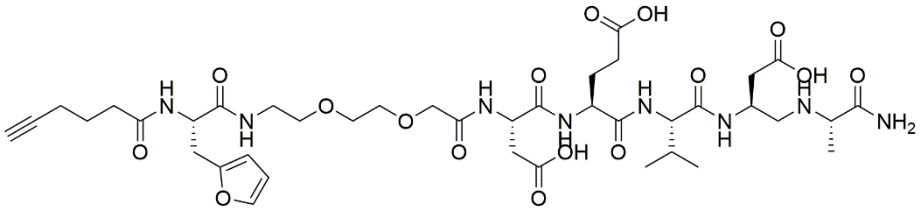	1

	Inhibitor structure	*Method*
26	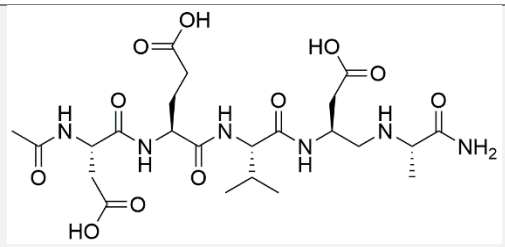	1
27	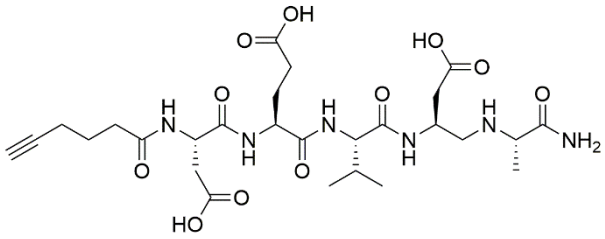	1
30	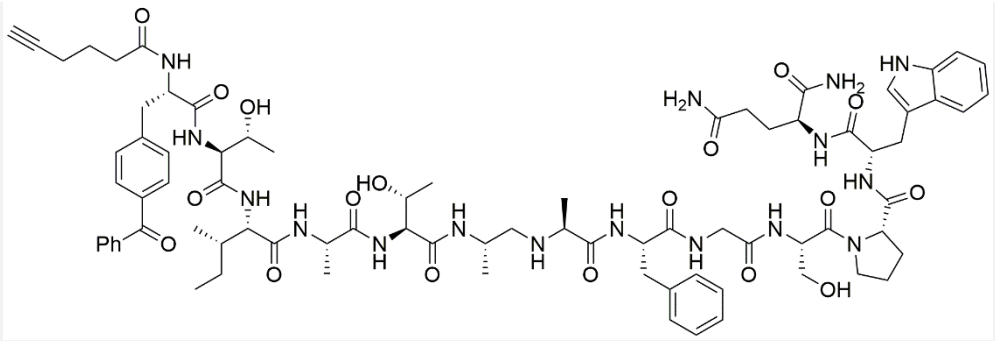	1
31	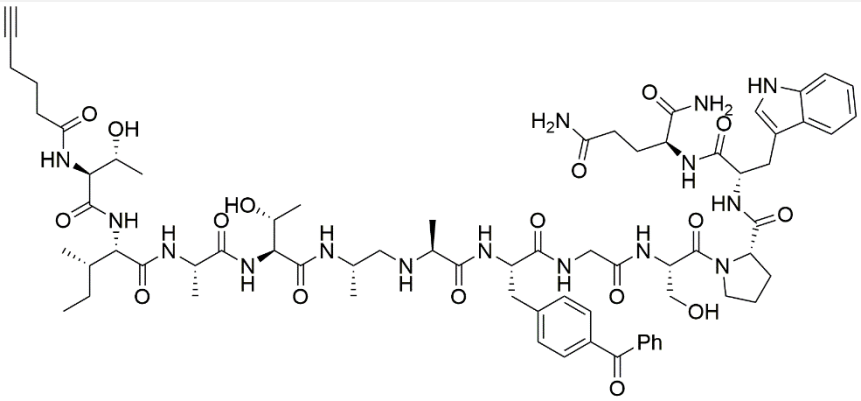	1
32	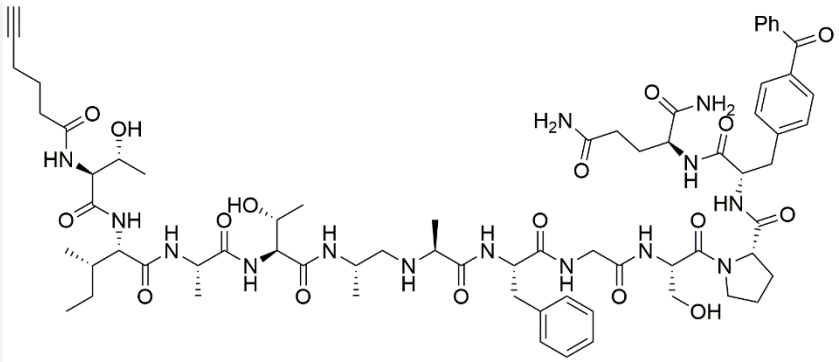	1

4.1.4 Synthesis of triazole inhibitors for caspase-3

The synthesis of inhibitors with a triazole as the peptide bond mimic was also envisioned to be entirely possible on solid support. The triazole could be formed by on-resin click chemistry. In order for this reaction to proceed, both reaction partners, the azide **10** and the alkyne **14**, had to be prepared in solution. The azide could be obtained via a diazotransfer reaction of L-alanine with imidazole-1-sulfonyl azide **9**. Before this reaction could be performed, the diazotransfer reagent **9** itself was synthesized in a two-step reaction [57]. In the first step, sulfuryl chloride was added to sodium azide. After that reaction was complete, imidazole was added to the intermediate. The diazotransfer reagent **9** was finally obtained as the HCl salt after crystallization.

The alkyne **14** proved to be a bigger challenge, as transforming a carboxylic acid into an alkyne is no straightforward reaction. A Seyferth-Gilbert homologation [58, 59] was the method of choice to obtain the alkyne from the amino aldehyde **13**, which was in turn synthesized using the optimized procedure described before. This reaction required the Bestmann-Ohira reagent, and this could be generated in situ by reacting dimethyl-2-oxopropylphosphonate with the diazotransfer reagent **9** and potassium carbonate as a base [60]. The amino aldehyde **13** was added to this mixture to obtain the amino alkyne **14**. Unfortunately, this reaction proved to be incompatible with the Fmoc protecting group, which was deprotected under the basic conditions. As the deprotection of the amine needs to proceed under acid-free conditions during the synthesis on solid support, the allyloxycarbonyl group was selected as the alternative protecting group, because it can be removed under neutral conditions and as compatible with SPPS. This group was introduced before the formation of the Weinreb amide via a reaction with N-(Allyloxycarbonyloxy)succinimide (Figure 4.6).

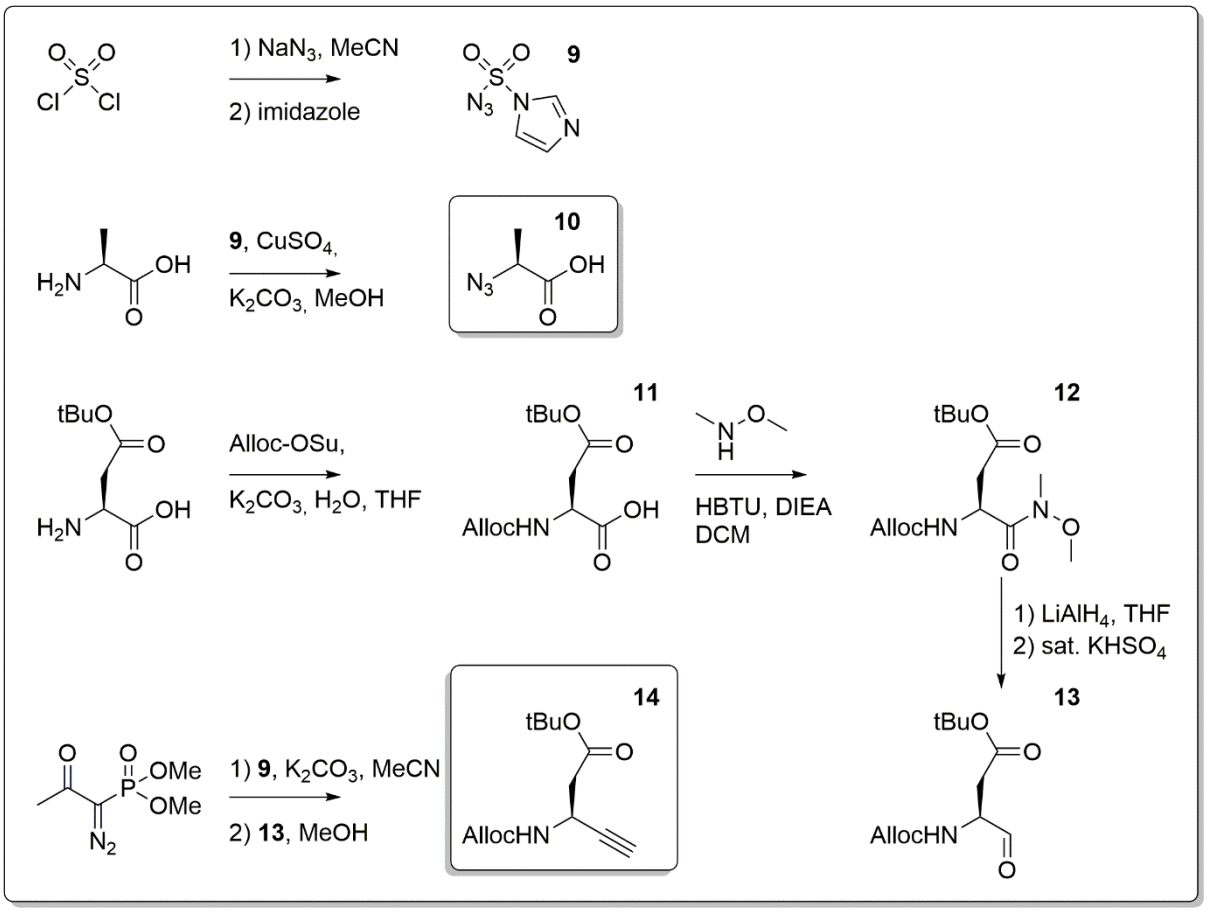

Figure 4.6 Synthesis of azide **10** and alkyne **14** as building blocks for the triazole synthesis

Now that both the azide and the aldehyde were synthesized, the inhibitors could again be constructed on the rink resin. After the coupling of the P1' alanine as the azide building block, the triazole was formed through a click reaction with the alkyne [61]. This was achieved with copper(I) bromide in the presence of sodium ascorbate, 2,6-lutidine and DIEA. The complete formation of the triazole was confirmed with a modified Kaiser test, where the resin was first treated with triphenylphosphine and water to reduce any remaining azides to amines. This reaction was followed by the deprotection of the Alloc group, which proceeded with $Pd(PPh_3)_4$ as catalyst and phenylsilane. The final synthesis steps were the standard amino acid couplings of valine, glutamic acid, aspartic acid, crosslinker, and tag. The fully protected resin-bound inhibitors were cleaved from the resin and purified as described before (Figure 4.7).

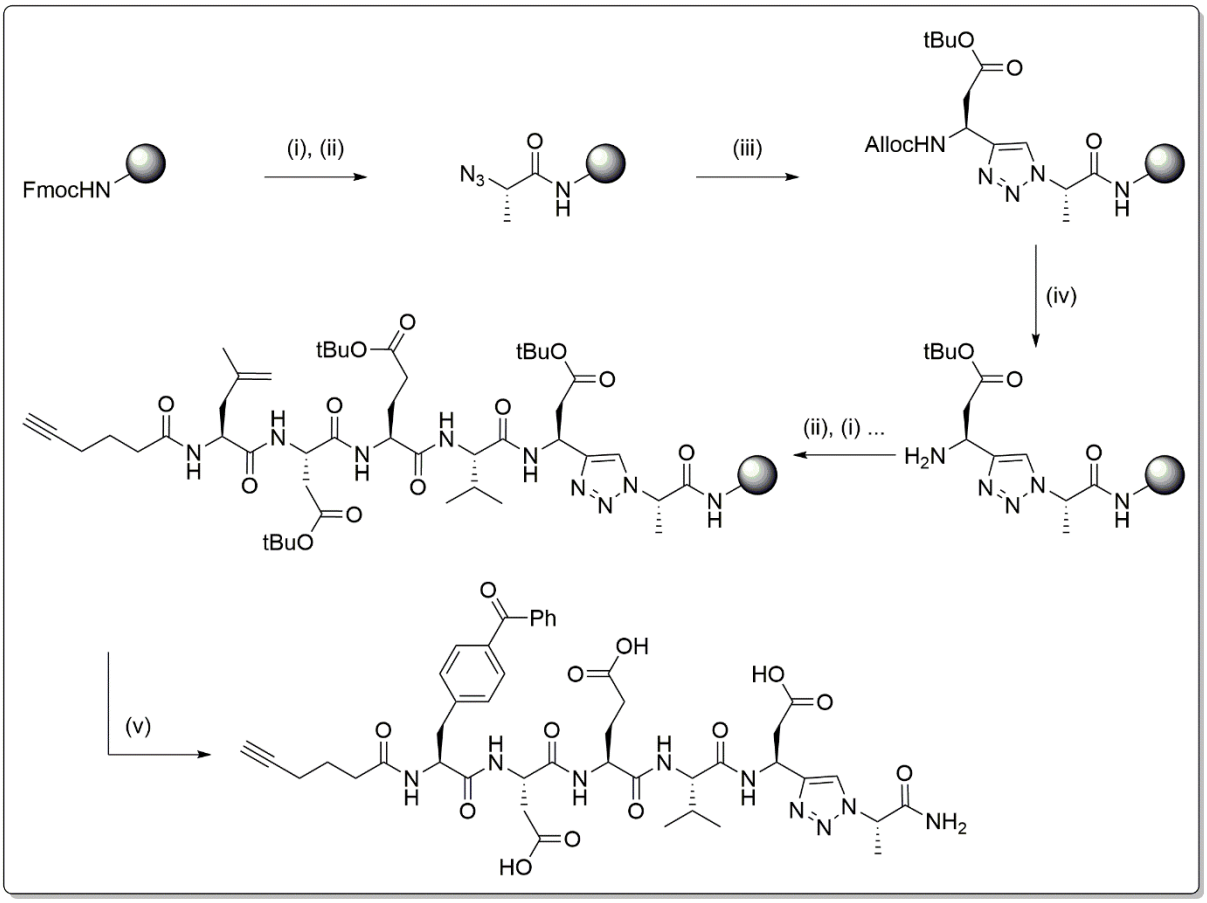

Figure 4.7 Synthesis of triazole inhibitor **28** on solid phase

(i) 20 % piperidine in DMF; (ii) azide **10** or Fmoc-amino acid, HBTU, DIEA, DMF; (iii) **14**, CuBr, sodium ascorbate, 2,6-lutidine, DIEA, MeCN, DMF; (iv) $Pd(PPh_3)_4$, phenylsilane, DCM; (v) TFA, TIS, H_2O.

Two inhibitors designed for caspase-3 were obtained this way, both with their benzophenone crosslinker in a different position (Table 4.3). Note that inhibitor **29** has an additional C-terminal glycine. This was introduced as a spacer between the crosslinker and the resin to circumvent the otherwise difficult coupling.

Table 4.3 Structures of both triazole inhibitors for caspase-3

	Inhibitor structure
28	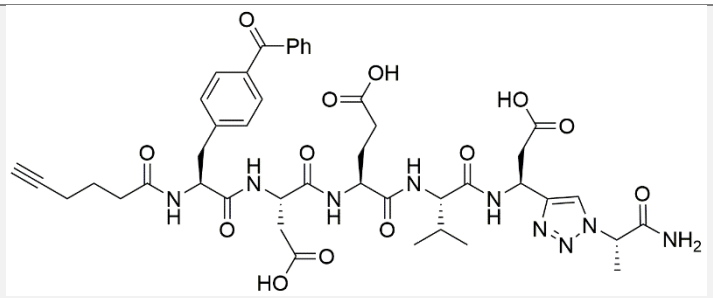
29	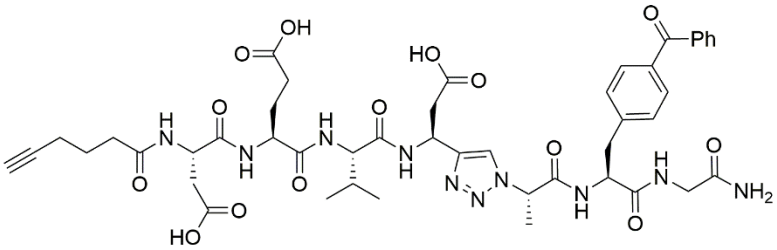

4.2 Potency assessment of the synthesized inhibitors for caspase-3

For the evaluation of the synthesized inhibitors, competitive activity-based protein profiling was performed [37]. The caspase-3-directed control ABP used here is **SV149** (Figure 4.8). This is a tetramethylrhodamine (TAMRA) derivative of KMB-01 that gives a fluorescent readout signal [62]. Unless otherwise specified, caspase-3 was always treated in a PBS buffer containing 1 mM DTT.

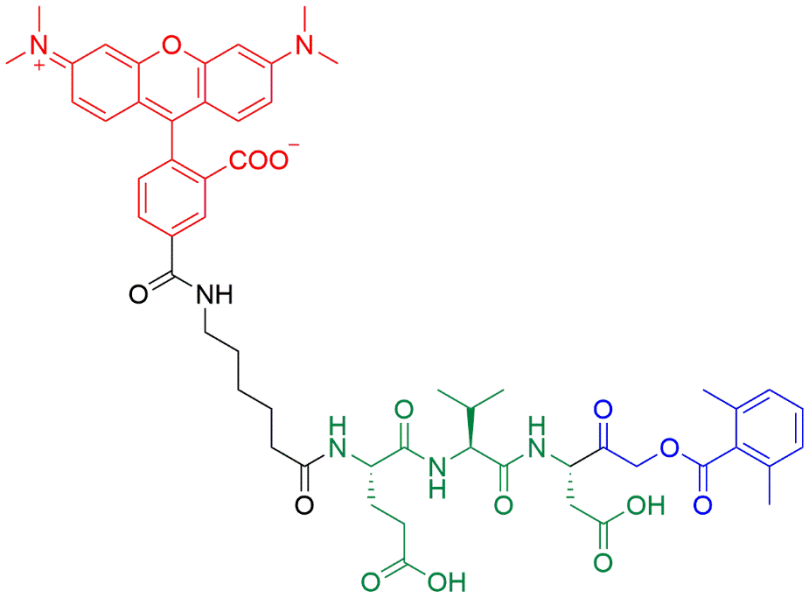

Figure 4.8 The structure of control ABP **SV149**

Red: the TAMRA fluorophore. Green: the EVD specificity element. Blue: the AOMK warhead.

4.2.1 Potency assessment of the reduced amide inhibitors

4.2.1.1 Influence of UV-irradiation on the protease activity

Before evaluating the potency of the photocrosslinking inhibitors, the influence of UV irradiation on caspase-3 activity had to be assessed. The irradiation did not seem to have an impact on the activity. However, when comparing UV lamps of different intensity (8 and 36 W), it appeared that the heat generated by the lamps had a direct negative effect on the activity. This was taken into account during the execution of all related experiments.

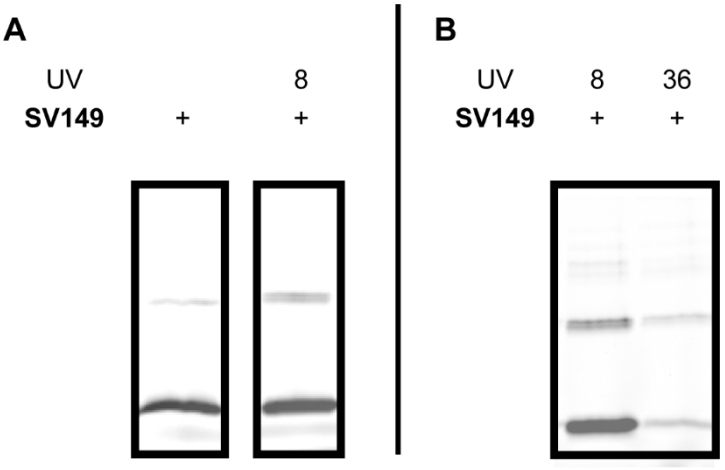

Figure 4.9 Influence of UV-irradiation on the caspase-3 activity

(A) An irradiation time of 30 min with a lamp of 8 W has no effect on the activity. (B) The stronger lamp of 36 W had a significant negative impact on the activity. This was attributed to the heat that was generated during the irradiation.

4.2.1.2 Inhibition of the inhibitors with a photocrosslinker

By making use of the standard protocol, inhibitors **15**, **16** and **17** with a benzophenone crosslinker showed complete inhibition of caspase-3 at a concentration of 10 µM with an irradiation of 30 minutes at 365 nm, whereas the non-irradiated samples showed little to no reduction of the labelling intensity. After optimization of the conditions for inhibitor **15**, it was concluded that even at 100 nM, 60 % inhibition remained, and that the irradiation time could be reduced to two minutes without any significant loss in potency. For this inhibitor, inhibition was also achieved in an apoptotic cell lysate. This was obtained by treating a lysate of HEK293 cells with dATP and cytochrome c to induce apoptosis.

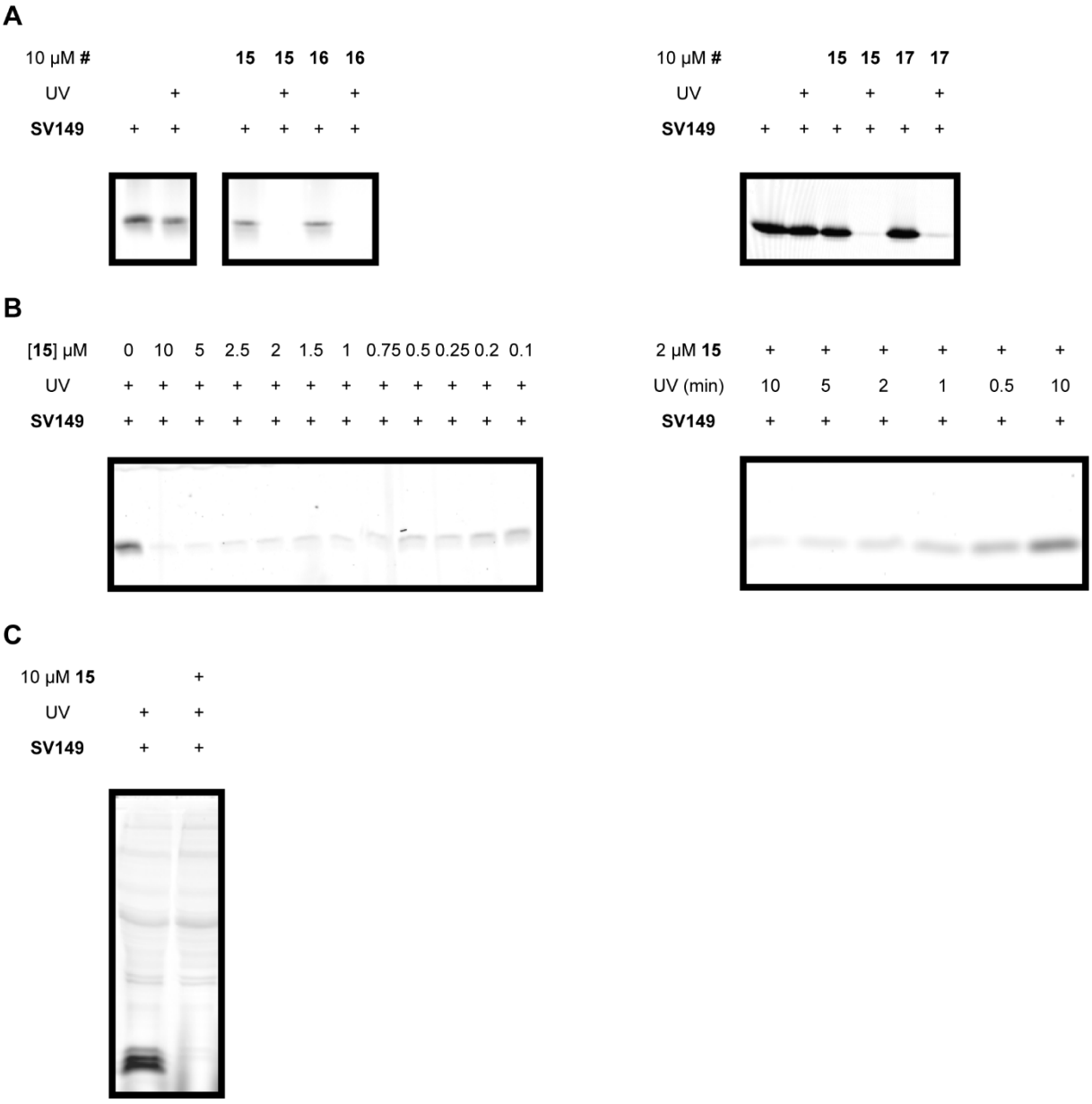

Figure 4.10 Competitive ABPP on caspase-3 with benzophenone inhibitors **15**, **16**, and **17**

(A) Inhibition of all three inhibitors at 10 µM. (B) Concentration titration of inhibitor **15** (left). Irradiation time optimization (right). (C) Inhibition with inhibitor **15** in an apoptotic HEK293 lysate. Apoptosis was induced with 1 mM dATP and 100 µM cytochrome c. Both caspase-3 and caspase-7 are inhibited.

As extra confirmation of the inhibition, substrate cleavage assays were performed using the fluorogenic substrate Ac-DEVD-AMC (Figure 4.11). Continued processing of this substrate will result in a steady increase of the fluorescence intensity, while inhibition of caspase-3 leads to a stagnation of the intensity. Inhibitors **15** and **17** were evaluated this way, and it was apparent from these experiments that both inhibitors show little to no inhibition without irradiation, but that substrate processing is completely inhibited after exposure to UV light.

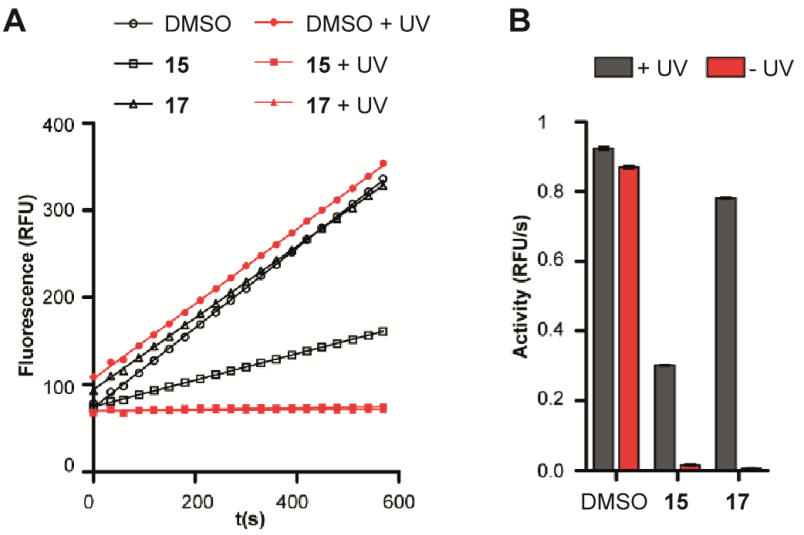

Figure 4.11 Substrate cleavage assays of Ac-DEVD-AMC with inhibitors **15** and **17**

Adapted from [53]. (A) Representative progress curves of fluorescence produced by Ac-DEVD-AMC (50 µM) cleavage by caspase-3, irradiated with or without 10 µM of the indicated compounds. (B) Bar graph of residual caspase-3 activity of replicate experiments (n = 2) of those in (A).

In the case of inhibitors **18** and **19**, containing diazirine photocrosslinker, a concentration of 100 µM and irradiation time of 30 minutes were required for complete inhibition (Figure 4.12). Hence, although they still show clear inhibition of caspase-3, they are clearly inferior to the benzophenone inhibitors.

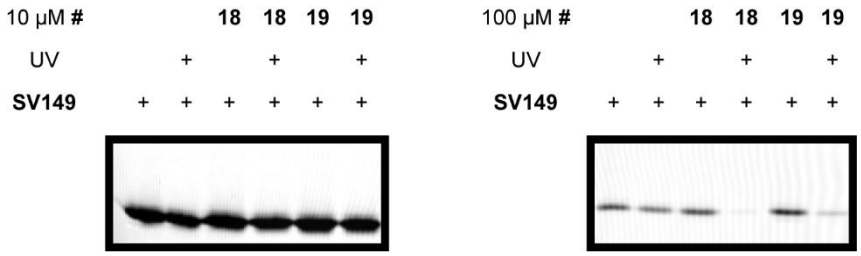

Figure 4.12 Competitive ABPP on caspase-3 with diazirine inhibitors **18** and **19**

The potency was evaluated at 10 µM (left) and 100 µM (right).

The last of the photocrosslinking inhibitors, **20** and **21**, with a phenyl azide, did not lead to any inhibition at all with a concentration of 10 µM. This was due to the incompatibility of the crosslinker with DTT, a reducing agent required for caspase-3 activity present in the buffer solution. This causes the phenyl azide to be reduced to its corresponding amine, and thus prevents any crosslinking. To circumvent this, the DTT was replaced with β-mercapto ethanol, a much milder reducing agent that supposedly leaves phenyl azides intact. However, this still yielded no inhibition of caspase-3 (Figure 4.13).

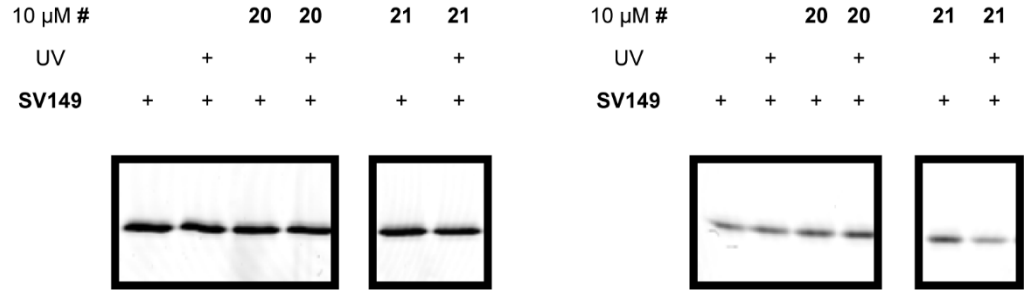

Figure 4.13 Competitive ABPP on caspase-3 with diazirine inhibitors **20** and **21**

Different reducing agents were used in the buffers: DTT (left) and β-mercapto ethanol (right).

4.2.1.3 Inhibition of the inhibitors with a furan crosslinker

As mentioned before, the inhibitors containing a furan crosslinker require oxidation as the trigger for their crosslinking. This creates an aldehyde that can crosslink to a nearby lysine or cysteine, requiring one of these residues to be in the close vicinity. For this reason, a docking of core structure inhibitor **26** in the caspase-3 active site was performed, and this revealed the presence of a lysine close to the N-terminal side (Figure 4.14).

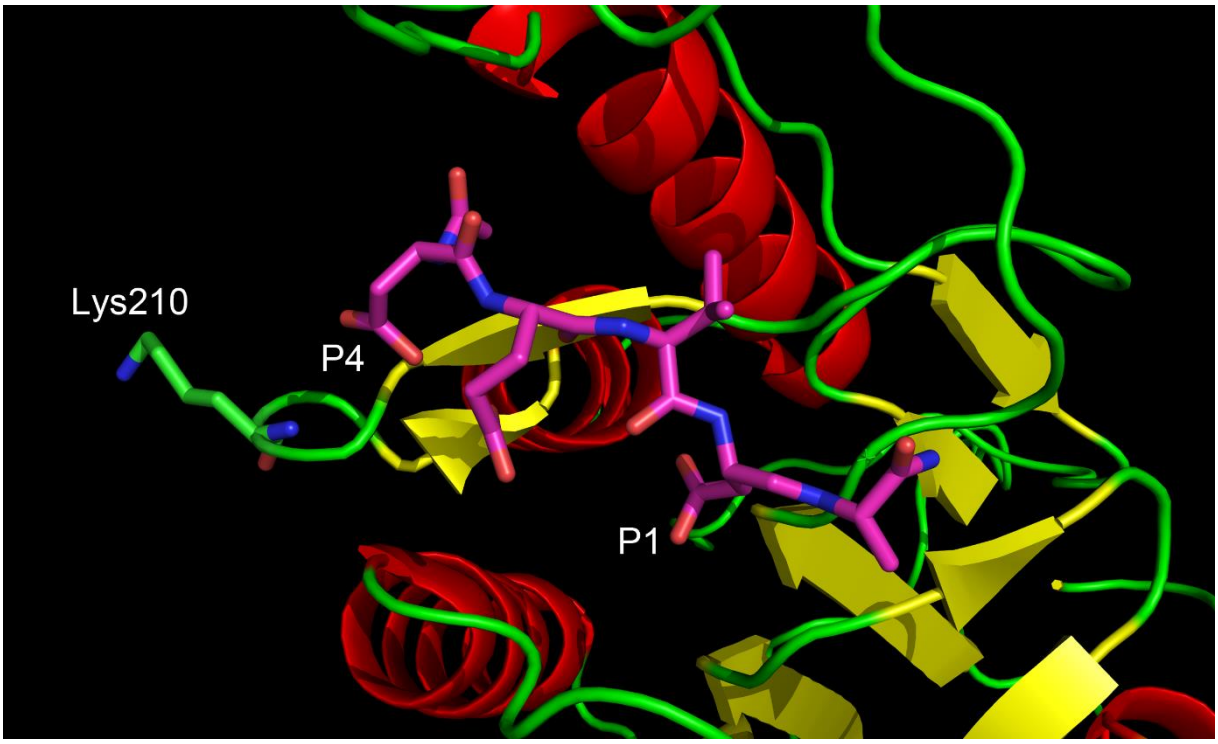

Figure 4.14 Docking of inhibitor **26** in the active site of caspase-3

Lys210 was identified to be in close proximity to the N-terminus of the inhibitor.

Four different inhibitors were synthesized, each with a different spacer between the furan moiety and the N-terminal side of the core structure. The most convenient method for the crosslinker activation was an NBS oxidation, which was added to the samples at the same concentration as the inhibitors. As expected, DTT counteracted the NBS and this resulted in either no inhibition (no furan oxidation due to a 100 times excess of DTT) or no caspase-3 activity (omission of DTT leads to oxidation of the active site cysteine). As a countermeasure for this, the oxidation was performed before the addition of caspase-3. All four inhibitors showed complete inhibition at 10 µM when evaluated in this manner (Figure 4.15).

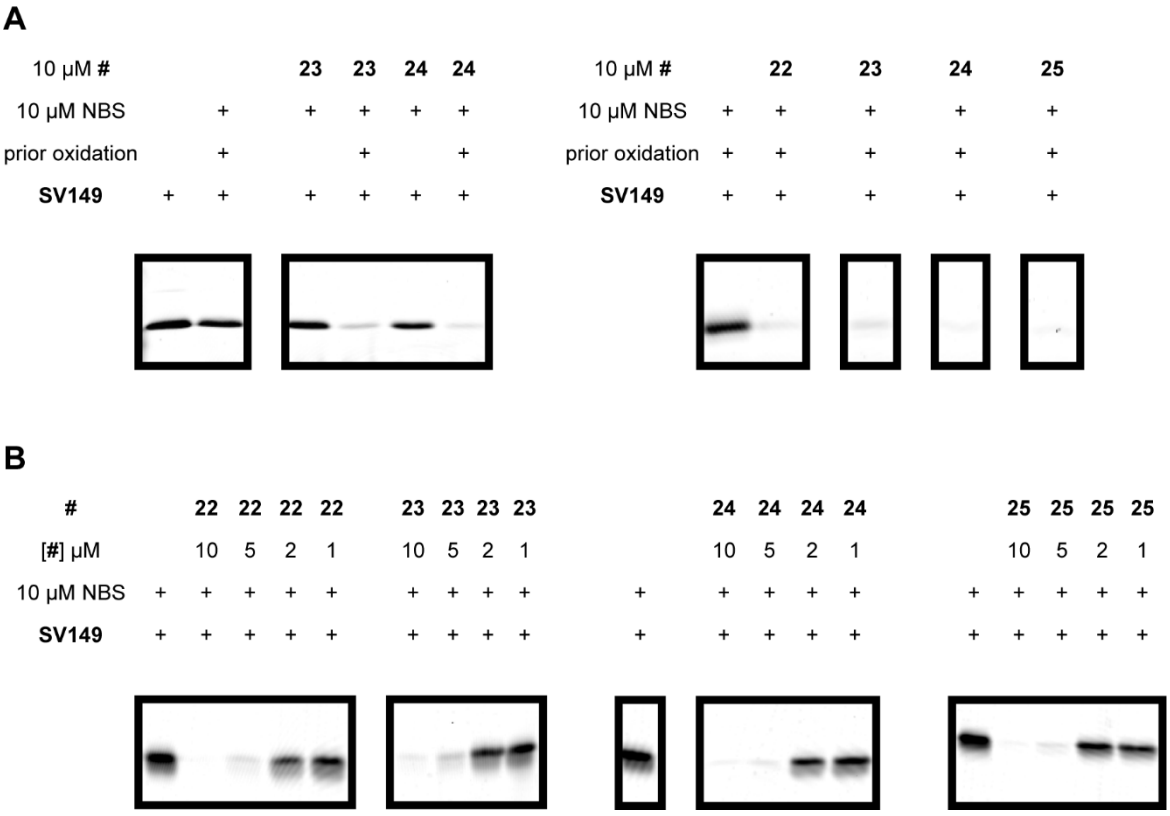

Figure 4.15 Competitive ABPP on caspase-3 with furan inhibitors **22**, **23**, **24**, and **25**

(A) Inhibition is only observed when furan is oxidized before incubation with caspase-3. (B) Concentration titration of all furan inhibitors.

4.2.2 Potency assessment of the triazole inhibitors

In addition to the reduced amide inhibitors, two inhibitors with a triazole as the peptide bond mimic were also synthesized. Both of these contained a benzophenone crosslinker, located at the N- and C-terminal positions respectively (**28**) and (**29**).

Competitive ABPP was also performed with these inhibitors, and it was found that inhibitor **29** displayed good inhibition of caspase-3 at 10 µM after an irradiation of 30 minutes at 365 nm. The other inhibitor, **28**, showed no inhibition at 10 µM. Only with an increased concentration of 100 µM did it show moderate inhibition (Figure 4.16). The potency of these inhibitors was much less pronounced compared with the ones with a reduced amide peptide bond mimic. As a result, the latter were the main focus in all further experiments.

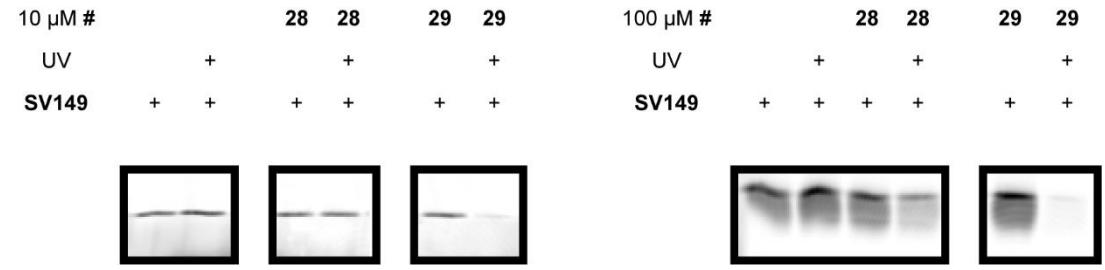

Figure 4.16 Competitive ABPP on caspase-3 with triazole inhibitors **28** and **29**

Both were evaluated at 10 µM (left) and 100 µM (right).

4.3 Direct labelling of the inhibitors complexed with caspase-3

In order to confirm the formation of the irreversible covalent complex, the inhibitors were equipped with an alkyne tag located at the N-terminus of all probes. This can be modified with a fluorescent (or other) label before or after complex formation via a click reaction (Figure 2.4). The label that was installed in the experiments below is a tetramethyl rhodamine fluorophore (5-TAMRA-azide, Figures 4.17).

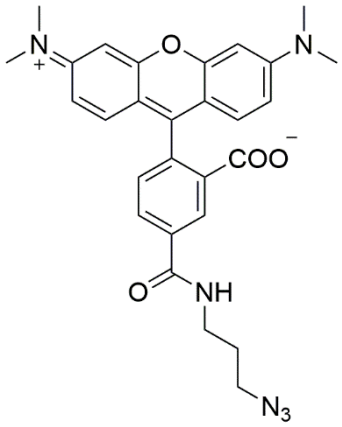

Figure 4.17 Structure of 5-TAMRA-azide

Before the labelling of the inhibitors was evaluated, the conditions for the click chemistry were optimized with an alkyne derivative of KMB-01 as control ABP **33**. Initially, the control experiment was performed in an optimal caspase assay buffer containing NaCl, sucrose, CHAPS, EDTA, and DTT. However, it turned out that the conditions for the click chemistry were not compatible with this buffer. By eliminating components from the buffer, the cause of this could be narrowed down to the presence of DTT, as exemplified by a click experiment in PBS buffer containing only DTT. Because caspase-3 requires the presence of DTT for its activity, this proved to be a major issue. As a solution, the click chemistry was performed prior to incubation with caspase-3 in PBS buffer. This resulted in the successful labelling of caspase-3 with the control ABP **33** (Figure 4.18).

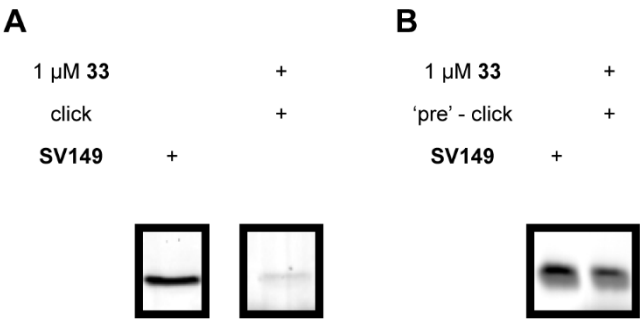

Figure 4.18 Optimization of the conditions for click chemistry

(A) Little to no labelling is observed, even when the click reaction is performed in a PBS buffer only containing 1 mM DTT. (B) Caspase-3 is successfully labelled with control probe 33 when the click is performed separately in PBS before the incubation with caspase-3.

The phenyl azide inhibitors, **20** and **21**, were not evaluated in this manner, as they didn't display any inhibition in the first place. All other inhibitors were labelled with the same conditions used for the control ABP. However, none of them showed any labelling, suggesting a reversible or non-covalent mechanism of action. In an attempt to at least confirm the formation of a complex between caspase-3 and the inhibitors, gels were loaded with samples without denaturing caspase-3 first. This way, bands corresponding to the dimeric active form of caspase-3 could be detected. In the case of inhibitors **15**, **16**, **22**, and **25**, these bands were successfully visualized, proving the existence of the complex (Figure 4.19).

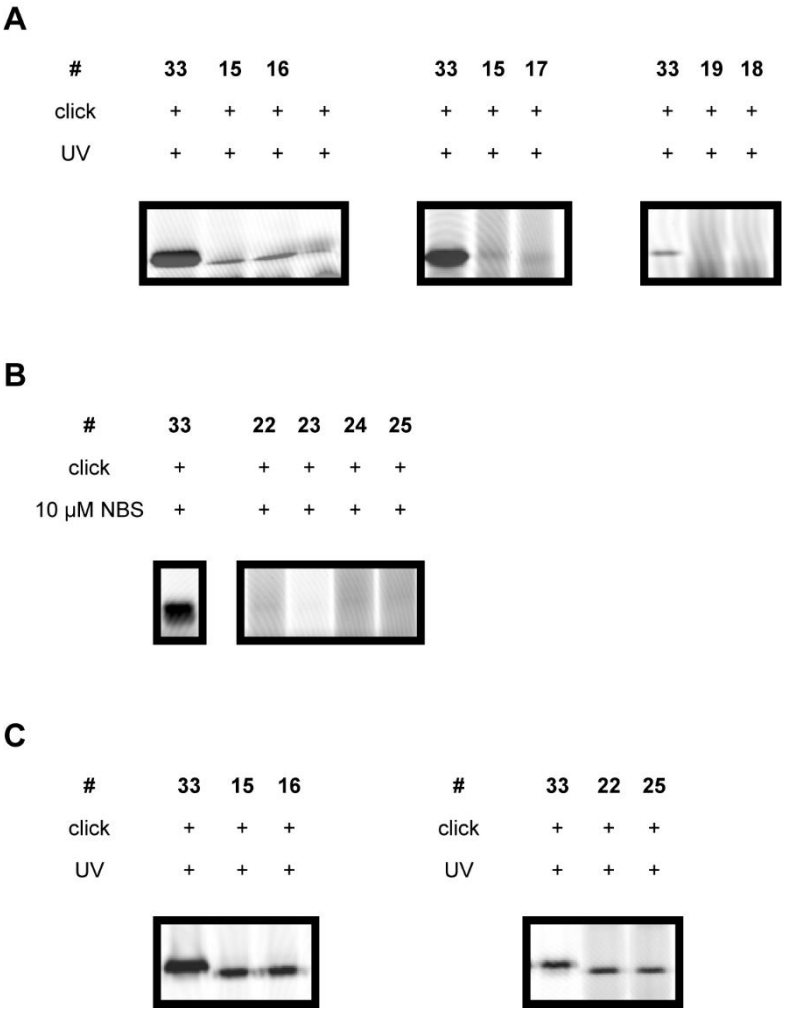

Figure 4.19 Direct labelling of caspase-3 with the reduced amide inhibitors

(A) photocrosslinkers. (B) furan. (C) When the samples are not denatured, labelling appears for inhibitors **15**, **16**, **22**, and **25**.

To exclude that these observations were due to the gel-based read-out, mass spectrometry experiments were performed. With ESI-MS on purified caspase-3, the small and large subunits could be identified. After treatment of caspase-3 with the fluorescent control probe **SV149**, the large subunit, where the active site cysteine is located, displayed a clear mass shift corresponding to the expected covalent modification. Performing the same experiment with benzophenone inhibitor **15** and furan probe **22b** (a biotin derivative of **22**) yielded no such shift (Figure 4.20). Similar experiments with MALDI-TOF-MS gave the same results for benzophenone inhibitor **17** and diazirine inhibitor **19** (Figure 4.21).

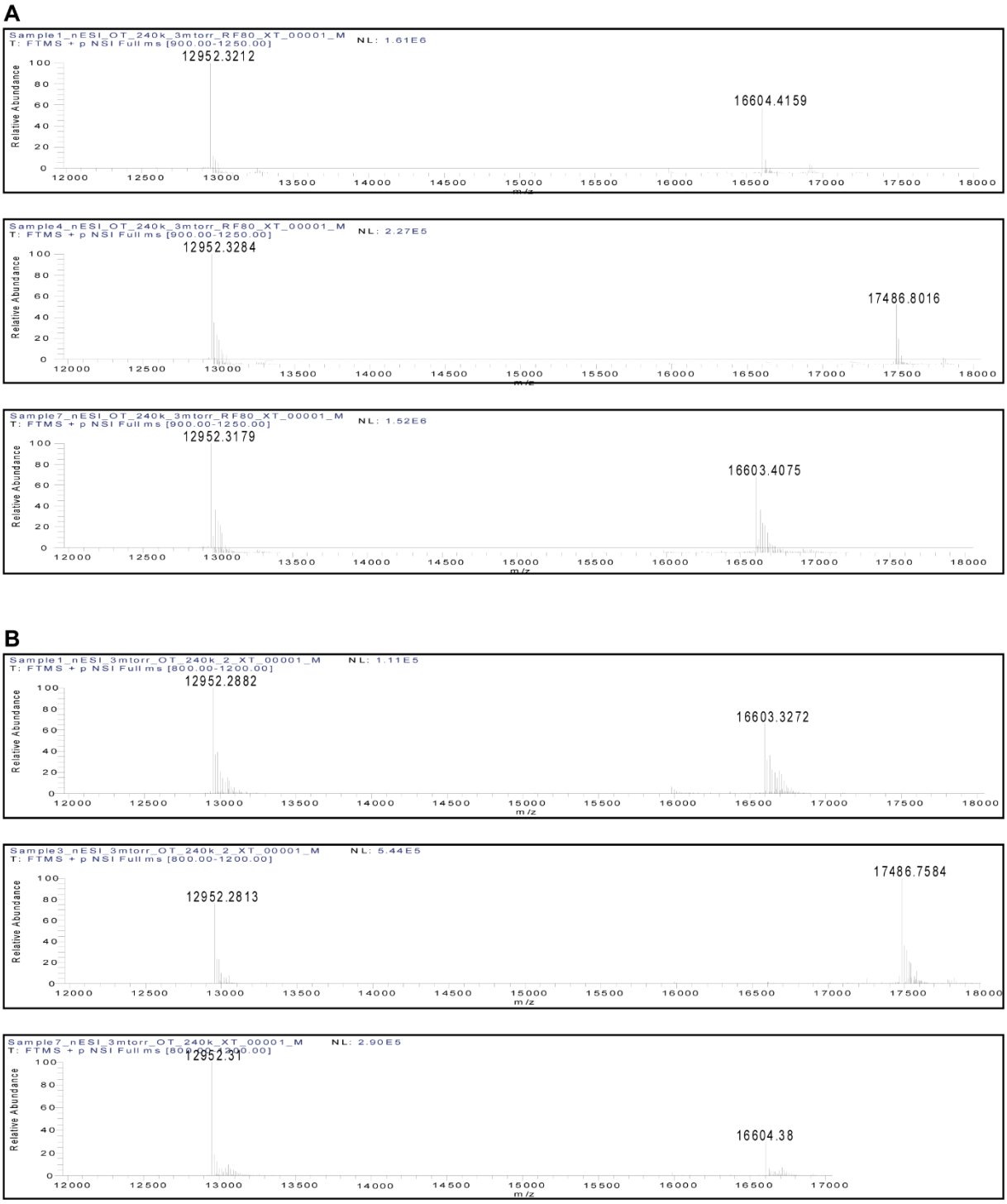

Figure 4.20 ESI-MS of purified caspase-3 reveals no covalent inhibitor-protease complex

(A) top: caspase-3, middle: caspase-3 + **SV149**, bottom: caspase-3 + **15**; (B) top: caspase-3, middle: caspase-3 + **SV149**, bottom: caspase-3 + **22b**.

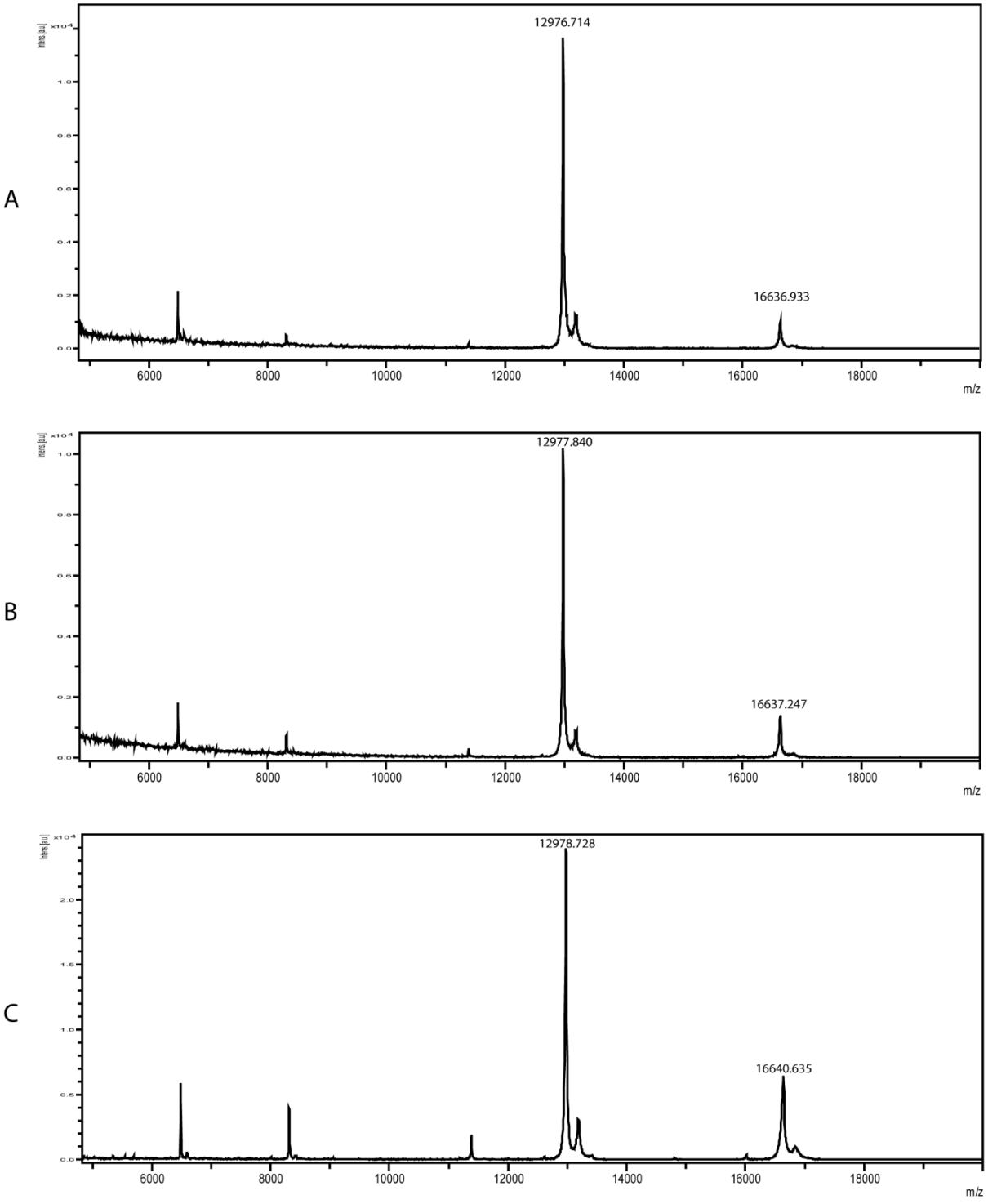

Figure 4.21 MALDI-MS of purified caspase-3 reveals no covalent inhibitor-protease complex

(A) caspase-3; (B) caspase-3 + **17**; (C) caspase-3 + **19**.

4.4 Elucidation of the mechanism of action

Originally, the synthesized inhibitors were designed to irreversibly crosslink to their target protease. However, it became clear from the competition and direct labelling experiments that although they successfully inhibit caspase-3, they don't form an irreversible covalent complex. It was hypothesized that the inhibitors might undergo an inter- or intramolecular reaction upon activation of their crosslinker, causing a substantial increase of their inhibitory potency. To investigate this, a series of experiments was performed where the photocrosslinkers were activated prior to incubation with caspase-3, similar to the competition experiments with oxidation of the furan inhibitors. With this setup, if a modification of the inhibitors themselves occurs, they would still display the previously observed inhibition, without their activated photocrosslinkers ever coming into contact with caspase-3. Surprisingly, both the benzophenone inhibitors, **15** and **17**, and the diazirine inhibitors, **18** and **19**, showed complete inhibition of caspase-3 at the same concentrations (resp 10 and 100 µM) as before (Figure 4.22A). Even more surprising was that although the phenyl azide probes, **20** and **21**, didn't show any inhibition at all before, they now also fully inhibited caspase-3 at 10 µM (Figure 4.22B). This indicated the formation of a stable inhibitor after crosslinker activation rather than a short-lived biradical or carbene species. As this same experiment did not result in any inhibition of caspase-3 with triazole inhibitor **29**, it appeared that the expected modification of the inhibitor occurred at the site of the peptide bond mimic (Figure 4.22C).

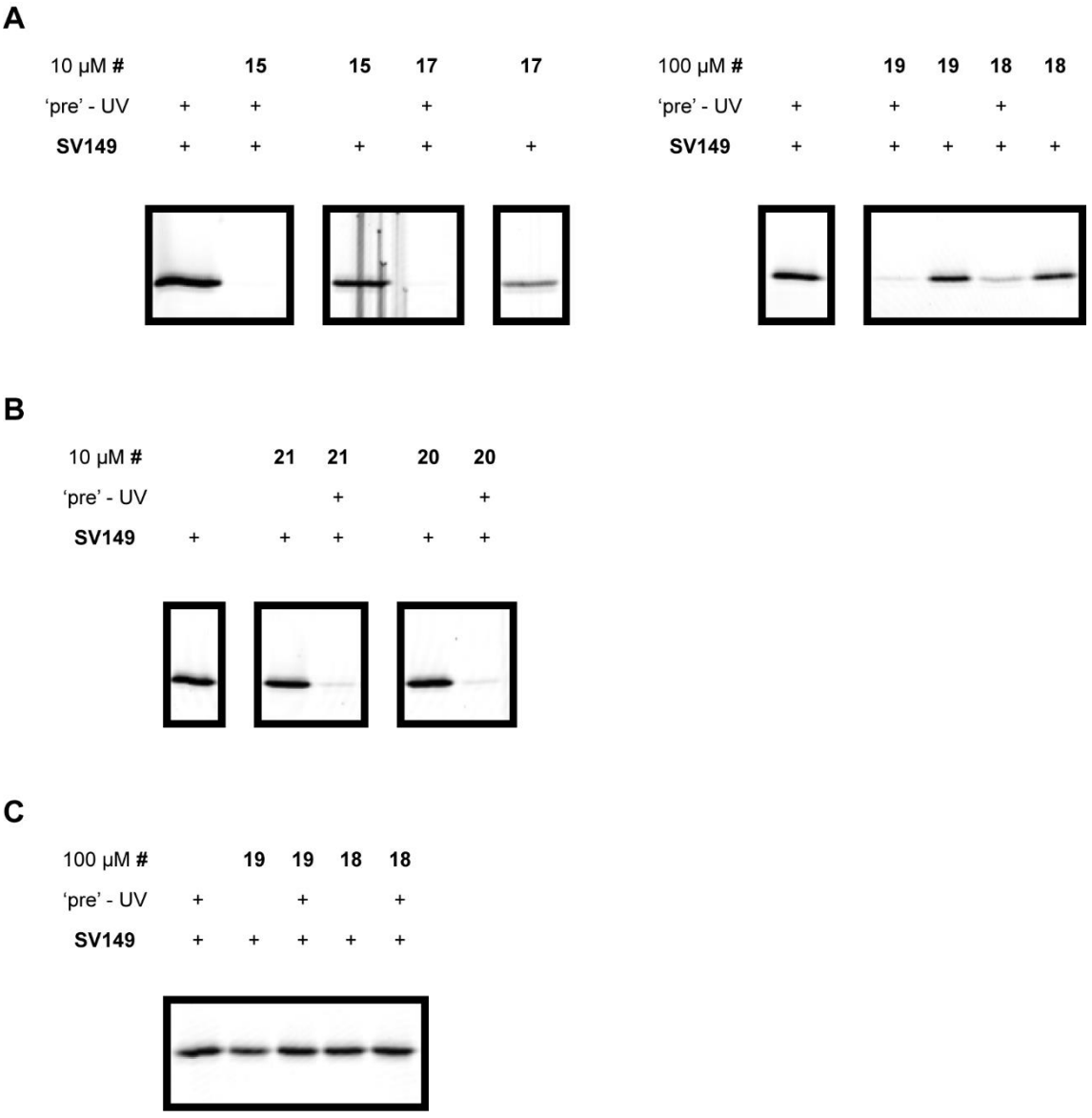

Figure 4.22 Competitive ABPP on caspase-3 with a 'pre'-activation of the photocrosslinkers
(A) Reduced amide inhibitors **15**, **17**, **18**, and **19**. (B) Reduced amide inhibitors **20** and **21**. (C) Triazole inhibitors **18** and **19**.

In an attempt to identify the generated inhibitors, LC-MS data was acquired before and after irradiation of the inhibitors (Figure 4.23). Unfortunately, no changes in mass or retention time were observed for the benzophenone inhibitors **15** and **17**. For the diazirine inhibitors, **18** and **19**, and the phenyl azide inhibitor, **21**, only the expected loss of nitrogen was observed, combined with the addition of water.

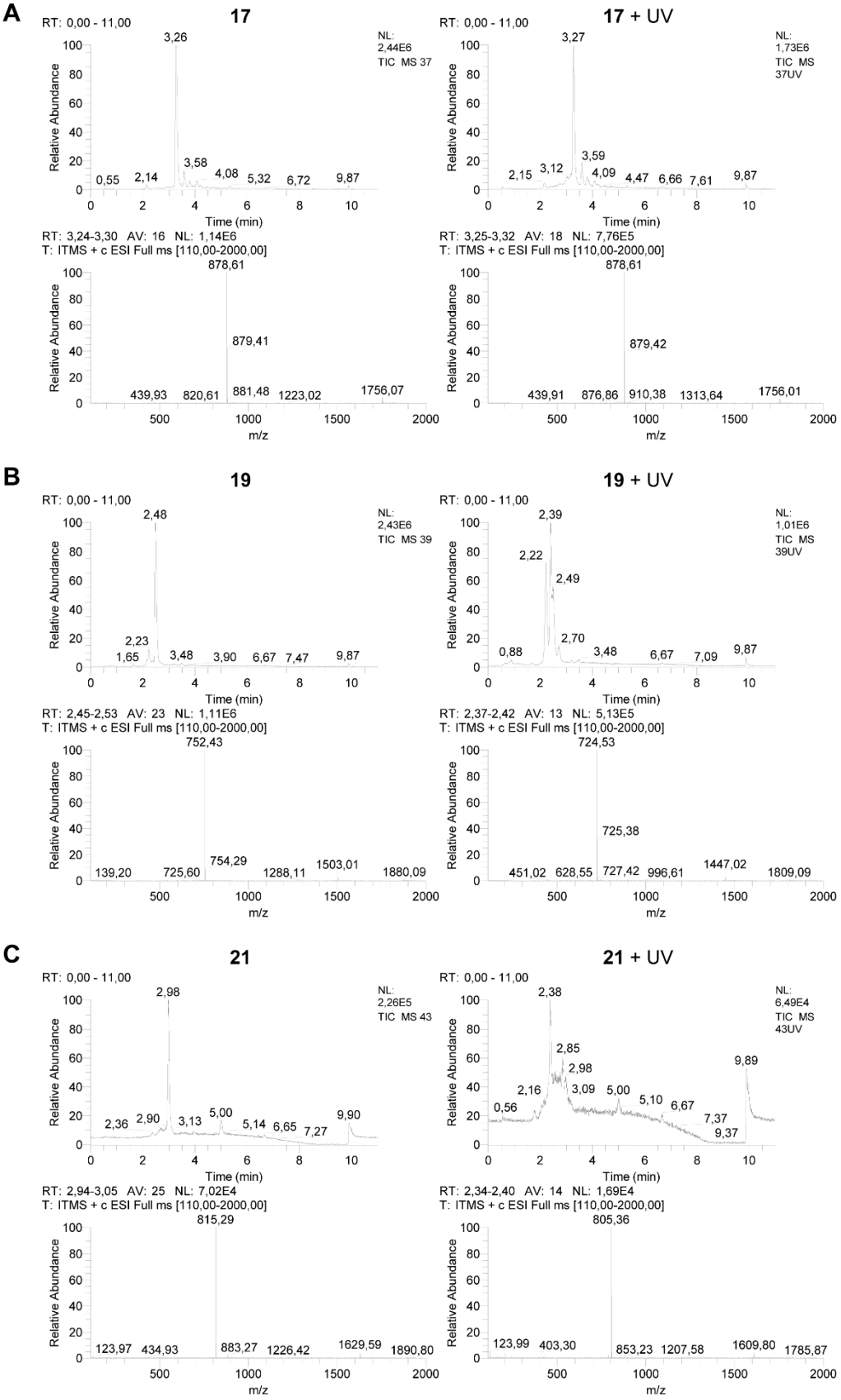

Figure 4.23 LC-MS data of the photocrosslinking inhibitors before and after irradiation

(A) Benzophenone inhibitor **15**. (B) Diazirine inhibitor **17**. The less intense peak at 2.22 min corresponds to a mass of 742.48. (C) Phenyl azide inhibitor **21**.

An intermolecular reaction between the inhibitors could be excluded because of these results, and the other option, an intramolecular reaction, also did not seem plausible. As there was no mass shift observed, a cyclization seemed like the only viable explanation. However, this usually corresponds to a significant shift of the retention time, which wasn't observed for the benzophenone inhibitors. Additionally, in the case of inhibitor **18**, ESI-MS-MS fragmentation only revealed the original intact inhibitor (Figure 4.24).

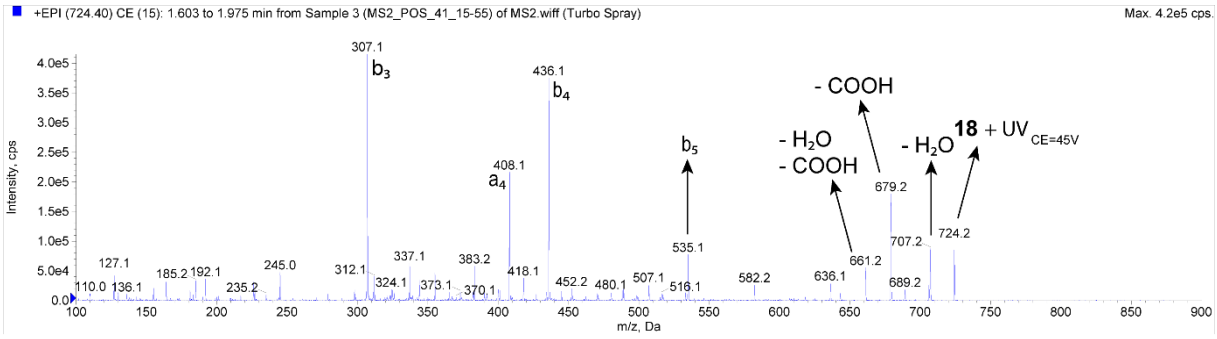

Figure 4.24 ESI-MS-MS of the irradiated diazirine inhibitor **18**

All the major peaks correspond to fragments of the original linear structure.

To further elucidate the identity of the inhibitors, a series of competition experiments was performed with two inhibitors not containing a crosslinker, where the N-terminus was either acetylated **26** or alkynylated **27**. Both with and without irradiation, these inhibitors did not show any inhibition towards caspase-3. However, after irradiating the inhibitors in the presence of an equimolar amount of benzophenone, they completely inhibited caspase-3 (Figure 4.25). Hence, the core structure of the probes and the crosslinker do not need to be present in the same molecule, but both the crosslinker and irradiation are required for successful inhibition. These experiments can completely exclude the occurrence of an intramolecular reaction during the activation of the inhibitors.

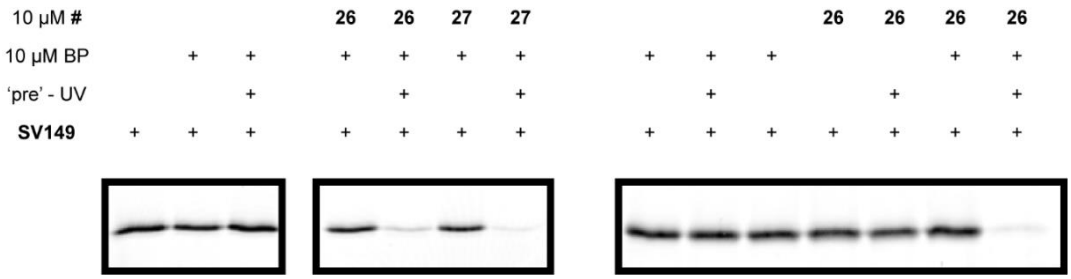

Figure 4.25 Pre'-activation experiments with inhibitors **26** and **27**

Both inhibitors inhibit caspase-3 after being treated with benzophenone (BP) and irradiated (left). Inhibition requires both BP and UV (right).

As the inhibitors were now expected to inhibit caspase-3 in a reversible manner, an experiment was performed to investigate if the protease can regain its activity over time after inhibition with probe **15**. After the inhibition was established, a dialysis was performed to remove (1,000,000 times dilution) the remaining 'free' inhibitor. An optimal assay buffer for caspase-3 (20 mM HEPES, pH 7.2, 100 mM NaCl, 10 % sucrose (w/v), 0.1 % CHAPS (w/v), 1 mM EDTA, 10 mM DTT) was used instead of the standard PBS buffer containing 1 mM DTT, as the latter resulted in an overnight loss of activity. While the non-inhibited caspase-3 clearly retained its activity, the inhibited sample showed no signs of activity recovery (Figure 4.26).

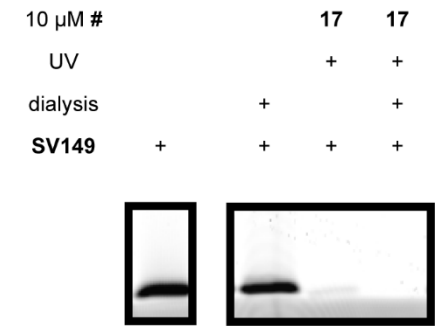

Figure 4.26 Dialysis of caspase-3 inhibited by inhibitor **17** to regain its activity

While caspase-3 clearly remains active after an overnight dialysis, it remains inhibited by caspase-3.

Because of the above results, it was hypothesized that a low abundant but highly potent reversible inhibitor was generated upon activation of the inhibitors. When looking at the structure of the inhibitors, the generation of small quantities of a peptide aldehyde seemed very plausible. Oxidation of the reduced amide to the imine and subsequent reaction with water could produce a C-terminal aldehyde (Figure 4.27).

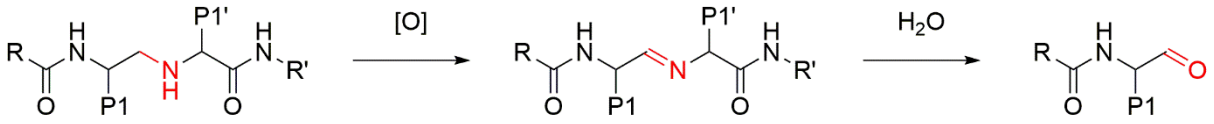

Figure 4.27 Proposed formation of a peptide aldehyde by oxidation of the reduced amide inhibitors

This hypothesis would also explain why no change was detected in the LC-MS data before and after irradiation. Very small quantities of a compound would not appear in a chromatogram containing a different highly abundant compound. That data was now reevaluated with the mass range narrowed down to the expected mass of the peptide aldehyde. It turned out that this mass could not be detected in the non-irradiated samples, but that it was present, in small quantities, in the irradiated samples for the benzophenone inhibitors **15** and **17** (Figure 4.28). Unfortunately, MS-MS fragmentation

of the signal proved to be impossible due to the high abundance of the original inhibitor, so the structural identity could not be confirmed in this manner.

Another method to prove the presence of the peptide aldehyde was pursued. It can be trapped with sodium bisulfite to form an adduct that cannot serve as an inhibitor anymore. If peptide aldehydes were the actual active species formed after irradiation of the inhibitors, caspase-3 would not be inhibited by their sodium bisulfite adducts anymore. These would be formed by treating the activated inhibitors with $NaHSO_3$. This procedure was first optimized with the commercial Ac-DEVD aldehyde, a potent inhibitor of caspase-3. Where the untreated inhibitor displayed complete inhibition at 100 nM, full activity of caspase-3 was retained after a pretreatment of the inhibitor with 10 mM sodium bisulfite. This optimized protocol was then repeated for the benzophenone inhibitors, **15** and **17**, phenyl azide inhibitors, **20** and **21**, and the core structure inhibitor **26** with equimolar addition of benzophenone. In all cases, there was full recovery of the activity of caspase-3, and this confirmed the generation of the peptide aldehyde upon crosslinker activation (Figure 4.29).

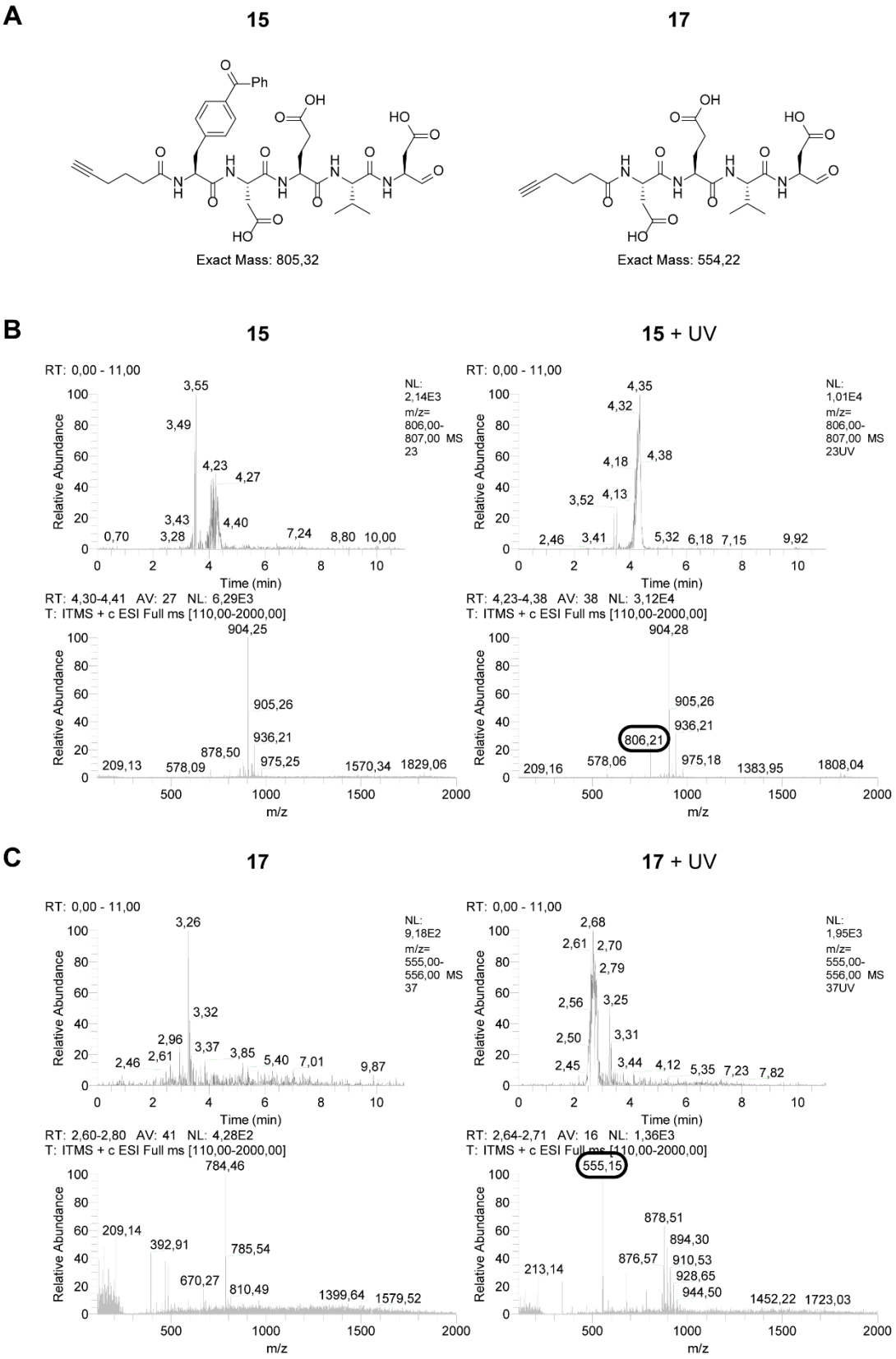

Figure 4.28 Detection of peptide aldehydes in the LC-MS data of irradiated benzophenone inhibitors

(A) Expected structures of the peptide aldehydes formed after oxidation of inhibitors **15** and **17**. (B) Data for inhibitor **15**. (C) Data for inhibitor **17**.

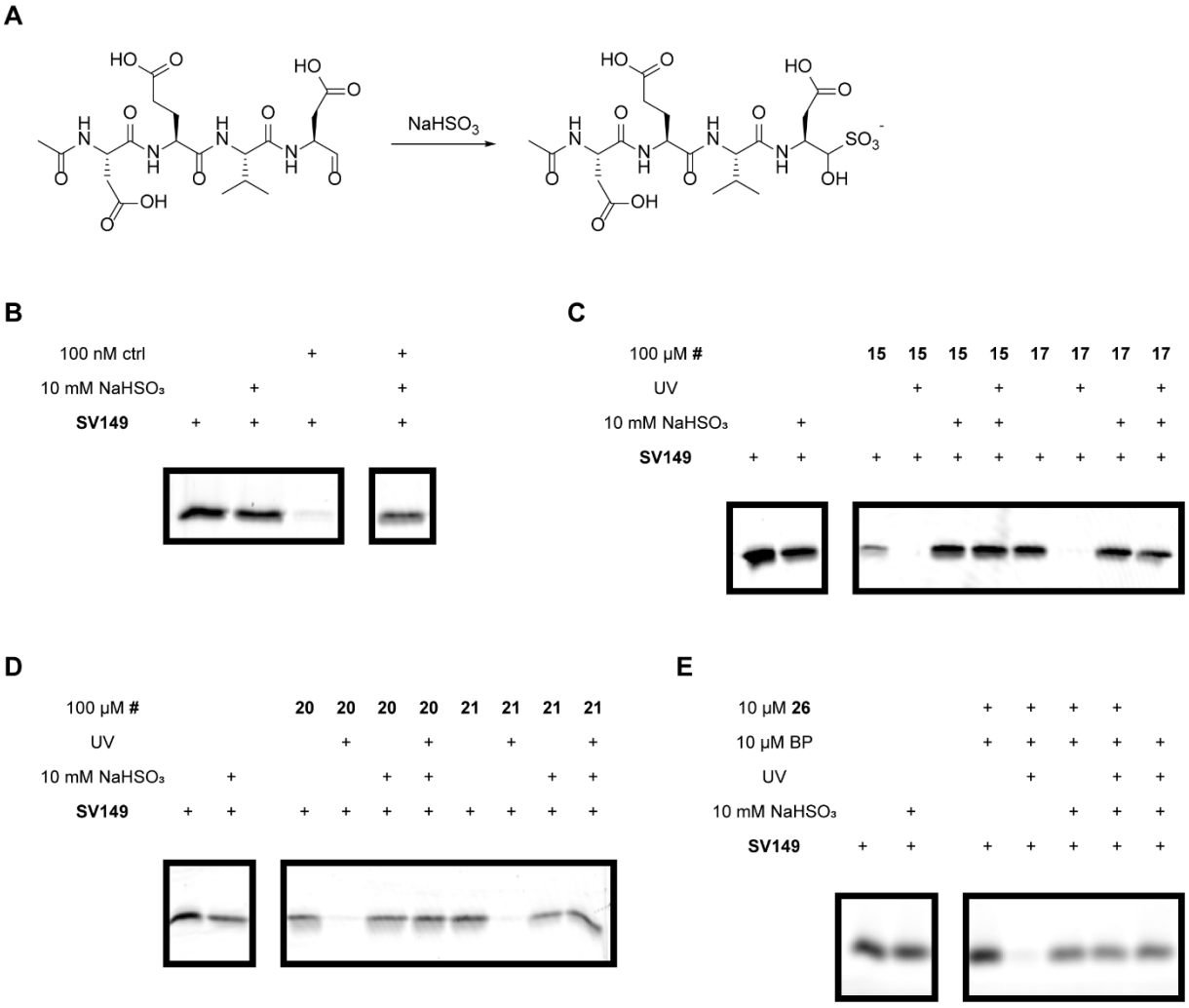

Figure 4.29 Detection of the presence of an aldehyde by treatment with sodium bisulfite

The treatment was always performed prior to the incubation with caspase-3. (A) Formation of the aldehyde-bisulfite adduct. (B) Control experiment with the commercial Ac-DEVD aldehyde. (C) Benzophenone inhibitors **15** and **17**. (D) Phenylazide inhibitors **20** and **21**. (E) Inhibitor **26**.

4.5 Evaluation of the inhibitors for GlpG

Similar to the inhibitors designed for caspase-3, the inhibitory potency of the GlpG inhibitors **30**, **31**, and **32** was assessed by competitive ABPP (Figure 4.30). In this case, only inhibitors with a benzophenone crosslinker were synthesized. The GlpG-targeting fluorescent ABP used here was fluorophosphonate-rhodamine, a general ABP for serine proteases.

All the synthesized GlpG inhibitors were identified to have a mass that is 26 a.u. higher than expected. This was caused by the reductive amination on solid support, as mentioned before. Nevertheless, because a lot of effort was required to obtain these inhibitors, they were evaluated despite this structural error. First, the influence of UV light was investigated, and a slight decrease in signal was observed. As expected, none of the probes showed any inhibition without activating the photocrosslinker. After irradiating the samples for 30 minutes at 365 nm, inhibitors **30** and **31** displayed minor inhibition at 500 µM, but inhibitor **32** completely inhibited GlpG (Figure 4.30A). After further investigation, the IC_{50} of inhibitor **32** was determined to be between 50 and 100 µM (Figure 4.30B). Unlike with caspase-3, the position of the crosslinker clearly had a huge impact on the potency of the inhibitors.

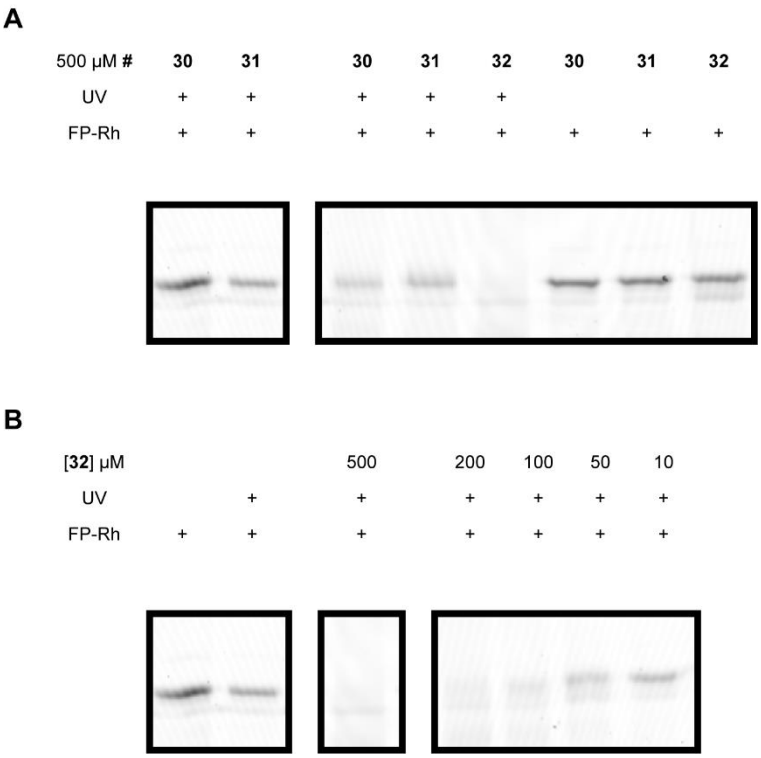

Figure 4.30 Competitive ABPP on GlpG with inhibitors **30**, **31**, and **32**

(A) Only inhibitor **32** displays promising inhibition. (B) Concentration titration of inhibitor **32**.

After the inhibition for inhibitor **32** was confirmed, a direct labelling experiment was again performed. Since inhibitors **30** and **31** only showed minor inhibition, they were not evaluated in this manner. Unlike caspase-3, the activity of GlpG can be investigated in a buffer that doesn't interfere with the click reaction, so the labelling of the inhibitor could be carried out after the inhibition itself was performed. Unfortunately, there was no control probe available for GlpG, implying that a negative result of the labelling experiment could possibly be attributed to the unoptimized conditions of the click reaction itself. Initially, no labelling of GlpG with inhibitor **32** was detected. However, just like with the inhibitors for caspase-3, bands for GlpG appeared when the samples were not denatured, proving the existence of a stable complex (Figure 4.31).

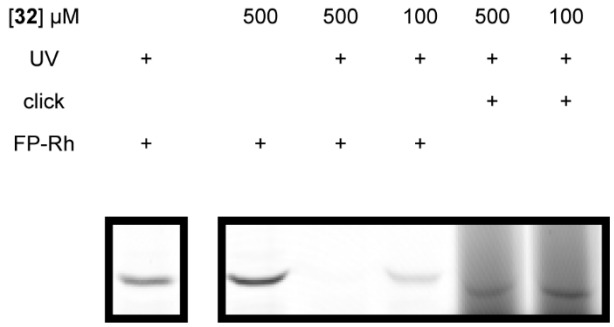

Figure 4.31 Direct labelling of GlpG with inhibitor **32**

5 Discussion

In this project, selective peptide-like inhibitors for proteases were designed by exploiting their substrate specificity. The idea was that these could be used as affinity-based probes after crosslinking to form an irreversible covalent bond with their target protease. As the recognition of these inhibitors would be solely dependent on their amino acid sequence, it was hypothesized that this strategy could be employed for all classes of proteins, regardless of their cleavage mechanisms.

The structure of the inhibitors is mostly that of a peptide substrate, with three additions: (1) a crosslinker, (2) an N-terminal detection tag, and (3) a peptide bond mimic that replaces the scissile bond in the substrate. For both mimics that have been described, the reduced amide and the triazole, the synthesis has been designed and optimized in such a way that it is compatible with most amino acids, using a combination of both solution and solid phase synthesis.

Most of the work described here focused on caspase-3, as this has a well-defined substrate specificity and was readily available. The optimal sequence required for recognition only spans five amino acids (Asp-Glu-Val-Asp-Ala, P4 to P1'). For this reason, aside from the generation of the peptide bond mimic, there was little synthetic effort required to obtain a range of inhibitors.

In addition, a number of inhibitors was also synthesized for the rhomboid GlpG, an intramembrane serine protease. This is a protease from a different class that also operates in a different environment. Unlike caspase-3, GlpG has a much less defined substrate preference. A sequence of twelve amino acids (P5 to P7'), based on the sequence of TatA, which acts as a substrate of GlpG, was used in the design of the inhibitors.

During initial experiments with caspase-3, it was found that UV irradiation did not have any influence on the activity, but the heat generated by the same lamps would substantially diminish it over time, as shown in figure 4.2. Therefore, care was always taken to avoid the generation of heat during the treatment of all samples, either by using an ice bath or by increasing the distance between the samples and lamp.

5.1 Inhibition of the reduced amide inhibitors

As presented in section 4.2.1.2, none of the reduced amide inhibitors with a photocrosslinker competed with the binding of ABP **SV149** without irradiation. This was concluded from the competitive ABPP experiment where caspase-3 didn't show any reduction in activity after incubation with those inhibitors (Figures 4.10 and 4.12). This could be explained by the covalent nature of **SV149** that might outcompete the reversible inhibitors over time. However, the low potency was confirmed during substrate cleavage assays of inhibitors **15** and **17** with the fluorogenic Ac-DEVD-AMC substrate, where no reduction in the enzyme activity was detected, as judged from the increase in fluorescence over time, compared with the untreated caspase-3 (Figure 4.11). When the samples were irradiated, the benzophenone inhibitors **15** - **17** suddenly showed complete inhibition, with an IC_{50} below 100 nM for inhibitor **15**. Additionally, inhibition was also observed for inhibitor **15** in an apoptotic cell lysate (Figure 4.10), which suggested its possible use in more complex systems. Although they were clearly less potent, the diazirine inhibitors **18** - **19** still showed complete inhibition (Figure 4.12). This was initially attributed to the higher light sensitivity of diazirines compared to benzophenones, already causing partial crosslinker activation during handling of the inhibitors. The phenyl azide inhibitors **20** – **21** still didn't show any inhibition at all, and this observation was attributed to the reduction of the azide by the DTT present in the buffer. A reducing agent is required for caspase-3 activity, and even exchanging DTT for the milder β-mercapto ethanol did not lead to any improvements (Figure 4.13). Therefore, the phenyl azide inhibitors could not be evaluated in this manner.

Section 4.2.1.3 described the inhibition the inhibition of caspase-3 with reduced amide inhibitors containing furan as their crosslinker. All of them contained the crosslinker in a position N-terminal to the core structure of the inhibitor, because the crosslinking would proceed through the interaction with a lysine in the active site of caspase-3. The location of the lysine was revealed via a docking of core structure inhibitor **26** into the caspase-3 active site (Figure 4.14). The difference between all these inhibitors, **22** - **25** is an increasing distance between their core structures and furan moieties. As expected, the oxidation required for crosslinker activation proved to be problematic because of the highly abundant reducing agent, DTT, which completely counteracted the oxidizing effects of NBS. In the end, a solution was found by oxidizing the inhibitors

in a neutral buffer prior to the incubation with caspase-3. This was not expected to bias the results as the crosslinking comprised the formation of a stable aldehyde intermediate anyway. As before, without activation of the crosslinker, no inhibition was observed in competitive ABPP experiments, and a prior oxidation of the inhibitors led to complete inhibition (Figure 4.15).

All of the above described potent inhibitors with photocrosslinkers contain their crosslinker either N-terminal (**15**, **16**, and **18**) or C-terminal (**17** and **19**) of the core structure. This allows the investigation of the crosslinker position on their potency. While there seems to be some minor differences between them, overall, the observed potency is mostly unaffected by the location of the crosslinkers. This result was more or less expected, as photocrosslinking as a non-specific method where the crosslinker can insert into any X-H bond (X = C, N, O). Contrary to this, the furan crosslinker requires the presence of a nearby lysine or cysteine for its crosslinking, and it was expected that the distance between the core structure and the furan moiety would greatly affect the potency of inhibitors **22** – **25**. The fact that all of these furan-containing inhibitors displayed an equal potency was surprising to say the least, and the flexibility of the linkers connecting both components was reasoned to be the cause of this.

Next, the three inhibitors for GlpG will be discussed, as they have the same peptide bond mimic, a reduced amide, and contain benzophenone as their crosslinker. Hence, they can be directly compared to the results above. Inhibitor **30** had its crosslinker in the P6 position, which is directly N-terminal to the core structure. Both the other inhibitors, **31** and **32**, had their crosslinker positioned within the core structure, in the P2’ and P6’ positions respectively. To evaluate these inhibitors, competitive ABPP was once again the preferred method. In this case, FP-rhodamine, a general ABP for serine proteases, was used to label residual GlpG activity. Unlike caspase-3, GlpG activity was clearly influenced by UV irradiation, and a substantial reduction in labelling intensity by FP-rhodamine was detected. However, this residual signal proved to be of sufficient intensity to evaluate the inhibitors. Similar to the results of the benzophenone inhibitors for caspase-3, no inhibition of GlpG was detected without activating the crosslinkers. After irradiation, only inhibitor **32** displayed complete inhibition, while the others only caused a minor reduction in GlpG activity compared to the irradiated protease (Figure 4.30). This result was in stark contrast with the expectations and what

was observed for caspase-3, where the position of the photocrosslinker within the inhibitor structure didn't influence the activity. The low potency of inhibitors **30** and **31** could possible explained when evaluating the crosslinker position in more detail. Inhibitor **30** has its crosslinker in the P6-position, which has been suggested to reside outside of the active site of GlpG during cleavage and be exposed to the solvent, so it might not interact with GlpG [63]. For inhibitor **31**, the benzophenone is located in the P2' position, which is quite close to the cleavage site. The reasoning for this was the similarity to Phe, which is naturally present at that location in TatA. However, benzophenone has twice the size the S2' pocket of GlpG might not accommodate this residue, as supported by previously reported crystal structures of β-lactam inhibitors bound to GlpG [64].

5.2 Inhibition of the triazole inhibitors

In the case of the triazole peptide bond mimic, only two inhibitors, **28** and **29**, were synthesized. Both were equipped with a benzophenone crosslinker, as this previously provided inhibitors with the highest potency for the reduced amide inhibitors. When they were evaluated, the inhibitors themselves again displayed no inhibition. Unexpectedly, only inhibitor **29**, with the benzophenone located at the P2' position, inhibited caspase-3 after irradiation, and inhibitor **28** did not (Figure 4.16). A tenfold increase in concentration only slightly improved those results. This difference in potency compared with the reduced amides could be explained by the structural differences. The size of triazoles is larger than both reduced amides and peptide bonds, which could result in a steric clash. Additionally, the conformational restriction imposed by the triazole might not be accepted by the active site of caspase-3 or proteases in general. This hypothesis is supported by a recent study that used substrate-derived triazole peptides as inhibitors for cathepsins, a family of cysteine proteases, where only very weak inhibition was observed [65].

5.3 Identification of the inhibitor-protease complexes

Identification of the complex formed between protease and inhibitor would further support the possible use of the inhibitors as photoactivatable affinity-based probes. However, while direct labelling experiments revealed the existence of a covalent complex between caspase-3 and control ABP **33** after incorporation of a fluorophore via click chemistry, that same complex surprisingly could not be detected with any of the synthesized benzophenone, diazirine, and furan inhibitors. Only in some cases, benzophenone inhibitors **15** and **16** and furan inhibitors **22** and **25**, were bands detected at a molecular weight corresponding to the active caspase-3 dimer, without prior denaturation of the samples (Figure 4.19). Under these conditions, a stable but reversible complex would remain intact. The same result was obtained for GlpG inhibitor **32** (Figure 4.31), which hints at a similar mechanism of action for the inhibitors of both proteases. Contrary to the expected irreversible covalent inhibition with the photocrosslinkers, this suggested a mechanism of action that relies on a reversible or non-covalent interaction between the inhibitors and proteases. This was supported by ESI-MS and MALDI-MS experiments on purified caspase-3, where a mass shift of the large subunit was detected with control ABP **SV149**, but no mass shift, either of the small subunit or the large subunit, was detected with inhibitors **15**, **17**, **19**, and **22b** (Figures 4.20 and 4.21).

5.4 Elucidation of the mechanism of inhibition

The results from the direct labelling experiments suggested that the crosslinkers might not actually behave as such for the synthesized inhibitors, as no covalent complex with the target proteases could be detected after their activation. To prove this, preactivation experiments similar to the competitive ABPP for the furan inhibitors, where the crosslinkers were activated prior to incubation with caspase-3, were performed. If the inhibitors crosslink to caspase-3, there should not be any detection of inhibition using this approach, because the reactive intermediates of the photocrosslinkers (either a biradical for the benzophenone or a carbene for the diazirine) are short-lived species. Surprisingly, inhibition was still observed for the benzophenone and diazirine inhibitors without reduction of the previously observed potency, actually proving that the crosslinkers don't bind to caspase-3. Additionally, the neglected phenyl azide inhibitors, **20** and **21**, were also evaluated in this manner. They previously couldn't be evaluated because of the crosslinker being incompatible with DTT, but this approach allowed the crosslinker to be activated in the absence of DTT. Similar to the other reduced amide inhibitors, these now also inhibited caspase-3 with a potency similar to the benzophenone inhibitors. The same experiment was also performed with triazole inhibitor **29**, but this time no inhibition was observed (Figure 4.22). This suggested a structural modification of the inhibitors upon photocrosslinker activation that involves the reduced amide peptide bond mimic. As the furan crosslinker forms a stable intermediate upon activation, the same conclusion could not be made for those inhibitors, although the mechanism of inhibition is probably the same for all reduced amide inhibitors.

For the suggested structural modification of the inhibitors, two possibilities were considered. An intermolecular reaction, where the crosslinker would interact with a different molecule, was proposed but deemed unlikely, as this would lead to a substantial increase in size and no longer result in a substrate-derived inhibitor. LC-MS data of inhibitors **15** and **17** before and after irradiation revealed no change in mass and retention time, so the idea of an intermolecular interaction was quickly rejected. In intramolecular cyclization was still possible because this doesn't result in a mass change. This was further supported by the observation that irradiation of the diazirine and phenyl azide inhibitors only resulted in the loss of expected loss of nitrogen, which points towards a cyclization in favor of a reaction with water (Figure 4.23). However,

cyclizations usually go hand in hand with a change in retention time, which wasn't observed for the benzophenone inhibitors. The cyclization route was finally abandoned after MS-MS fragmentation only revealed the existence of a linear compound (Figure 4.24).

To ultimately exclude the occurance of an inter- or intramolecular reaction, competitive ABPP was performed with two inhibitors, **26** and **27**, not containing a crosslinker. By themselves, they didn't display any inhibition of caspase-3, even upon irradiation. Addition of benzophenone still didn't lead to inhibition, but irradiation of this sample suddenly completely inhibited caspase-3 (Figre 4.25). This proved that both irradiation and the presence of benzophenone are crucial for efficient inhibition of the inhibitors, but that the core structure and the crosslinker don't need to be present in the same molecule. This suggested that a modification of the structure, imposed by the activation of the crosslinker, resulted in a potent inhibitor. As the previous LC-MS data didn't reveal any structural changes, only a minor fraction of the inhibitors would be converted, resulting in a highly potent active species. This was supported by a dialysis experiment intended to reveal the reversible nature of the inhibition. After inhibition, removal of the excess inhibitor did not cause caspase-3 to regain its activity, revealing the existence of a very stable complex between inhibitor and protease (Figure 4.26).

An oxidation of the reduced amide, induced by benzophenone activation, was proposed. This would first lead to the formation of an imine, which further reacts with water to a C-terminal aldehyde (Figure 4.27). This type of oxidation has been reported before [66], and would result here in small quantities of highly potent peptide aldehydes [67]. With this in mind, the previous LC-MS data was now scanned for the masses of the respective peptide aldehydes. While those masses couldn't be detected in the data of the non-irradiated samples, it was clearly present in the irradiated samples of the benzophenone and phenylazide inhibitors (Figure 4.28). The fact that it wasn't detectable in the samples with the diazirine inhibitors could explain the lower potency of those inhibitors compared to the other photocrosslinkers, meaning that the aldehyde might still be formed, but that it is below the detection limit in the data. The formation of the peptide aldehydes as inhibitory species was further confirmed after experiments where the inhibitors were treated with sodium bisulfite after crosslinker activation. This reacts with the peptide aldehydes to form stable bisulfite adducts, leaving them unable

to inhibit. The benzophenone, phenylazide, and core structure inhibitors lost all of their ability to inhibit caspase-3 after bisulfite treatment (Figure 4.29).

The formation of small quantities of peptide aldehyde upon crosslinker activation also explained most of the results observed for caspase-3 until this point. The absence of inhibition in the preactivation experiments of the triazole inhibitors and their much lower potency could be explained by the occurrence of a different (unknown) mechanism of inhibition. The interaction between aldehydes and cysteine or serine proteases is stable but reversible, and this explained why caspase-3 could only be labelled by the inhibitors when the samples were not denatured. The lower potency of the diazirine inhibitors could be attributed to a much less efficient oxidation. The furan inhibitors most likely employ the same mechanism, as this would explain the independency of the crosslinker position on their potency. Unfortunately, this cannot be confirmed with the bisulfite experiment, because crosslinker activation generates an aldehyde as well. To confirm that the observed inhibition is not due to crosslinking, the furan moiety could be selectively oxidized followed by a repeat of the competitive ABPP experiment, and a sudden drop in potency or dependency on crosslinker position would indicate exactly that.

In the case of the GlpG inhibitors, the results of the direct labelling support the formation of a peptide aldehyde. On the other hand, the dependency on the position of the benzophenone opposes this. After all, after oxidation to the peptide aldehyde, there should be no structural differences between inhibitors **31** and **32**, but only the latter successfully inhibits GlpG. Further experiments will reveal if the nature of this inhibition is the same as for the caspase-3 inhibitors.

6 Summary and outlook

In this work, a general strategy was explored for the construction of selective chemical probes targeting proteases. There was a need for this, because up until now, a whole range of chemical probes have been designed for all different kinds of proteases. However, the synthetic strategies to obtain them differ greatly.

The design of the probes pursued here exploited the substrate specificity of proteases and included the preferred amino acid residues around the scissile peptide bond in the structure. The scissile peptide bond itself was replaced with an uncleavable mimic. This way, the selectivity of the protease for its substrate is retained within the probe while it cannot be processed. Two mimics were discussed in this work: (1) a reduced amide, which is similar in size but differs in the electronic properties and conformational flexibility. (2) A triazole retains the dipole moment of a peptide bond, but is larger in size and conformationally more restricted. Both of these mimics can be conveniently synthesized on solid support after preparation of certain amino acid derivatives as building blocks in solution. The synthetic procedures to obtain these building blocks have been optimized to be compatible with most amino acids. In addition to these specificity elements, crosslinkers were introduced for covalent linkage to the protease. Lastly, an N-terminal alkyne handle would allow detection of the generated complex, allowing their use as chemical probes.

The unexpected finding of photoactivatable, reversible inhbibitors for the soluble cysteine protease caspase-3 is presented using the described approach. In contrast to the expectations, no covalent complex between the synthesized compounds and caspase-3 could originally be detected. However, they still served as inhibitors, but only after activation of their crosslinkers. It also turned out that the reduced amide inhibitors displayed a much higher potency compared to their triazole counterparts. Additionally, it appeared that in some cases a covalent complex was formed after all, but it could only be detected with SDS-PAGE and without denaturing the evaluated samples. The complex was detected only for the reduced amide inhibitors, and within this group only for inhibitors containing a benzophenone or furan crosslinker. This suggested a reversible mechanism of inhibition, in which the irreversible crosslinking plays no direct role. This was confirmed in experiments in which the inhibitor and

crosslinker (benzophenone), were not part of the same molecule, but where inhibition was still observed upon crosslinker activation.

The nature of the active species was still elusive at this point, as the original inhibitor structure was not expected to be strong enough to outcompete the covalent activity-based probe during the competitive ABPP experiments that were used to evaluate the potency. As such, a small structural modification of the inhibitors was proposed upon crosslinker activation, namely the oxidation of the reduced amide to the corresponding imine. After hydrolysis by solvent water molecules, this would generate a highly potent C-terminal peptide aldehyde. This hypothesis seemed plausible, as the highest potencies were observed for the furan inhibitors, where activation of the crosslinker relies on oxidation, and the benzophenone inhibitors, which have previously been reported as photosensitizers in the oxidation of amines. The formation of the peptide aldehyde was ultimately proven in experiments with sodium bisulfite, which can form adducts with aldehydes, rendering them unable to inhibit. After treating the activated inhibitor with sodium bisulfite, complete recovery of the activity of caspase-3 was observed, confirming the presence of an aldehyde as the active inhibitor species.

Aside from caspase-3, inhibitors containing a benzophenone crosslinker were also synthesized for the intramembrane serine protease GlpG. Similar to the results for caspase-3, there was no detection of a covalent complex despite complete inhibition of GlpG. Although this suggests a similar mechanism of inhibition, this has not yet been confirmed, and further experiments, similar to the ones described for the caspase-3 inhibitors are required. The most important ones will be the sodium bisulfite experiment and the synthesis of GlpG inhibitors with different or without crosslinkers to compare their potency.

The unexpected finding of photo-induced oxidation of caspase-3 targeting inhibitors that can lead to the formation of a potent peptide aldehyde is reported. In the future, this strategy could be expanded to other proteases, producing selective inhibitors for many proteases of different classes. Because of the inhibitor design, proteases could be selectively targeted in complex systems, where they could be inhibited at a specific time and location. As a result, this type of inhibitors may be used in the photopharmacological study of protease function.

7 Zusammenfassung

Für eine Menge von verschiedensten Proteasen wurden bereits chemische Liganden, die deren Aktivität verändern, entwickelt. Die Methodik zur Herstellung dieser Liganden unterscheidet sich jedoch erheblich. In dieser Arbeit sollte eine generelle Methode entwickelt werden, welche es erlaubt ein breites Spektrum von spezifischen, selektiven chemischen Liganden herzustellen. Dabei wurde die Substratspezifität der Proteasen ausgenutzt und die Aminosäuresequenz, welche die Hydrolysierungsposition im Molekül markiert, mit dem chemischen Liganden verknüpft. Des Weiteren wurde die genaue Schnittstelle durch eine unspaltbare Sequenz ersetzt, sodass die Protease zwar binden, die Hydrolyse aber nicht durchführen kann. In dieser Arbeit wurden zwei solcher unspaltbaren Ersatzsequenzen als mögliche Kandidaten diskutiert. Die erste beinhaltet ein reduziertes Amid, welches der Größe der Originalsequenz ähnelt, aber andere elektrochemische Eigenschaften sowie Konformitätsflexibilität aufweist. Die zweite besteht aus einem Triazol, welches das Dipolmoment einer Peptidbindung besitzt, aber größer als die Originalsequenz und in ihrer Konformität eingeschränkter ist. Beide Ersatzsequenzen können, nachdem die Grundbausteine in Lösung hergestellt wurden, in einem Festphasensystem synthetisiert werden. Als weiterer Baustein wurde ein Crosslinker verwendet der nach Bindung der Protease eine kovalente Bindung vermittelt und somit das Enzym permanent an den chemischen Liganden bindet. Zudem kann mittels einer eingebauten Alkyne-Gruppe ein Signalmolekül angeknüpft werden, welches eine nachträgliche Detektion von gebundenen Liganden ermöglicht.

Mit dem beschriebenen Ansatz konnte in dieser Arbeit ein photoaktivierbarer, reversibler Inhibitor für die lösliche Cystein-Protease Caspase-3 entwickelt werden. Entgegen der Erwartungen konnte kein kovalent gebundener Komplex festgestellt werden, jedoch zeigten alle synthetisierten Verbindungen eine inhibitorische Aktivität, nachdem der Crosslinker aktiviert wurde. Dabei zeigten die Verbindungen mit reduziertem Amid deutlich höhere Inhibitoraktivität als die entsprechenden Triazol-beinhaltenden Verbindungen. In Abhängigkeit des Crosslinkers konnte für einige reduzierte Amidverbindungen eine kovalent Bindung zur Protease festgestellt werden, wenn der Crosslinker ein Furan oder ein Benzophenon war. Dies indiziert einen reversiblen Inhibitionsmechanismus, in der die irreversible Crosslink-Verknüpfunk keine direkte Rolle spielt. Dies konnte bestätigt werden, indem das Experiment mit

dem Inhibitor und dem Crosslinker als getrennte Moleküle wiederholt wurde und ein inhibitorischer Effekt nach Aktivierung des Crosslinkers deutlich messbar war.

Da nicht erwartet wurde, dass der chemische Ligand in seiner ursprünglichen Struktur den kovalent bindenden aktivierbaren Liganden in seiner inhibitorischen Aktivität übertreffen würde, wurde die chemische Struktur des reduzierten Amids leicht verändert, wodurch nach der Crosslinkeraktivierung das reduzierte Amid zu einem Imine oxidiert wird. Dieses autohydrolysiert in wässriger Umgebung, wodurch ein reaktives, C-terminales Peptidaldehyd entsteht. Diese Reaktionsabfolge erscheint plausibel, da die höchste Inhibitoraktivität für die Furan-Crosslinker, deren Aktivierung auf Oxidation beruht, und für die Benzophenon-Crosslinker, die als Photosensibiliatoren in der Oxdiation von Aminen genutzt werden, gezeigt wurde. Die Bildung des Peptidaldehyds und die Bedeutung für die Inhibition konnte bewiesen werden, indem nach einer Reaktion mit Natriumhydrogensulfit, welches mit Aldehyden reagiert, die inhibitorische Aktivität der Verbindung nicht mehr nachgewiesen werden konnte und die Proteaseaktivität der Caspase-3 wieder vollständig hergestellt wurde.

Des Weiteren wurden Inhibitoren mit Benzophenon-Crosslinker für die Intramembran-Serine-Protease GlpG synthetisiert. Ähnlich wie bei den Caspase-3-Inhibitoren konnten auch hier keine kovalenten Komplexe trotz vollständiger Inhibition der GlpG-Proteaseaktivität festgestellt werden. Auch wenn ein ähnlicher Mechanismus wie bei der Caspase-3-Inhibiton wahrscheinlich ist, sind hier weitere Experimente zur Verifizierung notwendig.

Zusammenfassend lässt sich sagen, dass die unerwartete Beobachtung der photoinduzierten Oxidation, die ein stark inhibierendes Peptidaldehyd an einer spezifischen Stelle generiert, neue Möglichkeiten zur Untersuchung von Proteasen für pharmakologische Zwecke eröffnet.

8 References

1. Turk, B., *Targeting proteases: successes, failures and future prospects.* Nat. Rev. Drug Discovery, 2006. **5**: p. 785-799.
2. M. Verdoes, S.H.L.V., *Detection of protease activity in cells and animals.* Biochim Biophys Acta. , 2016. **1864**(1): p. 130-42.
3. Salvesen, G.S., *Caspases and apoptosis.* Essays Biochem., 2002. **38**: p. 9-19.
4. J. P. Jr. Riddel, B.E.A., C. Miaskowski, D. P. Lillicrap., *Theories of blood coagulation.* J Pediatr Oncol Nur, 2007. **24**(3): p. 123-31.
5. Chakrabarty S, K.J., van de Plassche MAT, Vanhoutte R, Verhelst SHL., *Recent Advances in Activity-Based Protein Profiling of Proteases.* Curr Top Microbiol Immunol., 2019. **420**: p. 253-281.
6. Jennifer L. Harris, B.J.B., Francesco Leonetti, Sami Mahrus, Jonathan A. Ellman, and Charles S. Craik, *Rapid and general profiling of protease specificity by using combinatorial fluorogenic substrate libraries.* Proc Natl Acad Sci U S A, 2000. **97**(14): p. 7754-9.
7. al., D.R.B.e., *Familial Alzheimer's Disease–Linked Presenilin 1 Variants Elevate Ab1–42/1–40 Ratio In Vitro and In Vivo.* Neuron, 1996. **17**(5): p. 1005-13.
8. He, G., et al., *Gamma-secretase activating protein is a therapeutic target for Alzheimer's disease.* Nature, 2010. **467**(7311): p. 95-8.
9. Sibley, L.D., *The roles of intramembrane proteases in protozoan parasites.* Biochim. Biophys. Acta, Biomembr., 2013. **1828**: p. 2908-2915.
10. Baldwin, M., et al., *Plasmodium falciparum signal peptide peptidase cleaves malaria heat shock protein 101 (HSP101). Implications for gametocytogenesis.* Biochem Biophys Res Commun, 2014. **450**(4): p. 1427-32.
11. M. Drag, G.S.S., *Emerging principles in protease-based drug discovery.* Nat. Rev. Drug Discovery, 2010. **9**: p. 690-701.
12. Szecsi, P.B., *The aspartic proteases.* Scand J Clin Lab Invest Suppl., 1992. **210**: p. 5-22.
13. Masao Fujinaga, M.M.C., Hiroshi Oyama, Kohei Oda, and Michael N. G. James, *The molecular structure and catalytic mechanism of a novel carboxyl peptidase from Scytalidium lignicolum.* Proc Natl Acad Sci U S A, 2004. **101**(10): p. 3364-9.
14. N. D. Rawlings, A.J.B., *Evolutionary families of metallopeptidases.* Methods Enzymol., 1995. **248**: p. 183-228.
15. Rawlings ND, B.A., *Families of cysteine peptidases.* Methods Enzymol., 1994. **244**: p. 461-86.
16. Rawlings ND, B.A., *Families of serine peptidases.* Methods Enzymol., 1994. **244**: p. 19-61.
17. Brannigan JA, D.G., Duggleby HJ, Moody PC, Smith JL, Tomchick DR, Murzin AG., *A protein catalytic framework with an N-terminal nucleophile is capable of self-activation.* Nature, 1995. **378**(6555): p. 416-9.
18. Rawlings, N.D., A.J. Barrett, and A. Bateman, *Asparagine peptide lyases: a seventh catalytic type of proteolytic enzymes.* J Biol Chem, 2011. **286**(44): p. 38321-8.
19. Fujinaga M, C.M., Tarasova NI, Mosimann SC, James MN., *Crystal structure of human pepsin and its complex with pepstatin.* Protein Sci., 1995. **4**(5): p. 960-72.
20. Verma RP, H.C., *Matrix metalloproteinases (MMPs): chemical-biological functions and (Q)SARs.* Bioorg Med Chem., 2007. **15**(6): p. 2223-68.
21. Sinisa Urban, J.R.L., and Matthew Freeman, *Drosophila Rhomboid-1 Defines a Family of Putative Intramembrane Serine Proteases.* Cell, 2001. **107**: p. 173-182.
22. Freeman, M., *The rhomboid-like superfamily: molecular mechanisms and biological roles.* Annu Rev Cell Dev Biol, 2014. **30**: p. 235-54.
23. Wang, Y., Y. Zhang, and Y. Ha, *Crystal structure of a rhomboid family intramembrane protease.* Nature, 2006. **444**(7116): p. 179-80.
24. Russell, C.W., et al., *The Rhomboid Protease GlpG Promotes the Persistence of Extraintestinal Pathogenic Escherichia coli within the Gut.* Infect Immun, 2017. **85**(6).

25. M. T. N. Nguyen, T.V.K., S. H. L. Verhelst, *Chemical Tools for the Study of Intramembrane Proteases.* ACS Chemical Biology, 2015. **10**(11): p. 2423-2434.
26. Schechter, I., and Berger, A., *On the size of the active site in proteases. I. Papain.* Biochem. Biophys. Res. Commun., 1967. **27**: p. 157-162.
27. Nguyen MTN, S.G., Zahedi RP, Verhelst SHL, *Protease Specificity Profiling in a Pipet Tip Using "Charge-Synchronized" Proteome-Derived Peptide Libraries.* J Proteome Res. , 2018. **17**(5): p. 1923-33.
28. P. L. Meisenheimer, M.A.O.B., and J. J. Cali, *Luminogenic enzyme substrates: the basis for a new paradigm in assay desing.* Promega - Enzyme Assays, 2008(22).
29. Heal, W.P., T.H. Dang, and E.W. Tate, *Activity-based probes: discovering new biology and new drug targets.* Chem Soc Rev, 2011. **40**(1): p. 246-57.
30. Serim, S., U. Haedke, and S.H. Verhelst, *Activity-based probes for the study of proteases: recent advances and developments.* ChemMedChem, 2012. **7**(7): p. 1146-59.
31. Powers JC, A.J., Ekici OD, James KE., *Irreversible inhibitors of serine, cysteine, and threonine proteases.* Chem Rev., 2002. **102**(12): p. 4639-750.
32. Speers, A.E. and B.F. Cravatt, *Profiling enzyme activities in vivo using click chemistry methods.* Chem Biol, 2004. **11**(4): p. 535-46.
33. Yang, Y., X. Yang, and S. Verhelst, *Comparative Analysis of Click Chemistry Mediated Activity-Based Protein Profiling in Cell Lysates.* Molecules, 2013. **18**(10): p. 12599-12608.
34. P. P. Geurinck, L.M.P., G. A. van der Marel, R. Bischoff, H. S. Overkleeft, *Photoaffinity Labeling in Activity-Based Protein Profiling.* Top. Curr. Chem., 2011. **324**: p. 85-113.
35. Saghatelian A, J.N., Joseph A, Humphrey M, Cravatt BF., *Activity-based probes for the proteomic profiling of metalloproteases.* Proc Natl Acad Sci U S A., 2004. **101**(27): p. 10000-5.
36. Leeuwenburgh MA, G.P., Klein T, Kauffman HF, van der Marel GA, Bischoff R, Overkleeft HS., *Solid-phase synthesis of succinylhydroxamate peptides: functionalized matrix metalloproteinase inhibitors.* Org Lett., 2006. **8**(8): p. 1705-8.
37. Cravatt, B.F., A.T. Wright, and J.W. Kozarich, *Activity-based protein profiling: from enzyme chemistry to proteomic chemistry.* Annu Rev Biochem, 2008. **77**: p. 383-414.
38. Kasperkiewicz, P., et al., *Emerging challenges in the design of selective substrates, inhibitors and activity-based probes for indistinguishable proteases.* FEBS J, 2017. **284**(10): p. 1518-1539.
39. Sanman LE, B.M., *Activity-based profiling of proteases.* Annu Rev Biochem., 2014. **83**: p. 249-73.
40. Haedke U, K.E., Vosyka O, Yang Y, Verhelst SH., *Tuning probe selectivity for chemical proteomics applications.* Curr Opin Chem Biol., 2013. **17**(1): p. 102-9.
41. Greenbaum D, M.K., Burlingame A, Bogyo M., *Epoxide electrophiles as activity-dependent cysteine protease profiling and discovery tools.* Chem Biol., 2000. **7**(8): p. 569-81.
42. Kato D, B.K., Berger AB, Nazif T, Blum G, Ryan C, Chehade KA, Salvesen GS, Bogyo M., *Activity-based probes that target diverse cysteine protease families.* Nat Chem Biol. , 2005. **1**(1): p. 33-8.
43. Barglow, K.T. and B.F. Cravatt, *Discovering disease-associated enzymes by proteome reactivity profiling.* Chem Biol, 2004. **11**(11): p. 1523-31.
44. Xue, Y. and Y. Ha, *Catalytic mechanism of rhomboid protease GlpG probed by 3,4-dichloroisocoumarin and diisopropyl fluorophosphonate.* J Biol Chem, 2012. **287**(5): p. 3099-107.
45. Thornberry NA, R.T., Peterson EP, Rasper DM, Timkey T, Garcia-Calvo M, Houtzager VM, Nordstrom PA, Roy S, Vaillancourt JP, Chapman KT, Nicholson DW., *A combinatorial approach defines specificities of members of the caspase family and granzyme B. Functional relationships established for key mediators of apoptosis.* J Biol Chem. , 1997. **272**(29): p. 17907-11.
46. Schilling O, O.C., *Proteome-derived, database-searchable peptide libraries for identifying protease cleavage sites.* Nat Biotechnol., 2008. **26**(6): p. 685-94.
47. Timmer JC, Z.W., Pop C, Regan T, Snipas SJ, Eroshkin AM, Riedl SJ, Salvesen GS., *Structural and kinetic determinants of protease substrates.* Nat Struct Mol Biol. , 2009. **16**(10): p. 1101-8.

48. Halila S, V.T., Clercq PD, Madder A., *Fine-tuning furan toxicity: fast and quantitative DNA interchain cross-link formation upon selective oxidation of a furan containing oligonucleotide.* Chem Commun (Camb). 2005(7): p. 936-8.
49. Kleiner, P., et al., *A Whole Proteome Inventory of Background Photocrosslinker Binding.* Angew Chem Int Ed Engl, 2017. **56**(5): p. 1396-1401.
50. Angell YL, B.K., *Peptidomimetics via copper-catalyzed azide-alkyne cycloadditions.* Chem Soc Rev., 2007. **36**(10): p. 1674-89.
51. Szelke M, L.B., Hallett A, Jones DM, Sueiras J, Atrash B, Lever AF., *Potent new inhibitors of human renin.* Nature, 1982. **299**(5883): p. 555-7.
52. Tong L, P.S., Pargellis C, Dô F, Lamarre D, Anderson PC., *Crystal structure of human immunodeficiency virus (HIV) type 2 protease in complex with a reduced amide inhibitor and comparison with HIV-1 protease structures.* Proc Natl Acad Sci U S A., 1993. **90**(18): p. 8387-91.
53. Van Kersavond T, K.R., Chakrabarty S, Blank-Landeshammer B, Sickmann A, Verhelst SHL, *Short Peptides with Uncleavable Peptide Bond Mimetics as Photoactivatable Caspase-3 Inhibitors.* Molecules, 2019. **24**(1).
54. Punna S, F.M., *A convenient colorimetric test for aliphatic azides.* Synlett, 2008. **1**: p. 99-100.
55. Stennicke HR, S.G., *Caspases: preparation and characterization.* Methods, 1999. **17**(4): p. 313-9.
56. Robert Pascal, R.S., *Preservation of the protective group under alkaline conditions by using CaCl2. Applications in peptide synthesis.* Tetrahedron Letters, 1998. **39**(28): p. 5031-4.
57. Goddard-Borger ED, S.R., *An efficient, inexpensive, and shelf-stable diazotransfer reagent: imidazole-1-sulfonyl azide hydrochloride.* Org Lett. , 2007. **9**(19): p. 3797-800.
58. Seyferth D, M.R., Hilbert P, *Reactions of Dimethylphosphono-Substituted Diazoalkanes—(Meo)2P(O)CR Transfer to Olefins and 1,3-Dipolar Additions of (Meo)2P(O)C(N2)R.* J. Org. Chem., 1971. **36**(1379-86).
59. Gilbert JC, W.U., *Diazoethenes—Their Attempted Synthesis from Aldehydes and Aromatic Ketones by Way of the Horner-Emmons Modification of the Wittig Reaction—A Facile Synthesis of Alkynes.* J. Org. Chem., 1982. **47**: p. 1837-45.
60. Jepsen, T.H. and J.L. Kristensen, *In situ generation of the Ohira-Bestmann reagent from stable sulfonyl azide: scalable synthesis of alkynes from aldehydes.* J Org Chem, 2014. **79**(19): p. 9423-6.
61. Rushia A. Turner, A.G.O., and R. Scott Lokey, *Click Chemistry as a Macrocyclization Tool in the Solid-Phase Synthesis of Small Cyclic Peptides.* Org. Lett., 2007. **9**(24): p. 5011-4.
62. Berger, A.B., et al., *Identification of Early Intermediates of Caspase Activation Using Selective Inhibitors and Activity-Based Probes.* Molecular Cell, 2006. **23**(4): p. 509-521.
63. Zoll, S., et al., *Substrate binding and specificity of rhomboid intramembrane protease revealed by substrate-peptide complex structures.* EMBO J, 2014. **33**(20): p. 2408-21.
64. Wolf, E.V. and S.H. Verhelst, *Inhibitors of rhomboid proteases.* Biochimie, 2016. **122**: p. 38-47.
65. Galibert, M., et al., *Substrate-derived triazolo- and azapeptides as inhibitors of cathepsins K and S.* Eur J Med Chem, 2018. **144**: p. 201-210.
66. Davidson, R.F.B.a.R.S., *The photosensitised oxidation of amines. Part I. The use of benzophenone as a sensitiser.* 1971: p. 2342-6.
67. RC., T., *Peptide aldehydes: potent inhibitors of serine and cysteine proteases.* Methods Enzymol. , 1977. **46**: p. 220-5.

9 Supplementary information

9.1 List of NMR spectra

Compound **1**:

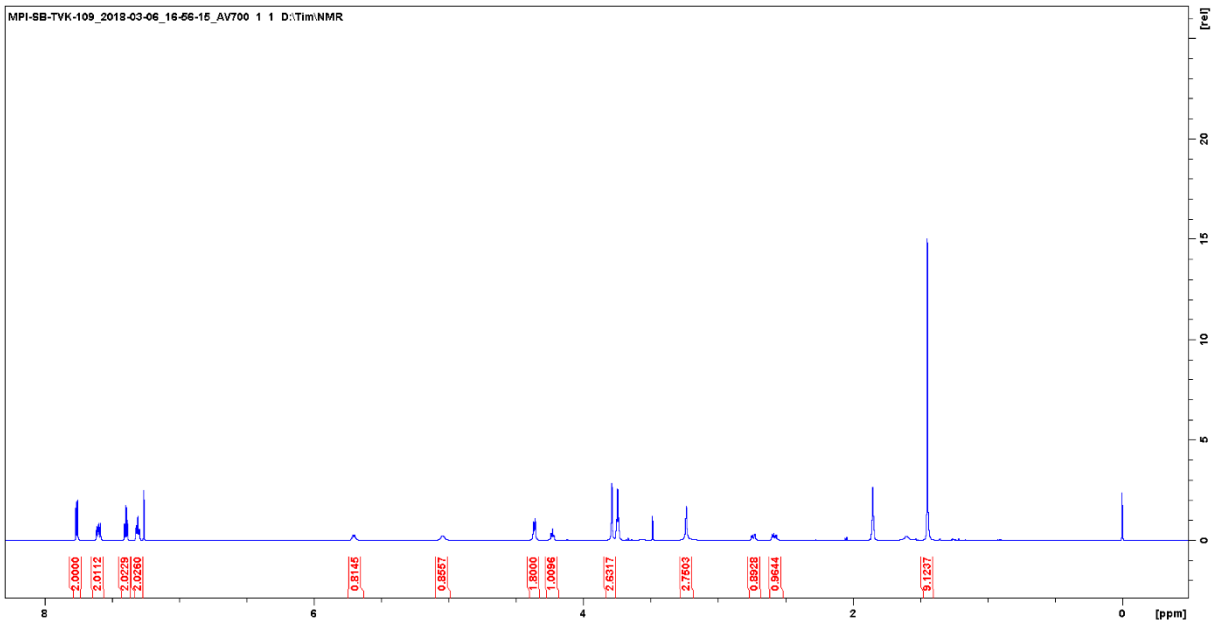

^{1}H NMR

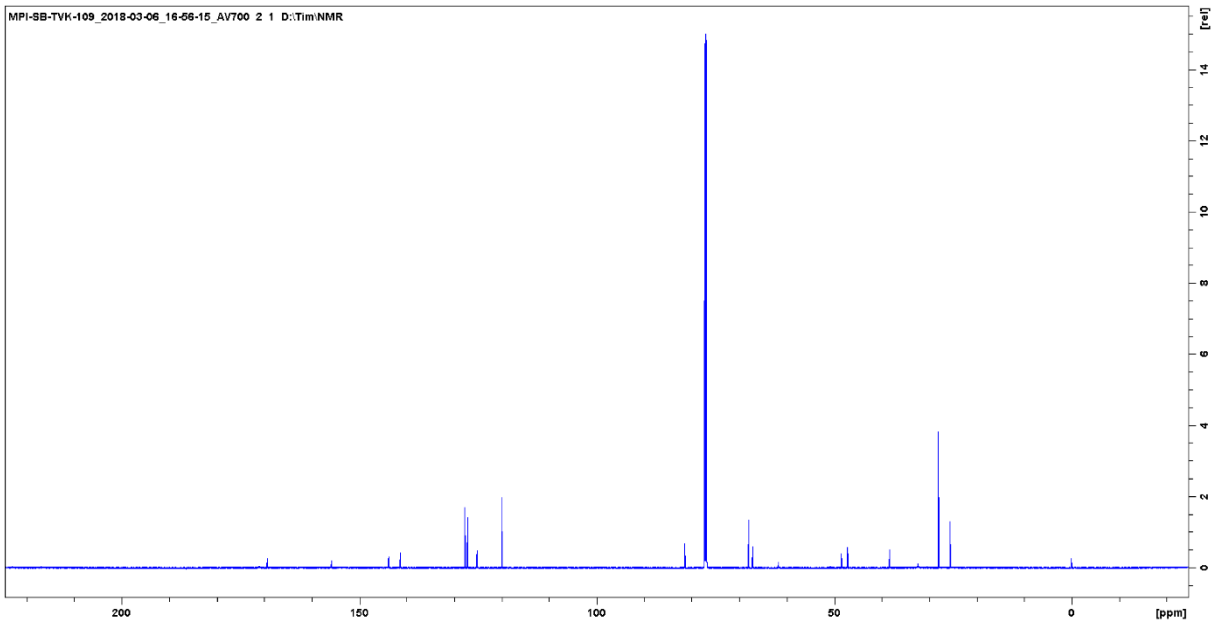

^{13}C NMR

Compound **2**:

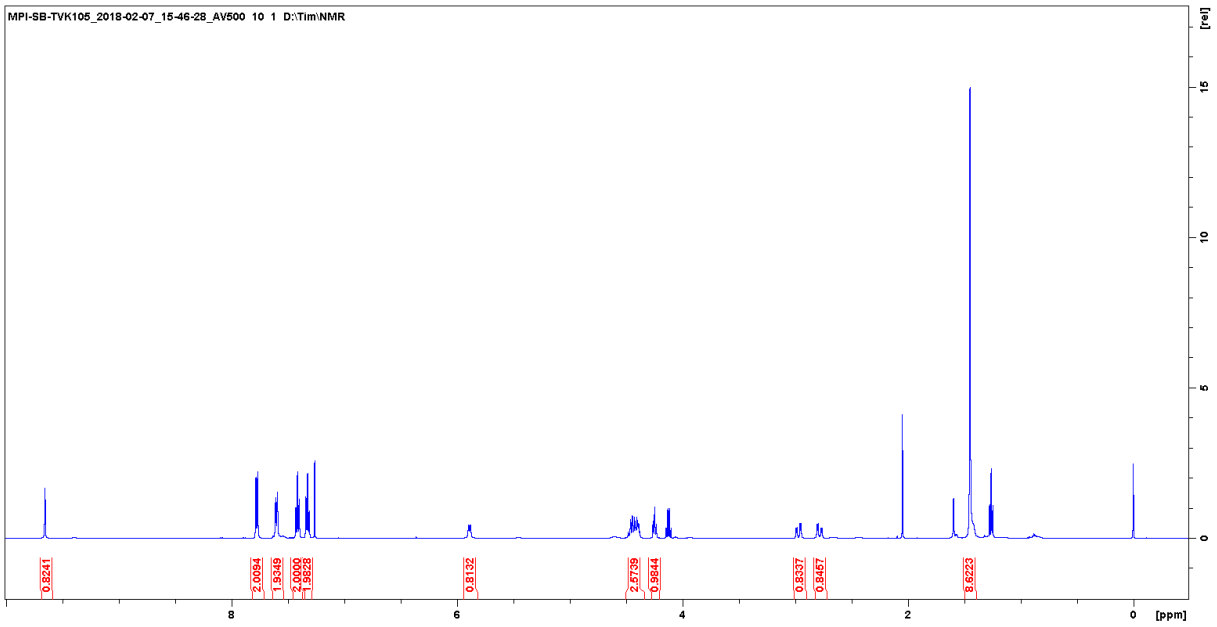

^{1}H NMR

Compound **5**:

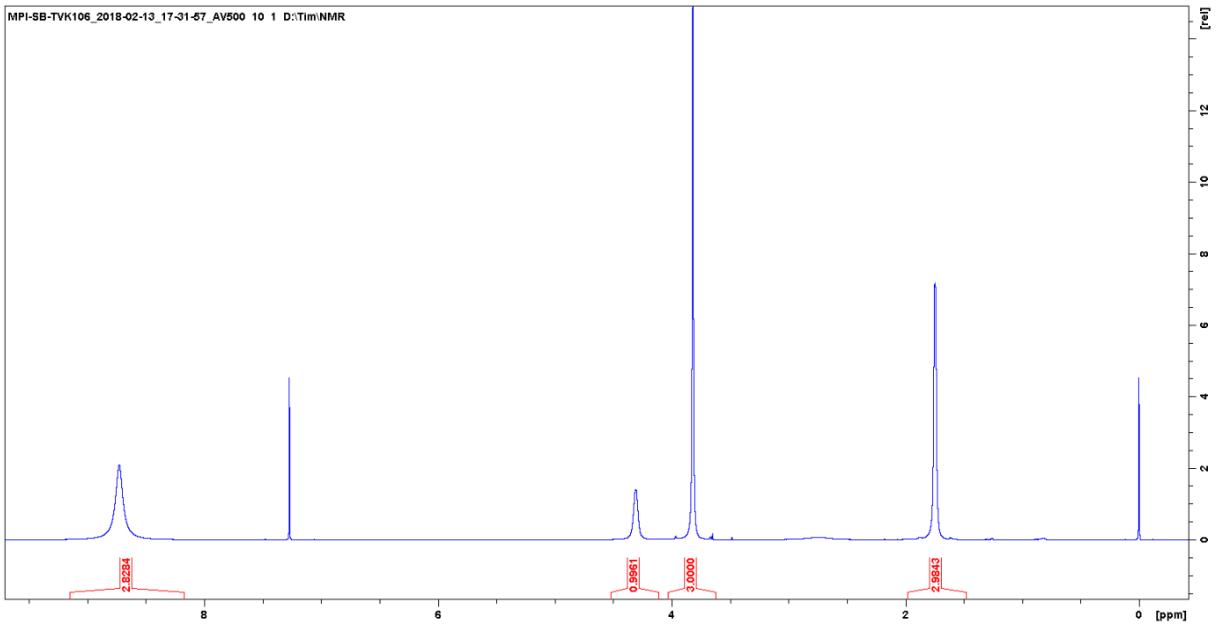

^{1}H NMR

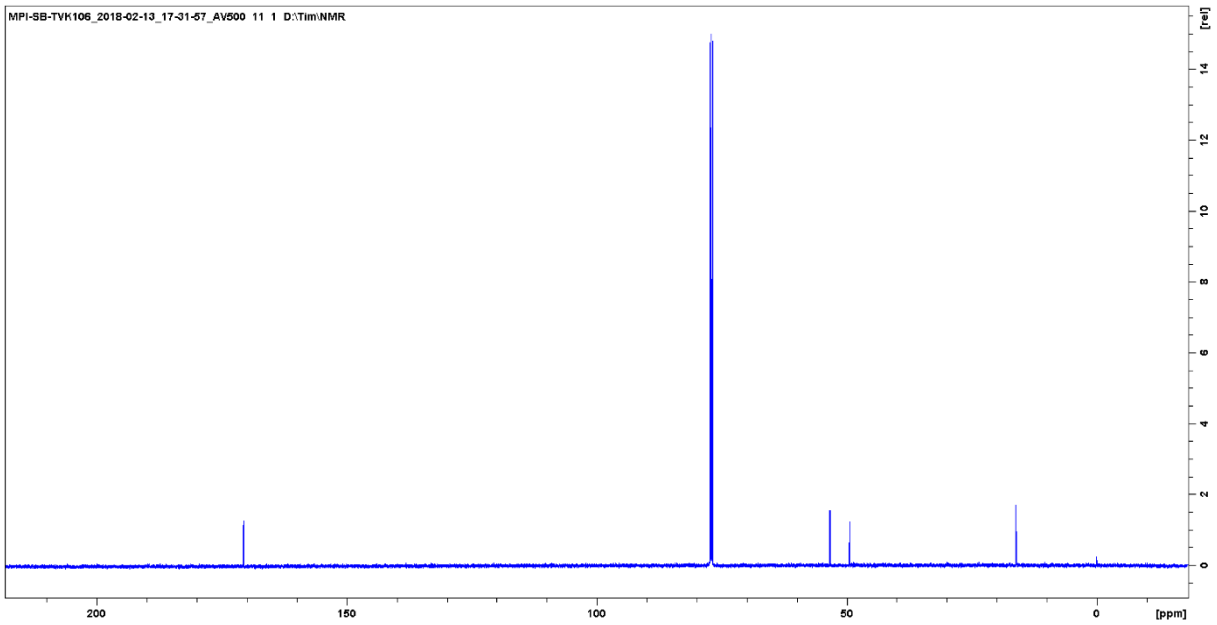

^{13}C NMR

Compound **6**:

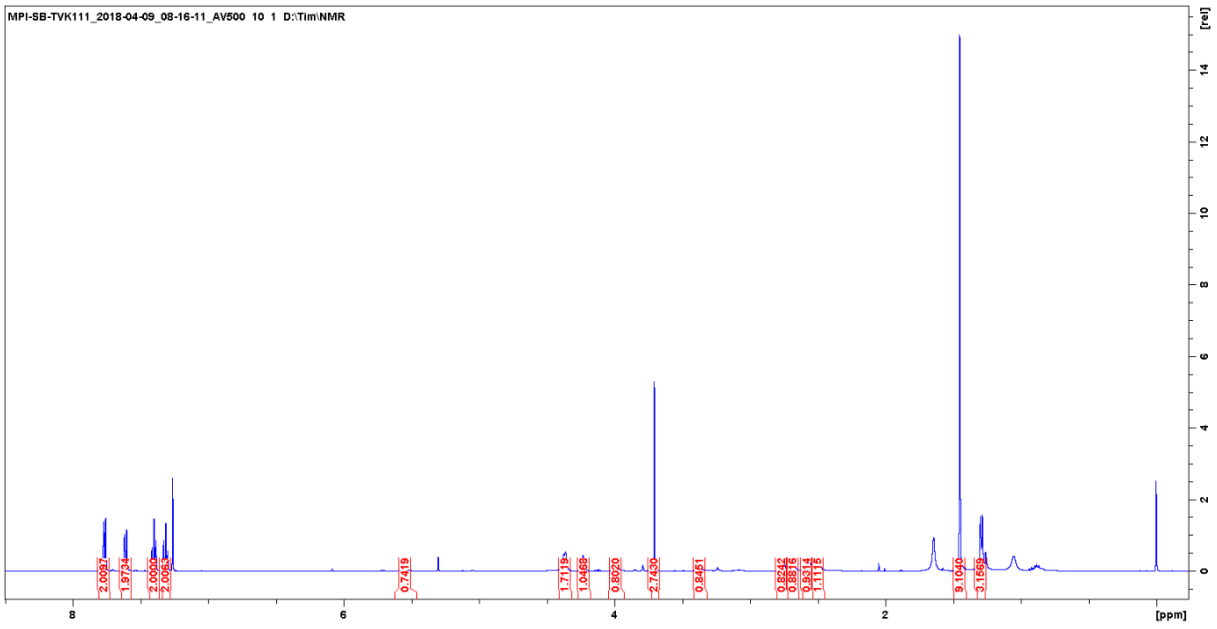

^{1}H NMR

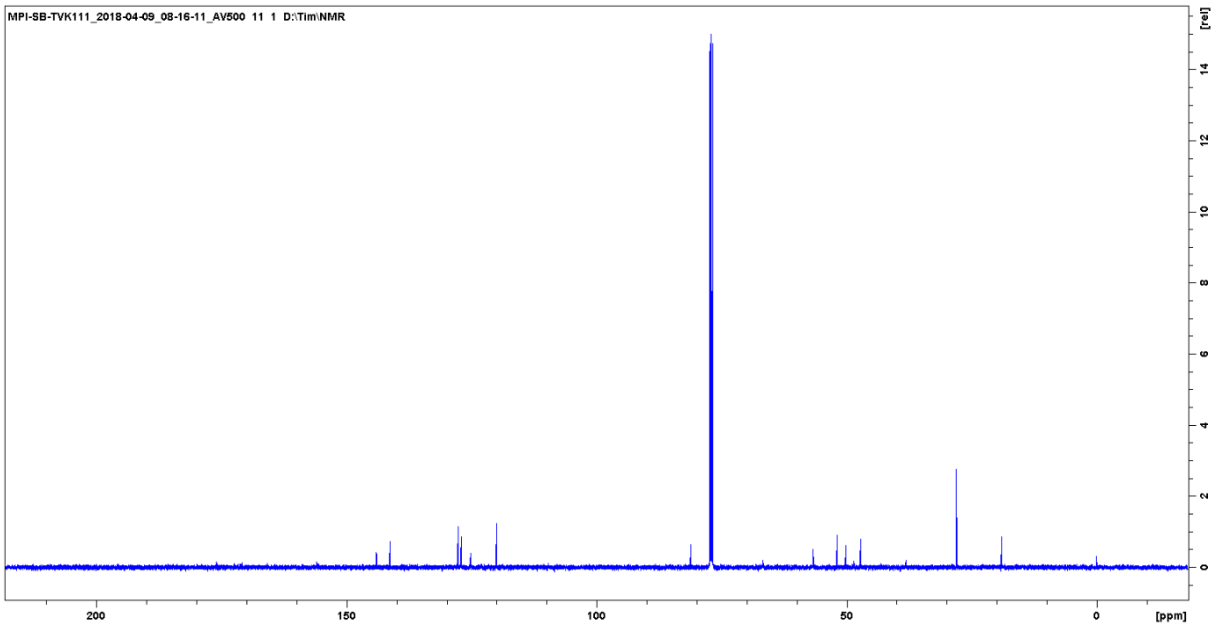

^{13}C NMR

Compound **7**:

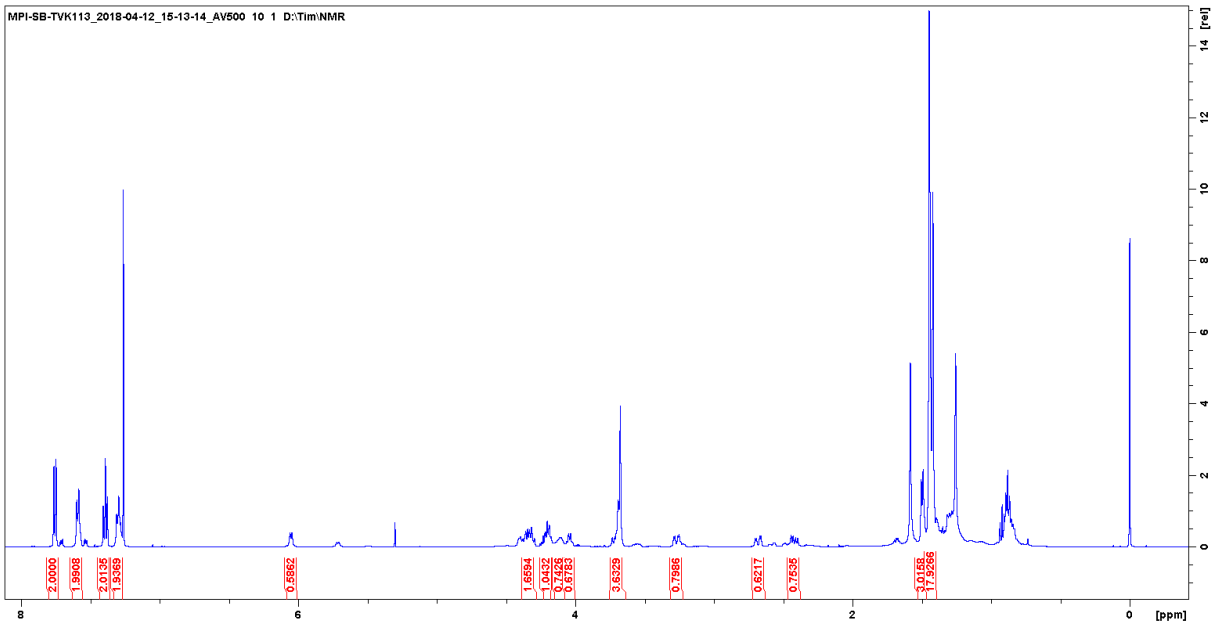

^{1}H NMR

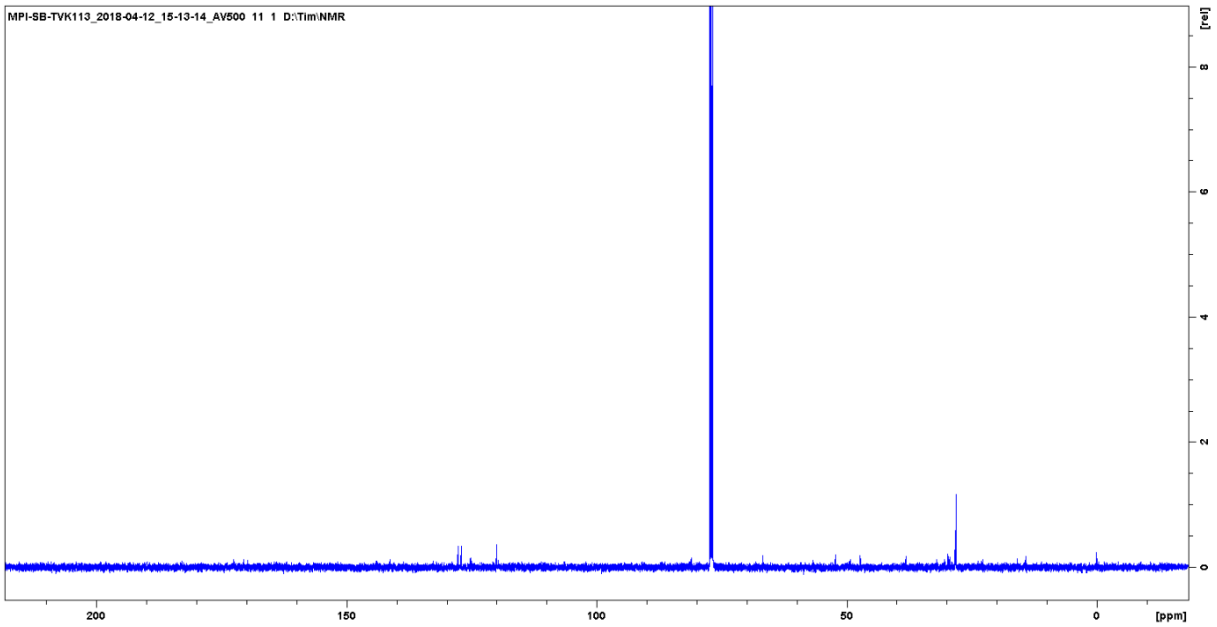

^{13}C NMR

Compound **8**:

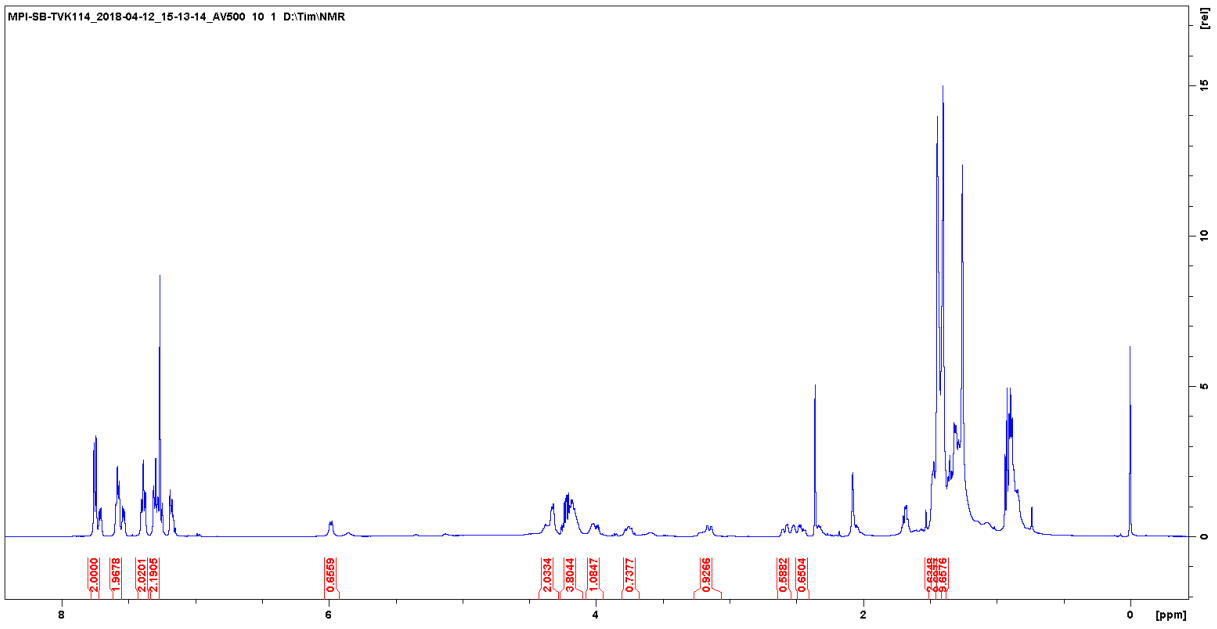

^{1}H NMR

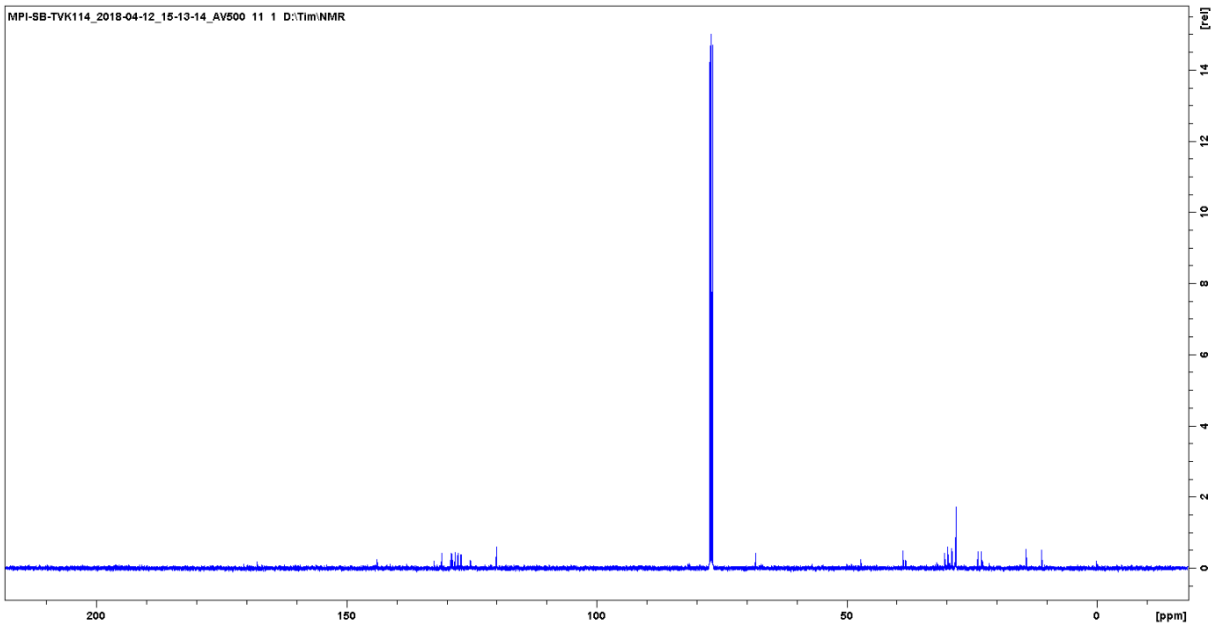

^{13}C NMR

Compound **10**:

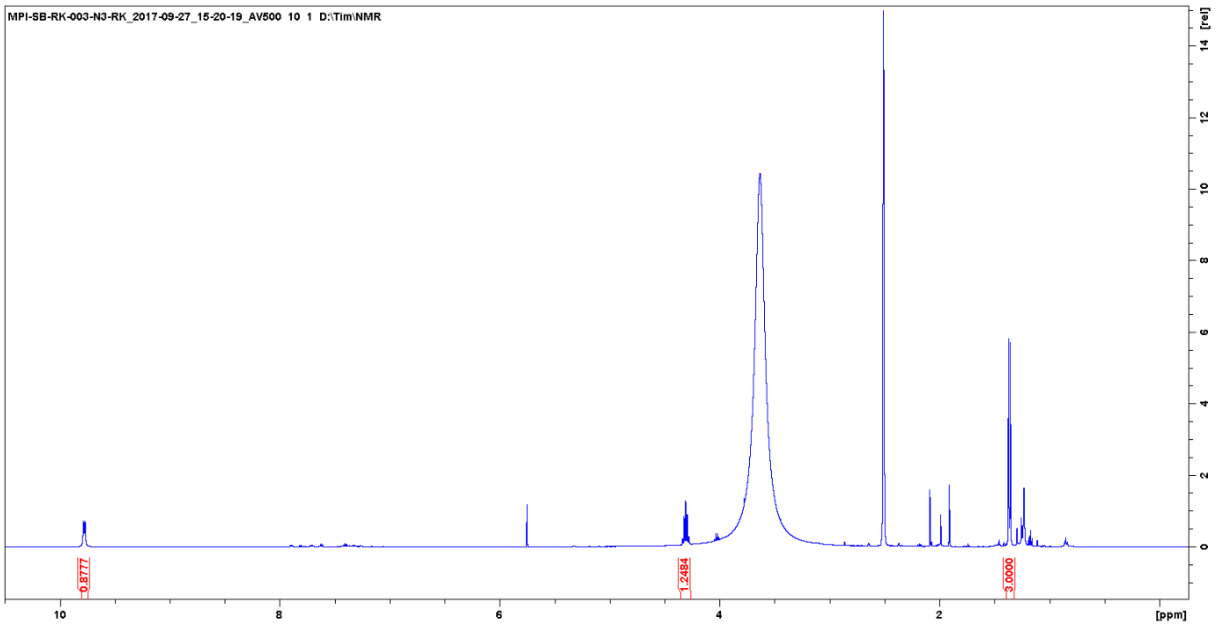

^{1}H NMR

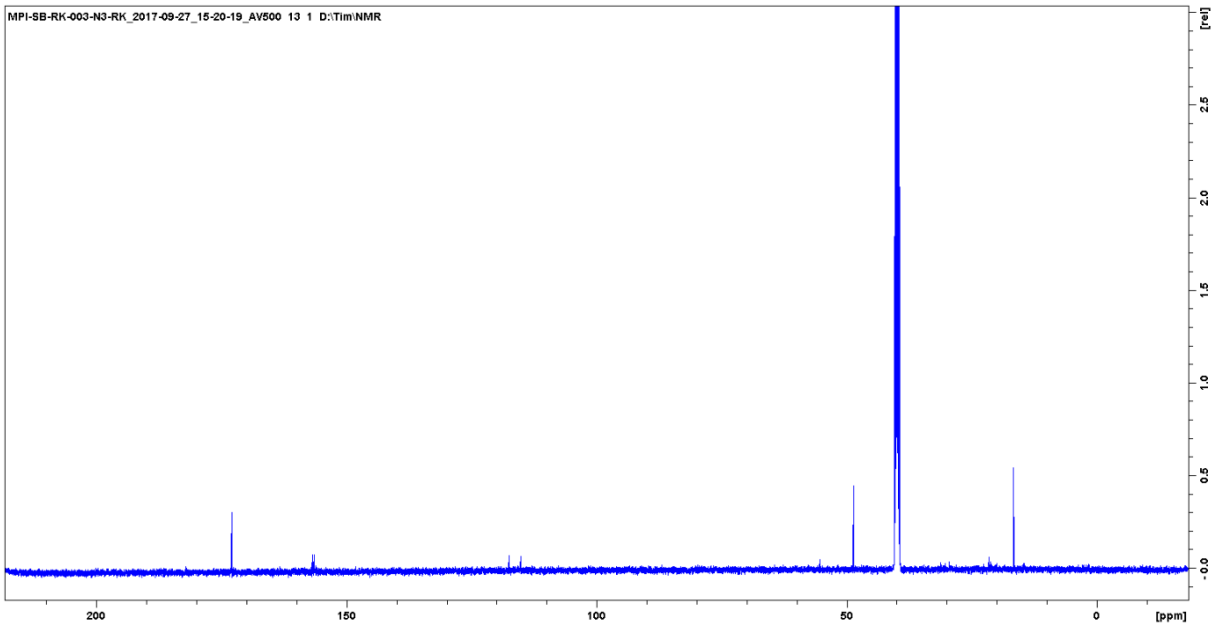

^{13}C NMR

Compound **11**:

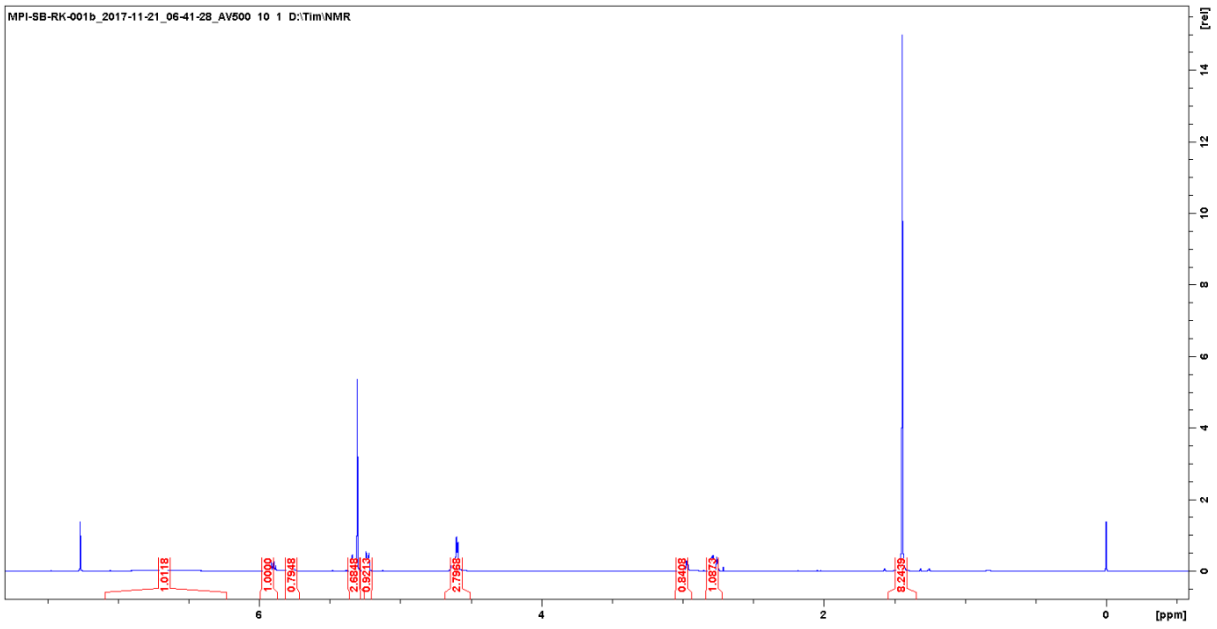

^{1}H NMR

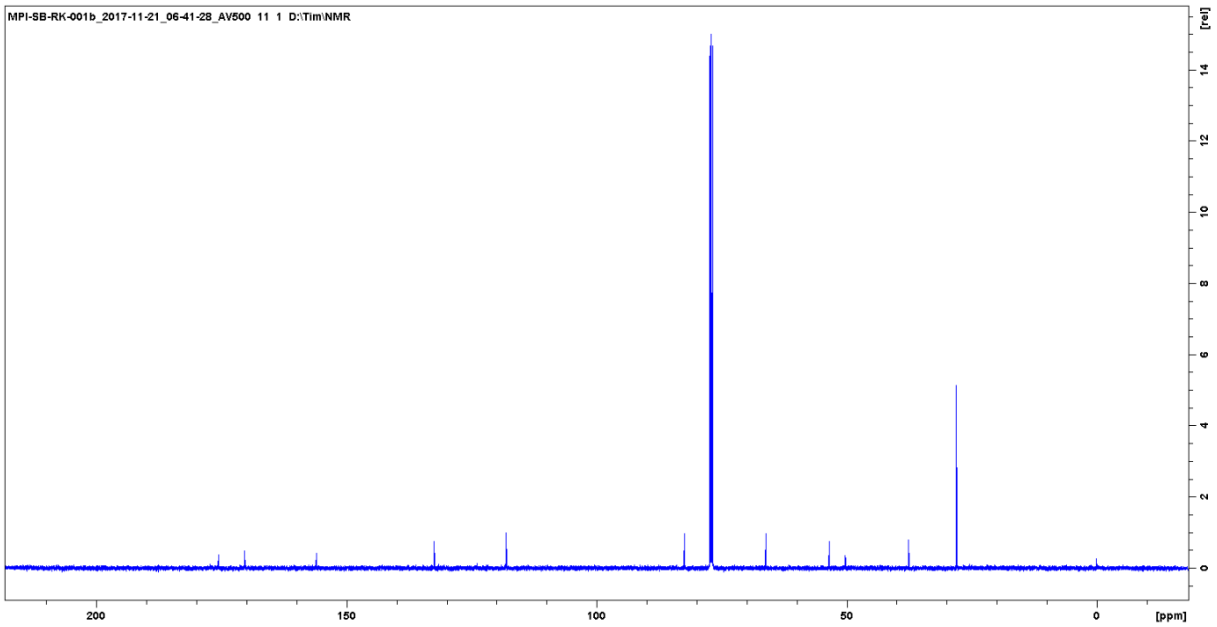

^{13}C NMR

Compound **14**:

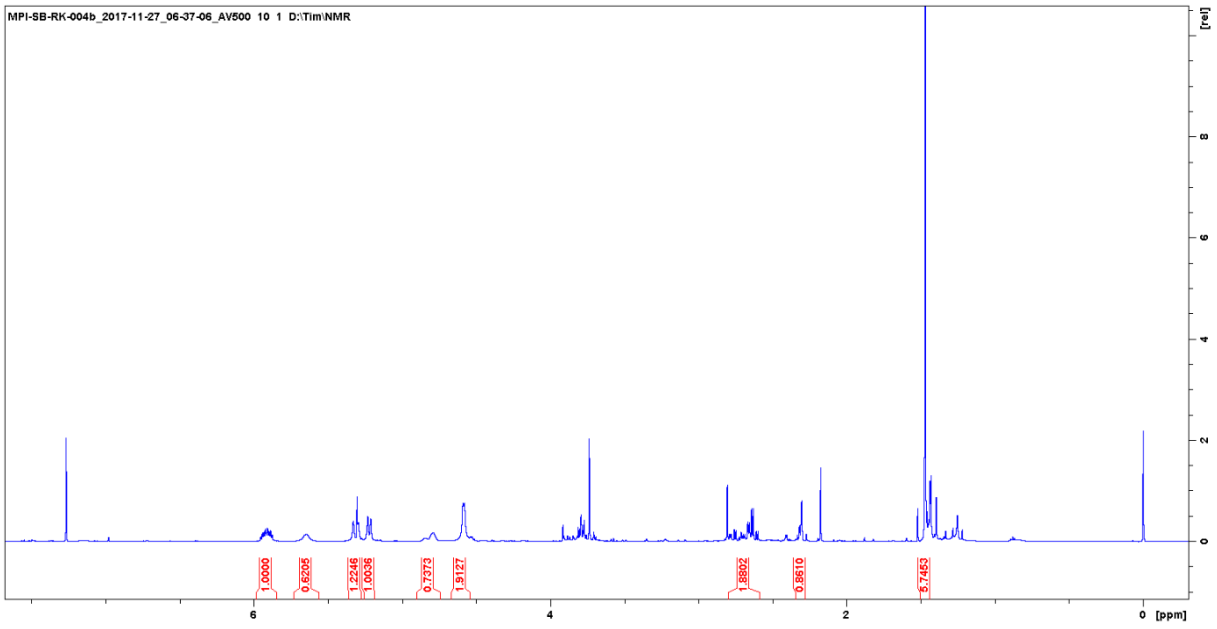

^{1}H NMR

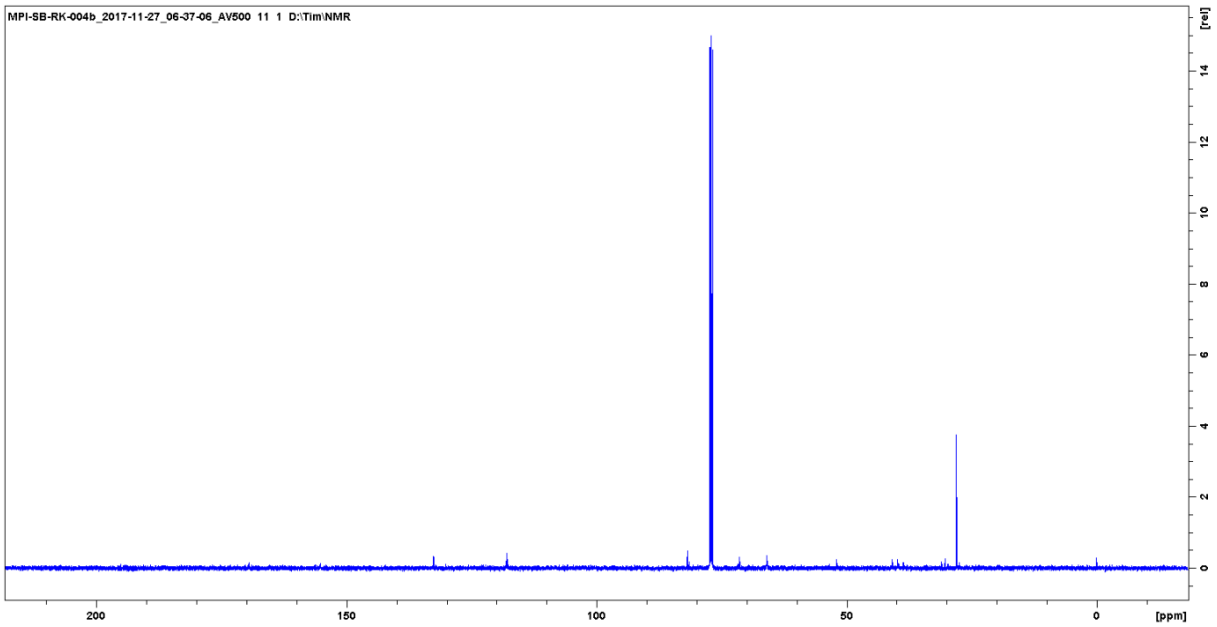

^{13}C NMR

9.2 List of mass spectrometry data

HR-MS (ESI) of inhibitor **15**:

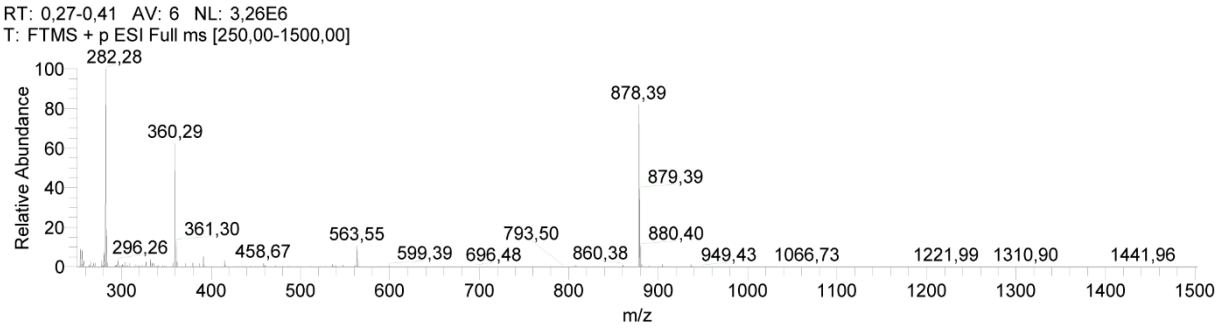

LC-MS (ESI) of inhibitor **16**:

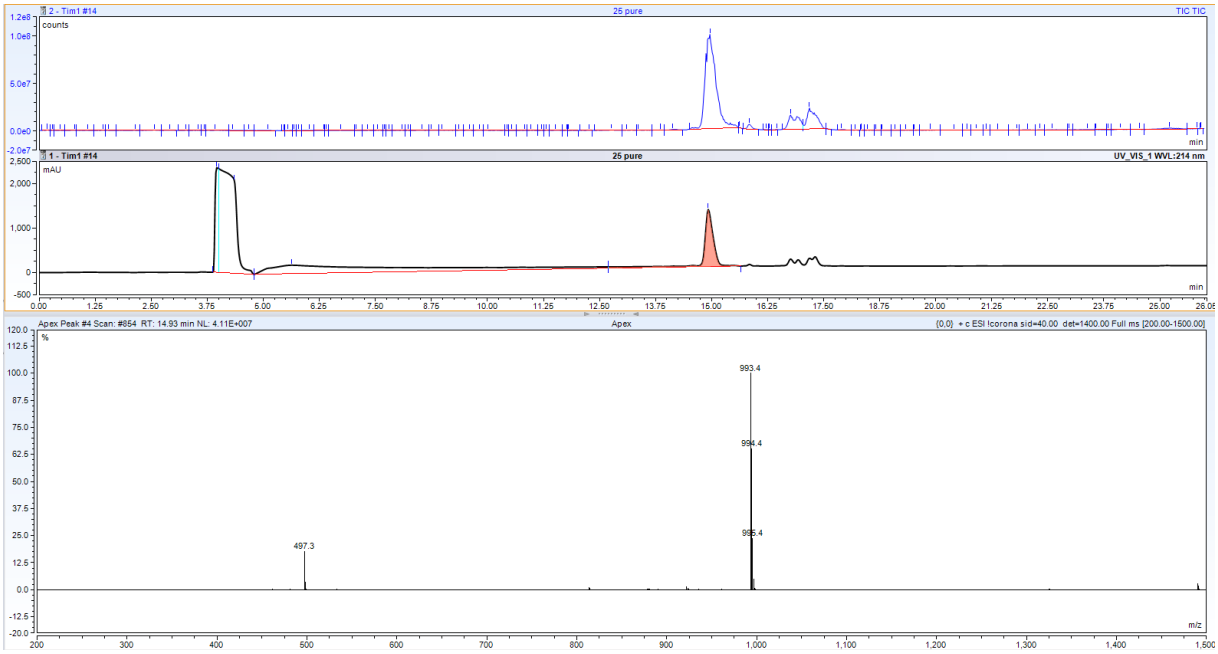

HRMS (ESI) of inhibitor **17**:

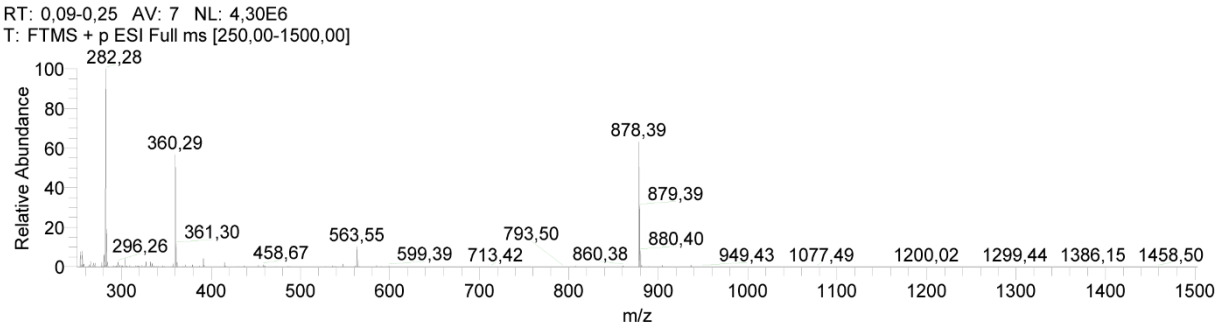

HRMS (ESI) of inhibitor **18**:

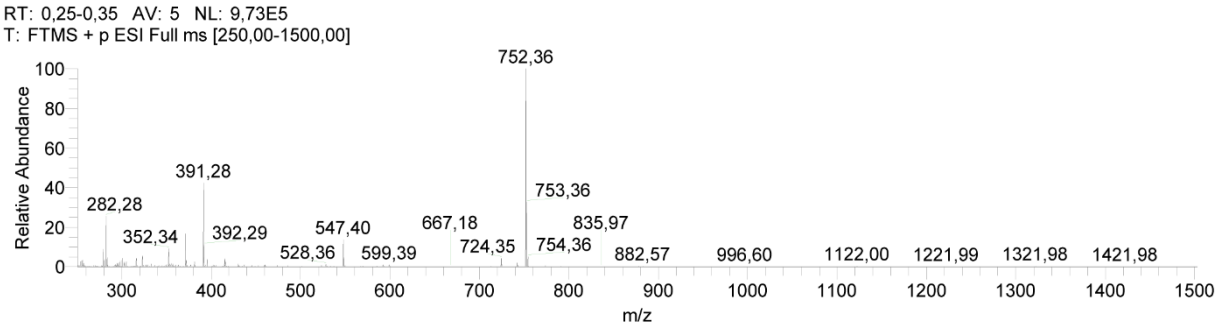

HRMS (ESI) of inhibitor **19**:

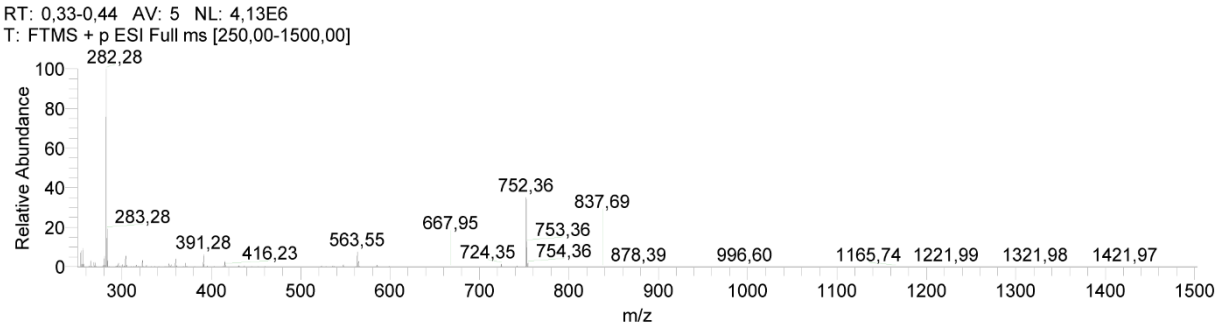

HRMS (ESI) of inhibitor **20**:

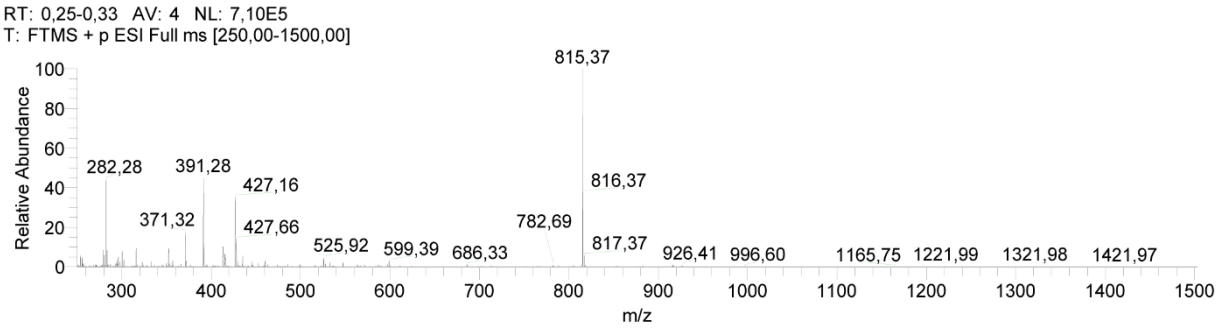

HRMS (ESI) of inhibitor **21**:

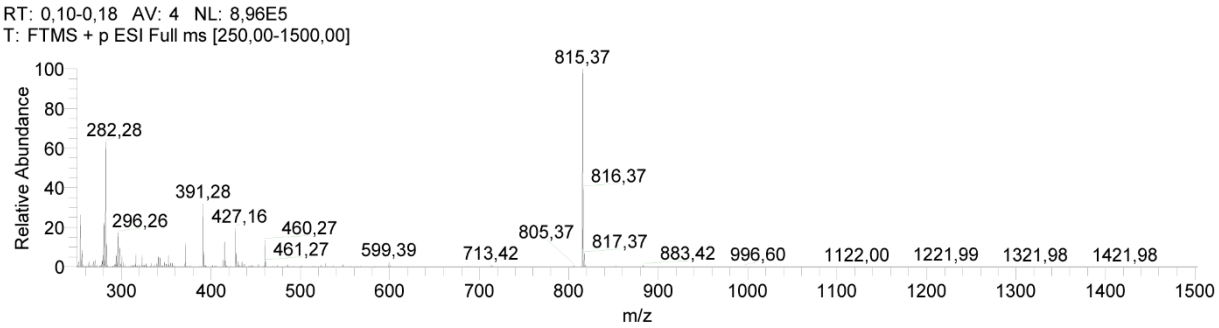

LC-MS (ESI) of inhibitor **22**:

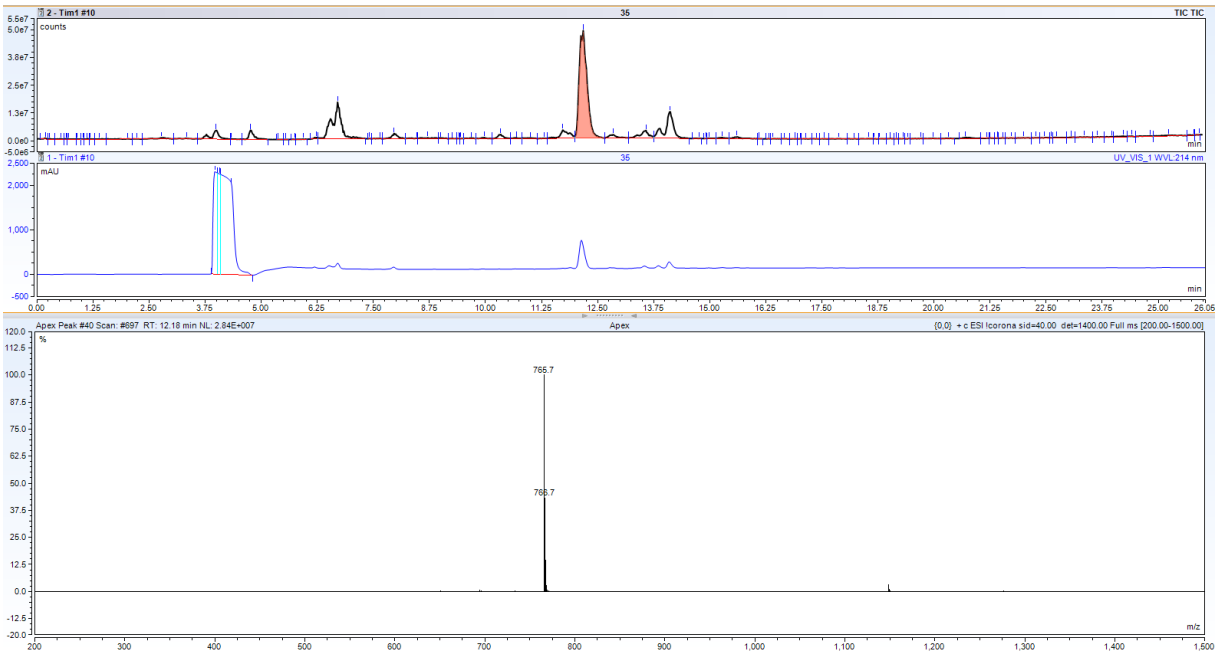

LC-MS (ESI) of inhibitor **23**:

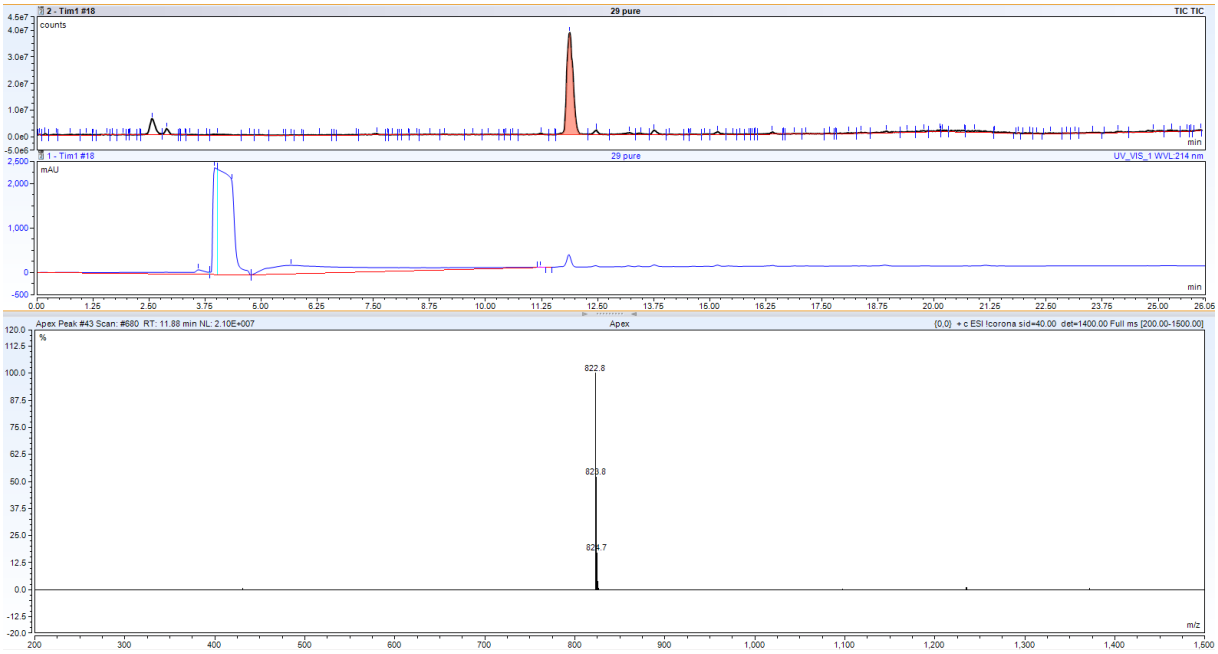

LC-MS (ESI) of inhibitor **24**:

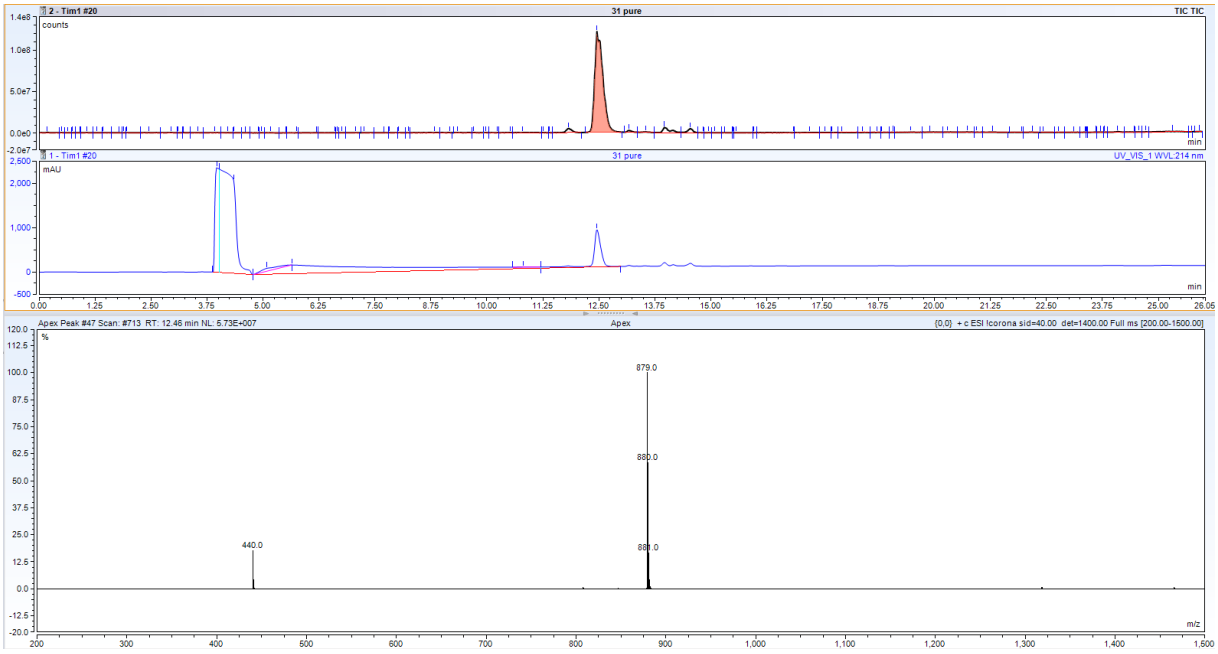

LC-MS (ESI) of inhibitor **25**:

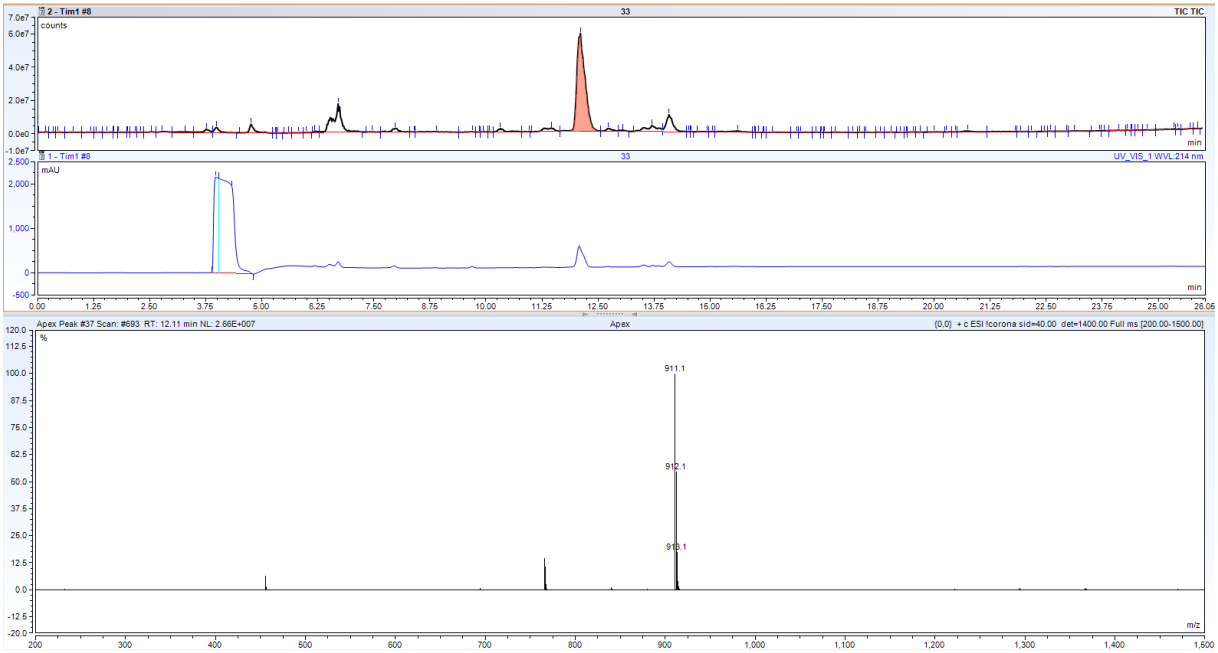

HRMS (ESI) of inhibitor **26**:

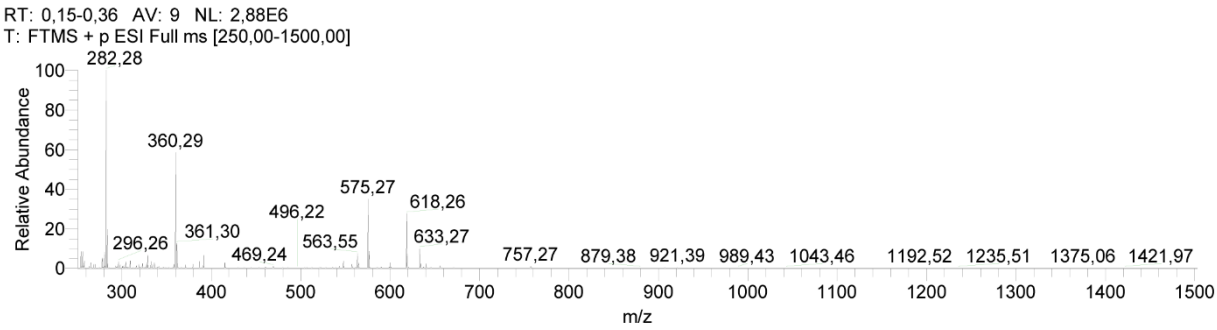

HRMS (ESI) of inhibitor **27**:

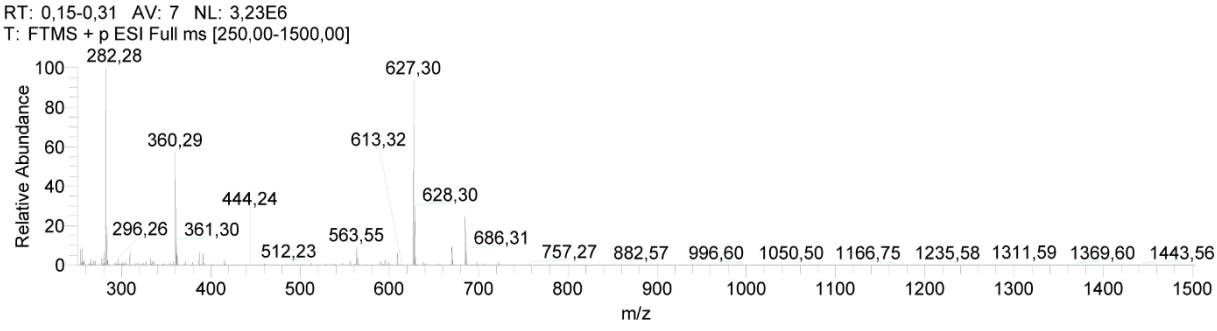

HRMS (ESI) of inhibitor **28**:

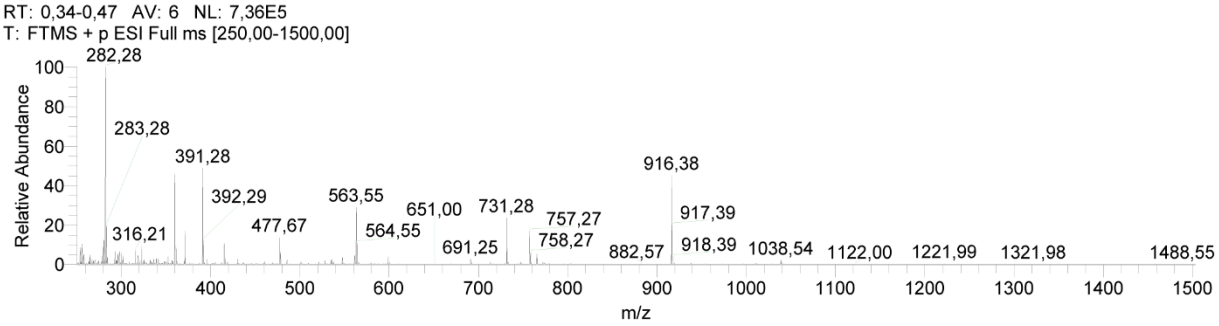

HRMS (ESI) of inhibitor **29**:

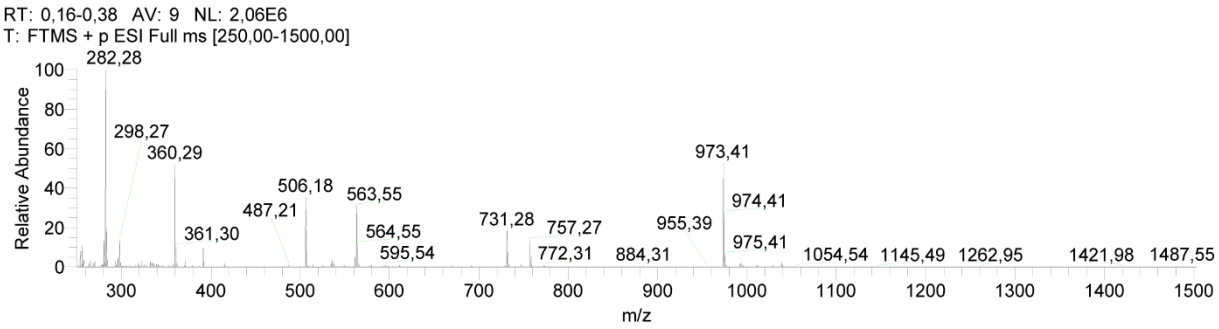

LC-MS (ESI) of inhibitor **30**:

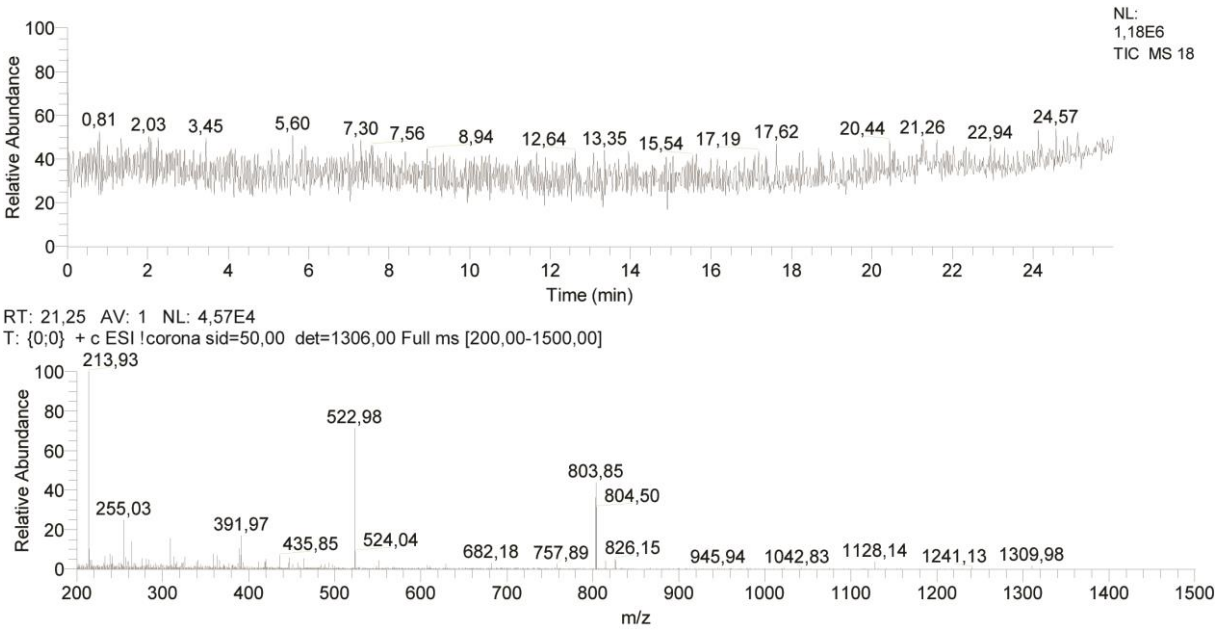

LC-MS (ESI) of inhibitor **31**:

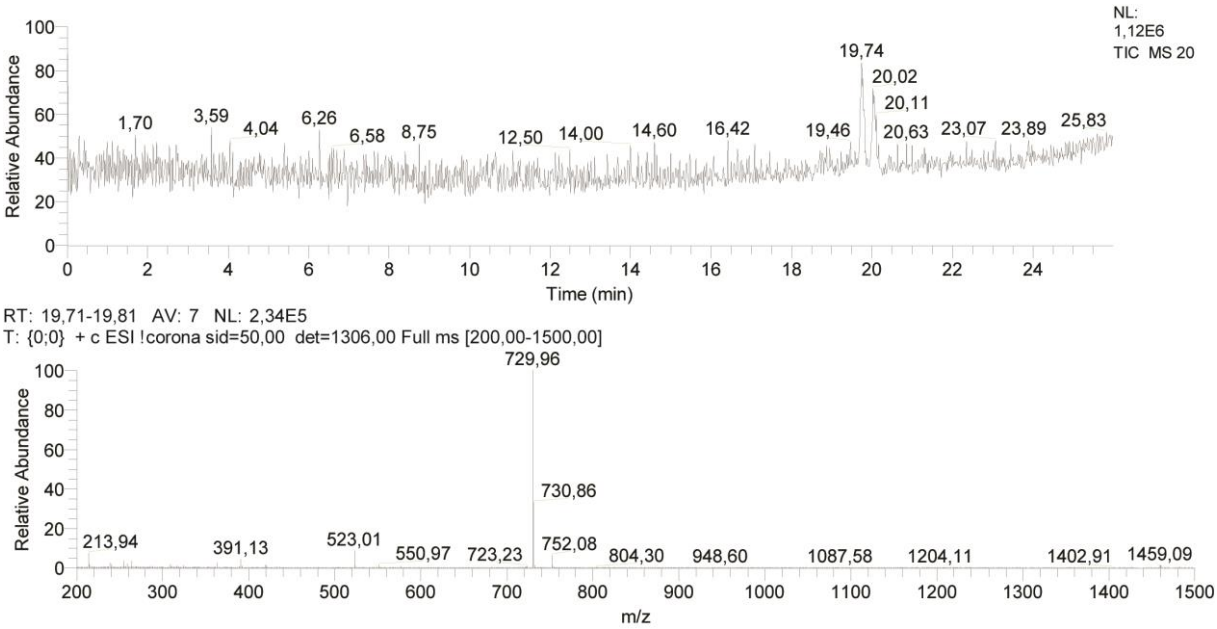

LC-MS (ESI) of inhibitor **32**:

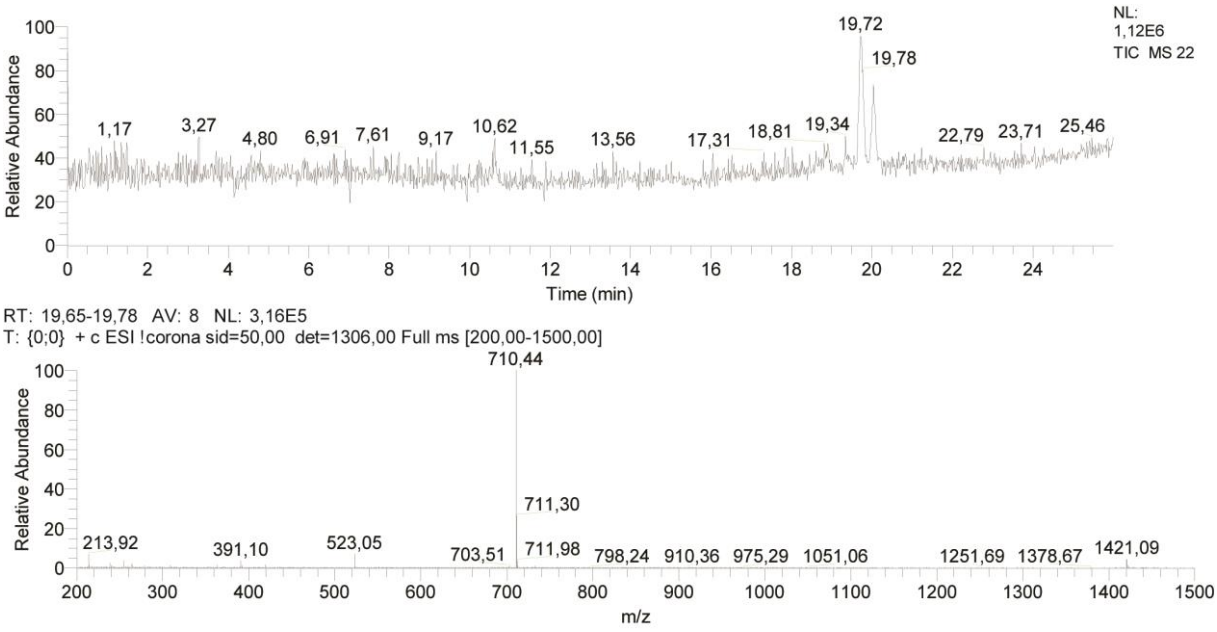

Acknowledgments

First and foremost, I would like to thank Prof. Dr. Steven Verhelst for giving me the unique chance to pursue a PhD and providing me with a challenging and fascinating project. As my direct supervisor, he was always available to provide me with advice and assistance where I needed it with unequaled enthusiasm.

A special thanks also goes to Prof. Dr. Markus Kaiser, without whom I would not have been able to complete my PhD at the Universität Duisburg-Essen.

I want to thank all members of the Chemical Proteomics group at ISAS and the Laboratory of Chemical Biology at the KU Leuven for being the most amazing colleagues. Special mentions go to Suravi for performing some of my measurements and Minh for the many fruitful discussions during the last few years.

I also want to thank all my other colleagues at ISAS, especially the members of the Lipidomics group, for keeping me entertained on a daily basis. Andreas, Bernhard, Bing, Cristina, and Philipp deserve a special mention. They helped me immensely with many of my mass spectrometry experiments and are just amazing people in general.

Thank you also to my friends from my time studying in Ghent, Gert-Jan, Giele, Jonas, Jorick, Niels, and Stephanie, and my friends from home, Jordy and Yannick, for always staying in touch and visiting me.

Last but not least, I want to thank my parents, sister and the rest of my family, for always showing their support in every way possible.

Curriculum Vitae

Eidesstattliche Erklärungen

Erklärung:

Hiermit erkläre ich, gem. § 7 Abs. (2) d) + f) der Promotionsordnung der Fakultät für Biologie zur Erlangung des Dr. rer. nat., dass ich die vorliegende Dissertation selbständig verfasst und mich keiner anderen als der angegebenen Hilfsmittel bedient, bei der Abfassung der Dissertation nur die angegeben Hilfsmittel benutzt und alle wörtlich oder inhaltlich übernommenen Stellen als solche gekennzeichnet habe.

Essen, den _____ _____

Unterschrift des Doktoranden

Erklärung:

Hiermit erkläre ich, gem. § 7 Abs. (2) e) + g) der Promotionsordnung der Fakultät für Biologie zur Erlangung des Dr. rer. nat., dass ich keine anderen Promotionen bzw. Promotionsversuche in der Vergangenheit durchgeführt habe und dass diese Arbeit von keiner anderen Fakultät/Fachbereich abgelehnt worden ist.

Essen, den _____ _____

Unterschrift des Doktoranden

Erklärung:

Hiermit erkläre ich, gem. § 6 Abs. (2) g) der Promotionsordnung der Fakultät für Biologie zur Erlangung der Dr. rer. nat., dass ich das Arbeitsgebiet, dem das Thema ***„Design, synthesis and application of peptide mimetics as photoactivatable inhibitors for proteases“*** zuzuordnen ist, in Forschung und Lehre vertrete und den Antrag von ***Tim Van Kersavond*** befürworte und die Betreuung auch im Falle eines Weggangs, wenn nicht wichtige Gründe dem entgegenstehen, weiterführen werde.

_____

Name des Mitglieds der Universität Duisburg-Essen in Druckbuchstaben

Essen, den _____ _____

Unterschrift eines Mitglieds der Universität Duisburg-Essen